AD NUMBER

ADB015271

LIMITATION CHANGES

TO:

Approved for public release; distribution is unlimited.

FROM:

Distribution authorized to U.S. Gov't. agencies only; Test and Evaluation; NOV 1976. Other requests shall be referred to Aeronautical Systems Division, Attn: ENFDA, Wright-Patterson AFB, OH 45433.

AUTHORITY

ASD, USAF ltr 2 Aug 1977

AEDC-TR-76-162

(2)

INLET PERFORMANCE CHARACTERISTICS OF A GENERALIZED 1/5.2–SCALE AIRCRAFT MODEL AT TRANSONIC AND SUPERSONIC MACH NUMBERS

PROPULSION WIND TUNNEL FACILITY
ARNOLD ENGINEERING DEVELOPMENT CENTER
AIR FORCE SYSTEMS COMMAND
ARNOLD AIR FORCE STATION, TENNESSEE 37389

November 1976

Final Report for Period November 24, 1975 – March 26, 1976

Prepared for

AERONAUTICAL SYSTEMS DIVISION (ASD/ENFDA)
WRIGHT-PATTERSON AIR FORCE BASE, OHIO 45433

NOTICES

When U. S. Government drawings specifications, or other data are used for any purpose other than a definitely related Government procurement operation, the Government thereby incurs no responsibility nor any obligation whatsoever, and the fact that the Government may have formulated, furnished, or in any way supplied the said drawings, specifications, or other data, is not to be regarded by implication or otherwise, or in any manner licensing the holder or any other person or corporation, or conveying any rights or permission to manufacture, use, or sell any patented invention that may in any way be related thereto.

Qualified users may obtain copies of this report from the Defense Documentation Center.

References to named commercial products in this report are not to be considered in any sense as an endorsement of the product by the United States Air Force or the Government.

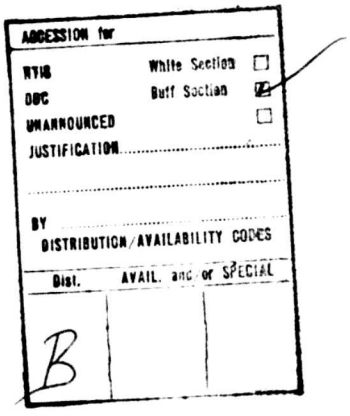

APPROVAL STATEMENT

This technical report has been reviewed and is approved for publication.

FOR THE COMMANDER

John C. Cardosi

JOHN C. CARDOSI
Lt Colonel, USAF
Chief Air Force Test Director, PWT
Directorate of Test

Alan L. Devereaux

ALAN L. DEVEREAUX
Colonel, USAF
Director of Test

UNCLASSIFIED

REPORT DOCUMENTATION PAGE	READ INSTRUCTIONS BEFORE COMPLETING FORM
1 REPORT NUMBER: AEDC-TR-76-162 (14)	2 GOVT ACCESSION NO. (9) Final rept. 24 Nov 75-26 Mar 76
4 TITLE (and Subtitle): INLET PERFORMANCE CHARACTERISTICS OF A GENERALIZED 1/5.2-SCALE AIRCRAFT MODEL AT TRANSONIC AND SUPERSONIC MACH NUMBERS (6)	5 TYPE OF REPORT & PERIOD COVERED: Final Report - November 24, 1975 - March 26, 1976 (8)
	6 PERFORMING ORG. REPORT NUMBER
7 AUTHOR(s): (10) Jimmy Walker, ARO, Inc.	8 CONTRACT OR GRANT NUMBER(s)
9 PERFORMING ORGANIZATION NAME AND ADDRESS: Arnold Engineering Development Center (XO) Air Force Systems Command Arnold Air Force Station, Tennessee 37389	10 PROGRAM ELEMENT, PROJECT, TASK AREA & WORK UNIT NUMBERS: Program Area 921A
11 CONTROLLING OFFICE NAME AND ADDRESS: Aeronautical Systems Division (ENFDA) Wright-Patterson Air Force Base Ohio 45433	12 REPORT DATE: (11) November 1976
	13 NUMBER OF PAGES: 99 (12) 103p.
14 MONITORING AGENCY NAME & ADDRESS(if different from Controlling Office)	15 SECURITY CLASS. (of this report): UNCLASSIFIED
	15a DECLASSIFICATION/DOWNGRADING SCHEDULE: N/A

16 DISTRIBUTION STATEMENT (of this Report)
Distribution limited to U.S. Government agencies only; this report contains information on test and evaluation of military hardware; November 1976; other requests for this document must be referred to Aeronautical Systems Division (ENFDA), Wright-Patterson Air Force Base, Ohio 45433.

17 DISTRIBUTION STATEMENT (of the abstract entered in Block 20, if different from Report)

18 SUPPLEMENTARY NOTES

Available in DDC

19 KEY WORDS (Continue on reverse side if necessary and identify by block number)
air intakes
induction systems
performance
wind tunnel tests
transonic flow
supersonic flow

20 ABSTRACT (Continue on reverse side if necessary and identify by block number)
A wind tunnel investigation was conducted at free-stream Mach numbers from 0.55 to 2.0 on a 1/5.2-scale composite inlet model to evaluate configuration factors which affected inlet performance. In addition, flow-field surveys were made at the inlet throat and on the fuselage, forward of the inlet cowl lip. Inlet performance parameters in terms of total-pressure recovery, distortion, and turbulence at the simulated compressor face, as well as compressor-

CONT ON NEXT

DD FORM 1 JAN 73 1473 EDITION OF 1 NOV 65 IS OBSOLETE

042 550

UNCLASSIFIED

20. ABSTRACT (Continued)

face and throat station total-pressure contours and diffuser duct static-pressure distributions, are presented for various Mach numbers and angles of attack and sideslip. The basic air induction system consisted of a normal-shock-type inlet with a long splitter plate assembly and was located beneath the wing glove in proximity to the fuselage. The total-pressure recovery for the basic inlet system was slightly better than normal shock recovery for cruise attitudes at supersonic Mach numbers. At Mach numbers approaching 2.0, the basic inlet system was operating close to the buzz limit at design engine airflow. Reductions in total-pressure distortion were achieved by increasing the fuselage-to-inlet standoff distance and by inlet duct boundary-layer blowing.

AFSC
Arnold AFS Tenn

PREFACE

The work reported herein was conducted by the Arnold Engineering Development Center (AEDC), Air Force Systems Command (AFSC), at the request of the Aeronautical Systems Division (ASD/ENFDA), for the Convair Aerospace Division of General Dynamics Corporation under Program Area 921A. The results of the test were obtained by ARO, Inc. (a subsidiary of Sverdrup & Parcel and Associates, Inc.), contract operator of AEDC, AFSC, Arnold Air Force Station, Tennessee, under ARO Project Number P41T-A2A. The author of this report was Jimmy Walker, ARO, Inc. The tests were conducted from November 24, 1975 to March 26, 1976, and the data analysis was completed on June 18, 1976. The manuscript (ARO Control No. ARO-PWT-TR-76-99) was submitted for publication on August 27, 1976.

CONTENTS

ILLUSTRATIONS

Figure | Page

TABLES

Page

APPENDIX

1.0 INTRODUCTION

At the request of the Aeronautical Systems Division (ASD), Air Force Systems Command (AFSC), tests were conducted for the Convair Aerospace Fort Worth Division, General Dynamics Corporation, in the Propulsion Wind Tunnels (16T and 16S), Propulsion Wind Tunnel Facility (PWT) on a 1/5.2-scale composite inlet model. The primary objective of these tests was to evaluate inlet configuration factors which affect inlet performance, such as inlet standoff distance, splitter plate length, side plate geometry, inlet duct vortex generators, and inlet duct boundary-layer blowing system. In addition, flow-field surveys were made at the inlet throat and on the fuselage, forward of the inlet cowl lip. The data acquired from the subject test program will supplement an inlet system data bank which is used to provide data for evaluating air-induction-system parameters that affect the performance of the flight vehicle.

The Tunnel 16S phase of testing began on November 24, 1975, and was completed on November 27, 1975. The Tunnel 16T phase of testing was conducted during March 19-26, 1976. Inlet performance data were obtained at free-stream Mach numbers from 0.55 to 2.0 at angles of attack and sideslip from -2.5 to 13 deg and ±4 deg, respectively.

2.0 APPARATUS

2.1 TEST FACILITY

Tunnels 16T and 16S are closed-circuit, continuous flow tunnels which are currently capable of being operated in the Mach number ranges from 0.20 through 1.55, and 1.50 through 2.40, respectively. Tunnel 16T can be operated within a stagnation pressure range of 120 to 4,000 psfa depending on Mach number, and stagnation temperature can be varied from about 80 to 160°F as a function of cooling water temperature. Tunnel 16S can be operated at stagnation temperatures from 300 to 620°F and stagnation pressures from 200 to 1,600 psfa, depending on Mach number. The tunnels are equipped with a plenum evacuation system, and the test sections are formed by fixed, parallel top and bottom walls, and variable angle side walls. The test sections are 16 by 16 ft in cross section and 40 ft long. A more complete description of the tunnels and their operating characteristics may be found in Ref. 1.

2.2 TEST ARTICLE

2.2.1 Overall Model Description

The basic configuration tested during this investigation was a 1/5.2-scale inlet-forebody model which was not necessarily representative of a specific aircraft. A

photograph and sketch of the model installed in Tunnel 16T are shown in Fig. 1. The model scale was derived by using existing model hardware from other test programs. The compressor-face units, airflow plugs, and the structural beam built for the Tailor-Mate Program models (Refs. 2 and 3) were used in the design of the model. A more complete description of the model details may be found in Ref. 4.

The model was inverted on a support beam which was in turn attached to an auxiliary pitch system on top of a yaw table and strut (see Fig. 1). For this series of tests, it was possible to obtain the model angle-of-attack requirements of $-2.5 \leq \alpha \leq 13$ deg by using the strut pitch-angle capability. The model sideslip requirements of $-4 \leq \beta \leq 4$ deg were obtained by using the yaw table.

2.2.2 Inlet Configuration Description

The basic inlet configuration consisted of the long splitter plates and long diverters with the inlets located at buttock line (B.L.) 43.82. For the first tunnel entry of the test, the configuration of the right-hand inlet was fixed, but the left-hand inlet could be varied in its configuration. Therefore, design changes (splitter plates, diverter length) were evaluated with the left-hand inlet. Flow-field surveys at the inlet throat and on the fuselage forward of the inlet cowl lip were made with the right-hand inlet (see Fig. 2a). The effect of inlet buttock-line position on inlet performance was examined using both inlets, each of which could be moved outboard from the fuselage by up to 4.45 in. (full-scale). The inlet, duct, and flow control unit all moved together when the buttock-line position of the model inlets was changed. The left-hand inlet side and glove plates as well as the fuselage and glove diverters could be removed and replaced by shortened hardware to give an alternate splitter plate configuration (see Figs. 2b and c).

Before the second tunnel entry of the test, both inlets were modified to accept two additional alternate side plates for the long splitter configuration (see Fig. 2d). In addition, vortex generators were installed in the left-hand duct during the second entry of the test. Three different vortex generator patterns (see Figs. 2e and f) were tested. Another configuration change made during the second entry was the installation of a high-pressure air duct boundary-layer blowing system in the right-hand duct. This system is discussed in greater detail in Section 4.6. The left-hand inlet had a throat design Mach number of 0.8 and a full-scale throat area of 1052.4 sq in. The right-hand inlet had a throat design Mach number of 0.7 and a full-scale throat area of 1118.0 sq in. The left-hand compressor face had an ogive-nose rotor hub (Fig. 3a), and the right-hand compressor face had a mallet-nose rotor hub (Fig. 3c). A summary of the various inlet configurations tested is given in Table 1.

2.3 INSTRUMENTATION

The left-hand inlet and duct were instrumented for the determination of steady- and unsteady-state inlet performance, and for the evaluation of turbulence and distortion at the compressor-face plane. The left-hand inlet incorporated steady-state instrumentation at the compressor face, in the primary duct and cowl, forward of the inlet on the fuselage and glove sideplates and diverters, and on the fuselage and glove surfaces. Unsteady-state instrumentation was located at the compressor face, in the primary duct, and at the cowl throat. The left compressor-face instrumentation consisted of 40 high-response and 40 steady-state total-pressure probes located on centroids of equal areas (see Fig. 3a). The eight, five-probe compressor-face rakes were mounted in a plane forward of the simulated engine fan rotor hub. In addition to the compressor-face high-response total-pressure probes, there were nine flush-mounted unsteady-state pressure transducers installed in the left-hand inlet and subsonic duct so that any source of inlet-generated turbulence could be identified. The steady- and unsteady-state static pressure locations in the left-hand duct are shown in Fig. 3b. Another unsteady-state pressure transducer was mounted in the nose of the model to sense free-stream turbulence.

The right-hand inlet was instrumented to obtain steady-state pressure data for investigating the inlet-related flow field and cowl throat pressure distributions. The right-hand compressor-face instrumentation consisted of 40 steady-state total-pressure probes located on centroids of equal areas (see Fig. 3c). There were no high-response pressure transducers installed at either the right-hand compressor face or in the right-hand duct.

There were a total of up to 350 steady-state and 50 high-response static- and total-pressure probes located on the model, depending upon the configuration.

The primary airflow-metering plug positions were determined from the output of potentiometers mounted in the plug assemblies. Model pitch angle was measured with an angular position indicator mounted on the main structural beam of the model. The strut pitch angle was also measured with an angular position indicator, and the yaw angle was measured with a potentiometer mounted on the bottom of the yaw table. Model angles of attack and sideslip were calculated from the combined measurements of strut pitch angle, auxiliary pitch angle, and yaw table angle.

During the test, data from all steady-state channels were transmitted to the AEDC-PWT digital computer from the AEDC-PWT scanner system, data reduction was performed, and the computed parameters tabulated on a line printer in the control room.

The unsteady-state pressure transducer signals were recorded on the AEDC-PWT 98-channel FM multiplex magnetic tape recording system which has a frequency response of 8 kHz. Additionally, all 50 of the unsteady-state pressure signals were paralleled to root-mean-square (rms) meters whose outputs were recorded by the steady-state data system. A more complete description of the AEDC-PWT instrumentation system and capability may be found in Ref. 1.

Selected instrumentation channels were paralleled to a high-speed digital data acquisition system that was used to calculate inlet performance parameters in a real-time mode and display them on a cathode ray tube (CRT). In this manner, values of recovery, full-scale corrected airflow, and model positions were available in real time for operational information.

3.0 PROCEDURE

3.1 TEST OPERATING PROCEDURE

In Tunnel 16T, test Mach numbers were 0.55, 0.65, 0.75, 0.85, 1.20, 1.40, and 1.50. In Tunnel 16S, data were obtained at Mach numbers 1.60, 1.62, 1.70, 1.80, 1.90, and 2.00. Free-stream total temperature was maintained at 100°F in 16T and 140°F in 16S. Tunnel free-stream total pressures and dynamic pressures corresponding to the above Mach number conditions are shown in Table 2.

After the tunnel conditions had been established and the model positioned at the desired attitude, the primary airflow was varied in increments through a predetermined range and steady- and unsteady-state data were recorded at each airflow setting. Design engine airflow requirements are listed in Table 3.

3.2 DATA REDUCTION

Left-hand inlet performance in terms of total-pressure recovery, circumferential and radial distortion, inlet/engine distortion index, and rms turbulence was determined from the steady-state and high-response pressure measurements acquired at the compressor face. Right-hand inlet steady-state performance was obtained in a similar manner. The steady-state compressor-face total pressures were used to calculate two primary distortion descriptors: maximum radial and maximum circumferential distortions. These two descriptors were then used to calculate an inlet/ engine distortion index. The equations used in computing the distortion descriptors and index are presented in Appendix A. An inlet/engine distortion index value less than unity demonstrates acceptable engine/inlet compatibility, and a value equal to or greater than unity indicates potential compressor surge. It should be noted that at a given Mach number, the limiting values of the

distortion descriptors, IDCLMAX and IDRLMAX, for an inlet/engine distortion index (IDLMAX) equal to unity are defined by the engine sensitivity constants (KR, KC, A, B, and C) tabulated in Appendix A and are not independent of each other. For instance, in the Mach number range from 0.85 to 1.7, the limiting value of IDCLMAX is 0.105 for IDRLMAX = 0, but at IDRLMAX = 0.063, the limiting value of IDCLMAX is zero. The interrelationship of IDCLMAX and IDRLMAX for IDLMAX = 1.0 through the Mach number range 0.55 to 2.0 is shown in Fig. A-1.

3.3 MEASUREMENT UNCERTAINTY

Listed in Table 4 are estimates of the uncertainties for selected model test parameters. The uncertainties in these parameters include the inaccuracies in the tunnel reference systems, the recording systems, and the measuring devices themselves. The errors presented are combined errors (the square root of the sum of the squares of the individual errors) and were derived for a two-standard-deviation confidence level using the Taylor series expansion method. Uncertainty is expressed as

$$U = \pm(B + 2S)$$

where B is the bias (systematic error) and S is the precision index (random error for unity standard deviation). A detailed description of the measurement uncertainty methodology may be found in Ref. 5.

4.0 RESULTS

4.1 PERFORMANCE OF BASIC CONFIGURATION

The basic inlet configuration consisted of the long splitter plates with the "triangular" side plates (see Fig. 2c) and the inlets located at buttock line 43.82. Inlet performance characteristics, in terms of total-pressure recovery, rms turbulence, circumferential and radial distortion descriptors, and inlet/engine distortion index (a value equal to or greater than unity indicates a potential compressor surge) at the simulated engine compressor face, are presented in Fig. 4 for Mach numbers 0.65, 0.85, 1.20, 1.50, 1.80, and 2.0.

In general, the basic inlet configurations exhibited satisfactory performance throughout the Mach number range investigated. There was no indication of a potential compressor surge, although the inlet/engine steady-state distortion index (IDLMAX) approached a value of 0.9 for design engine airflow at M_∞ = 1.2 (see Fig. 4c) and was essentially independent of angle of attack (0 to 13 deg). Inlet total-pressure recovery (RECL) for design engine airflow at Mach numbers from 0.65 to 1.2 was relatively

insensitive (< 1.0-percent change in recovery) to changes in angle of attack at low angles of attack (0 to 5 deg), but was significantly affected (> 1.0-percent change in recovery) by changes in angle of attack in the angle-of-attack range from 5 to 13 deg. For Mach numbers from 1.5 to 2.0, recovery generally increased with increasing angle of attack as a result of the wing glove serving as a compression surface for the flow approaching the inlet (as angle of attack was increased from 5 to 13 deg at M_∞ = 1.8, this characteristic resulted in a 9-percent increase in recovery). At low angles of attack ($\alpha < 2.0$ deg) and for M_∞ = 1.8 and 2.0, the inlet operated close to the buzz limit (at design engine airflow). This was also true for data obtained at M_∞ = 1.90 (not shown). It should be noted that the inlet operated closer to the buzz limit at M_∞ = 2.0 (essentially at the buzz limit at α = -2.4 deg) than at M_∞ = 1.8, and as a result, maneuverability was more limited at M_∞ = 2.0 than at M_∞ = 1.8. It should also be noted that although the inlet/engine steady-state distortion index (IDLMAX) was near 0.5 at M_∞ = 2.0 and α = -2.4 deg, the inlet turbulence (TI2) approached seven percent; this characteristic portends the possibility of a compressor surge as a result of instantaneous peak distortion exceeding the allowable limit (IDLMAX > 1.0). In summary, the total-pressure recovery (at α = 5 deg and for design engine airflow) for the basic inlet configuration decreased approximately linearly from 0.97 at M_∞ = 0.55 to 0.95 at M_∞ = 1.4 and was slightly better than normal-shock recovery from M_∞ = 1.5 (1 percent) to 2.0 (6 percent) (see Fig. 5). Presented in Fig. 6 are left-hand duct static-pressure distributions obtained at design engine airflow for Mach numbers 0.65, 0.85, 1.20, 1.50, 1.80, and 2.00. These data show a well-behaved duct pressure recompression characteristic.

The effect of angle of sideslip (-4 to 4 deg) on the basic inlet configuration performance design engine airflow is shown in Fig. 7 for Mach numbers 0.85, 1.20, and 1.80. At subsonic Mach numbers, the sidewash of the flow approaching the inlet did not appreciably affect the inlet performance (recovery at M_∞ = 0.85 decreased 1.2 percent from 0- to 4-deg sideslip at α = 5 deg). However, the supersonic Mach number data indicate that this under-wing-fuselage-type inlet was quite susceptible to adverse flow sidewash at model sideslip attitudes (recovery at M_∞ = 1.8 decreased 2.9 percent from 0- to 4-deg sideslip angle at α = 5 deg).

Left compressor-face total-pressure and turbulence contours for the basic configuration at Mach numbers 0.65, 0.85, 1.20, 1.50, 1.80, and 2.00, design engine airflow, and several model attitudes are presented in Figs. 8 through 13. Note that the low-pressure region was always positioned on the outboard location and the high-turbulence region was generally located on the inboard side of the compressor face.

4.2 EFFECTS OF INLET STANDOFF DISTANCE

The model was designed such that both the left- and right-hand inlets could be moved outboard from the fuselage by 4.45 in. full-scale. The basic configuration was tested with

the inlet positioned at B.L. 43.82. In addition, data were obtained with the inlet positioned at B.L. 45.64 and B.L. 47.45. The data presented in Fig. 14 indicate that, for design engine airflows, moving the inlet from B.L. 43.82 to B.L. 45.64 resulted in about 25-percent lower circumferential and radial distortion, about 15-percent lower inlet/engine distortion index, and approximately the same compressor-face recovery and turbulence. This was true for all Mach numbers (0.55, 0.65, 0.75, 0.85, 1.2, 1.4, 1.5) at which data were acquired.

The data presented in Fig. 15 show a comparison between inlet performance at M_∞ = 1.62 for inlet buttock-line positions of 43.82 and 47.45. At angles of attack of 5 deg or less, the B.L. 47.45 inlet position resulted in slightly lower circumferential and radial distortion and a lower inlet/engine distortion index. However, the B.L. 47.45 position gave one- to two-percent lower compressor face total-pressure recovery and a slightly higher turbulence index. The inlet stable range was, however, better at B.L. 47.45 (stability limit at MFRL = 0.54) than at B.L. 43.82 (stability limit at MFRL = 0.62). At angles of attack of 10 deg and greater, the B.L. 47.45 inlet position gave slightly better overall performance than the B.L. 43.82 position (see Fig. 15b).

In summary, the predominant effect of increasing the inlet standoff distance was to decrease circumferential and radial distortion and, therefore, the inlet/engine distortion index at design engine airflow. Moving the inlet from B.L. 43.82 to B.L. 45.64 (full scale) resulted in a 15-percent decrease in the inlet/engine distortion index in the Mach number range from 0.55 to 1.5 at α = 5 deg.

4.3 COMPARISON OF SHORT AND LONG SPLITTERS

The basic inlet configuration consists of the long splitter, that is, long side and upper plates, and long fuselage and glove diverters. One test in Tunnel 16S was conducted with a short splitter inlet configuration. The data presented in Fig. 16 show that, at M_∞ = 1.60, the short splitters gave approximately one- to two-percent higher compressor-face total-pressure recovery than the long splitters. The circumferential and radial distortion, the inlet/engine distortion index, and the turbulence index were about equal for both long and short splitters. The short splitter configuration was tested only at M_∞ = 1.60.

4.4 EFFECTS OF ALTERNATE SIDE PLATES

The inlet throat rake data obtained during the Tunnel 16S entry indicated that there was significant shock wave/ boundary-layer interaction at the entrance to the inlet. This was caused by a large boundary-layer buildup along the fuselage and the external normal shock impinging on this boundary layer. For the subsequent Tunnel 16T entry of the test, the side plates on the left- and right-hand inlets were modified to accept two different extensions. The purpose of these modified side plates was to attempt to provide normal shock

impingement in a region free from the fuselage boundary layer. The throat-rake contours shown in Figs. 17 and 18 indicate that at $M_\infty = 1.50$ the basic side plate actually gave slightly better pressure recovery at the inlet throat than alternate side plate 2.

The throat rake contour plots presented in Fig. 19 indicate that at $M_\infty = 0.85$ and cruise attitude of $\alpha = 5$, $\beta = 0$, both of the alternate side plates produced a slight improvement in the pressure recovery at the inlet throat. However, the data presented in Fig. 20 show that at $M_\infty = 0.85$ and model attitude of $\alpha = 10$, $\beta = 0$, there was essentially no improvement gained from the alternate side plates.

The data presented in Figs. 21 through 24 show the right-hand compressor-face recovery and distortion values corresponding to the data shown in the throat rake contours in Figs. 17 through 20. The data obtained at $M_\infty = 1.50$ show that alternate side plate 2 gave slightly lower inlet/engine distortion index than the basic side plate; however, recovery was decreased by about two percent (see Figs. 21 and 22). At $M_\infty = 0.85$ the installation of the alternate side plates resulted in very little change in recovery and distortion (Figs. 23 and 24).

4.5 EFFECTS OF VORTEX GENERATORS

For the Tunnel 16T portion of the test, vortex generators were installed at various locations within the left-hand duct. There were three different vortex generator (V.G.) patterns tested. The purpose of testing with these vortex generators was to attempt to decrease the compressor-face distortion and improve the inlet/engine distortion index. The data presented in Fig. 25a at $\alpha = 5$ deg indicate that V.G. pattern 1 decreased circumferential distortion and improved the inlet/engine distortion index, but it also decreased compressor-face total-pressure recovery approximately two percent; radial distortion and the turbulence index were not changed. Data in Fig. 25b show that at $\alpha = 10$ deg, distortion, turbulence, and inlet/engine distortion index were not affected by the addition of V.G. pattern 1, but compressor-face total-pressure recovery was adversely affected by approximately two percent.

Inlet performance with V.G. patterns 2 and 3 compared with the basic inlet configuration is shown in Fig. 26. At Mach number 0.85 and cruise attitude ($\alpha = 5$ deg, $\beta = 0$ deg), the data show that V.G. pattern 3 resulted in better overall inlet performance than either the basic configuration or V.G. pattern 2. Compared with the basic configuration, V.G. pattern 3 produced approximately 25-percent improvement in circumferential distortion and about 13-percent improvement in inlet/engine distortion index. However, at $\alpha = 10$ deg (Fig. 26b) distortion, turbulence, and inlet/engine distortion index were not affected by the V.G. patterns, and recovery was slightly better for the basic configuration. Similar results were also obtained at Mach number 1.40 (see Fig. 27).

4.6 EFFECT OF THE HIGH-PRESSURE AIR DUCT BOUNDARY-LAYER BLOWING SYSTEM

For the last test in Tunnel 16T, a high-pressure air duct boundary-layer blowing system was installed in the right-hand duct. This installation consisted of small air jets installed through the wall of the inlet, with the opening of the jets pointed downstream and located 0.1 in. from the duct wall. One group of these jets was installed on the outboard side of and about halfway down the inlet, and the other group of jets was located on the inboard side of and near the throat of the inlet. The purpose of testing with this boundary-layer blowing system was an attempt to improve the compressor-face distortion and the inlet/engine distortion index. Various combinations of inboard and outboard blowing were tested. The steady-state compressor-face contour plots presented in Fig. 28 show that at Mach number 0.85 and cruise attitude of α = 5 deg and β = 0 deg, the greatest improvement in circumferential and radial distortions and inlet/engine distortion index occurred with the outboard jets blowing (see Fig. 28a) at a mass-flow rate of approximately 0.023 lbm/sec, compared with the model-scale inlet airflow of about 20.5 lbm/sec. The circumferential distortion decreased by 50 percent, and the inlet/engine distortion index improved by 22 percent. The outboard blowing actually produced about 97 percent of the total improvement in inlet/engine distortion index, whereas the inboard boundary-layer jets made no significant contribution. The data presented in Fig. 28b show that at α = 10 deg and β = 0 deg, the duct boundary-layer blowing system produced no significant improvements in distortion or inlet/engine distortion index.

At Mach number 1.40, notable improvements in circumferential distortion and inlet/engine distortion index were obtained with the use of the duct boundary-layer blowing system (Fig. 29). At α = 5 deg and β = 0 deg, circumferential distortion decreased by 28 percent and inlet/engine distortion index decreased by 13 percent. At α = 10 deg and β = 0 deg, circumferential and radial distortions decreased by 6 percent and 10 percent, respectively, and inlet/engine distortion index improved by about 7 percent. These inlet performance improvements resulted from operating both the inboard and outboard boundary-layer jets at a mass-flow rate of approximately 0.025 lbm/sec, compared with the model-scale inlet airflow of 19.7 lbm/sec.

In summary, the data indicate that the duct boundary-layer blowing system improved the compressor-face distortion and the inlet/engine distortion index. In addition, this type of system would apparently require engine bleed air on the order of 0.1 percent of total inlet airflow.

5.0 SUMMARY OF RESULTS

An investigation was conducted in Tunnels 16T and 16S of the Propulsion Wind Tunnel Facility on a 1/5.2-scale inlet/forebody model to support continued research in the

field of inlet design. The primary objective of this test program was to evaluate inlet configuration factors which affected inlet performance, such as inlet standoff distance, splitter plate length, side plate geometry, inlet duct vortex generators, and inlet duct boundary-layer blowing system. The basic inlet configuration consisted of the long splitter with the triangular-shaped side plate and with the inlet located at buttock line 43.82 in. (full scale). Data were obtained at free-stream Mach numbers from 0.55 to 2.0 at angles of attack and sideslip from -2.5 to 13 deg and ±4 deg, respectively. The significant test results are as follows:

1. For the basic inlet configuration, compressor-face total-pressure recovery at 5-deg angle of attack and for design engine airflow decreased linearly from 0.97 at Mach numbers 0.55 to 0.95 at Mach number 1.4 and was slightly better than normal-shock recovery from Mach number 1.5 (1 percent) to Mach number 2.0 (6 percent).

2. For supersonic Mach numbers in the range from 1.5 to 2.0, inlet total-pressure recovery for the basic inlet configuration (at design engine airflow) generally increased with increasing angle of attack as a result of the wing glove serving as a compression surface for the flow approaching the inlet. As angle of attack was increased from 5 to 13 deg at Mach number 1.8, this characteristic resulted in a 9-percent increase in recovery.

3. Angle-of-sideslip effects on inlet total-pressure recovery for the basic inlet configuration were more detrimental at supersonic Mach numbers than at subsonic Mach numbers. At Mach number 0.85 and for design engine airflow, recovery decreased 1.2 percent from 0- to 4-deg sideslip angle (inlet shielded by fuselage) at 5-deg angle of attack. At Mach number 1.8, recovery decreased 2.9 percent.

4. At Mach numbers 1.8 and 2.0 and for design engine airflow, the basic inlet configuration operated close to the buzz limit. In particular, at Mach number 2.0 and for an angle of attack of -2.4 deg, the inlet operated essentially at the buzz limit.

5. The predominant effect of increasing the inlet standoff distance was to decrease the inlet/engine distortion index. The inlet/engine distortion index decreased approximately 15 percent (at design engine airflow) as a result of moving the inlet outboard 1.8 in. (full scale) in the Mach number range from 0.55 to 1.5 at 5-deg angle of attack.

6. Inlet total-pressure recovery (at design engine airflow) for the short splitter configuration was from 1 to 2 percent higher than that for the long splitter at Mach number 1.6. The effect of splitter plate length at other Mach numbers is not known since the short splitter configuration was tested only at Mach number 1.6.

7. Vortex generators installed within the inlet on the outboard and lower walls midway down the duct resulted in decreasing the inlet/engine distortion index at design engine airflow. At Mach number 0.85 and for an angle of attack of 5 deg, the distortion index decreased approximately 13 percent.

8. An inlet duct boundary-layer blowing system decreased the inlet/engine distortion index approximately 22 percent at Mach number 0.85 and 13 percent at Mach number 1.4 at design engine airflow and 5-deg angle of attack. The system required a mass-flow rate on the order of 0.1 percent of the total inlet mass flow.

REFERENCES

1. Test Facilities Handbook (Tenth Edition). "Propulsion Wind Tunnel Facility, Vol. 4." Arnold Engineering Development Center, May 1974.

2. Sanders, M. E. and Christenson, R. J. "Inlet Performance Characteristics of Generalized 1/4-Scale and 1/2.83-Scale Tactical Aircraft Models at Transonic and Supersonic Mach Numbers." AEDC-TR-72-188 (AD906161L), December 1972.

3. Lauer, R. F., Jr. "Inlet Performance Characteristics of Generalized 1/4-Scale Tactical Aircraft Models at Transonic and Supersonic Mach Numbers." AEDC-TR-71-87 (AD515022L), May 1971.

4. Ammann, V. R., Jr. and Johnson, J. R. "Model and Test Information Report 1/5.2-Scale Composite Inlet Model Test in AEDC PWT 16T, 16S." General Dynamics FZT-267, October 1975.

5. Abernethy, R. B. and Thompson, J. W., Jr. "Handbook-Uncertainty in Gas Turbine Measurements." AEDC-TR-73-5 (AD755356), February 1973.

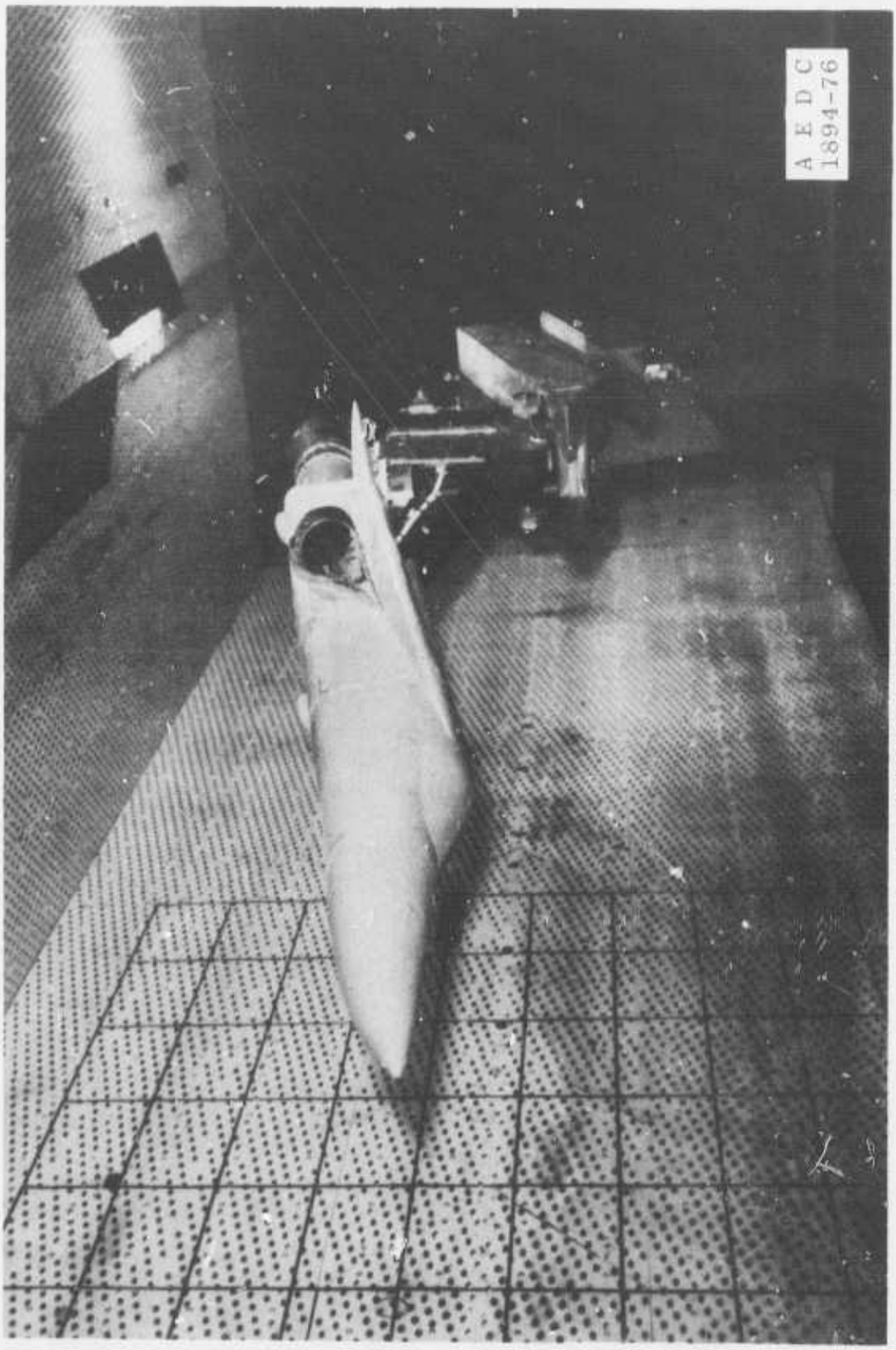

a. Tunnel 16T installation photograph

Figure 1. Model installation.

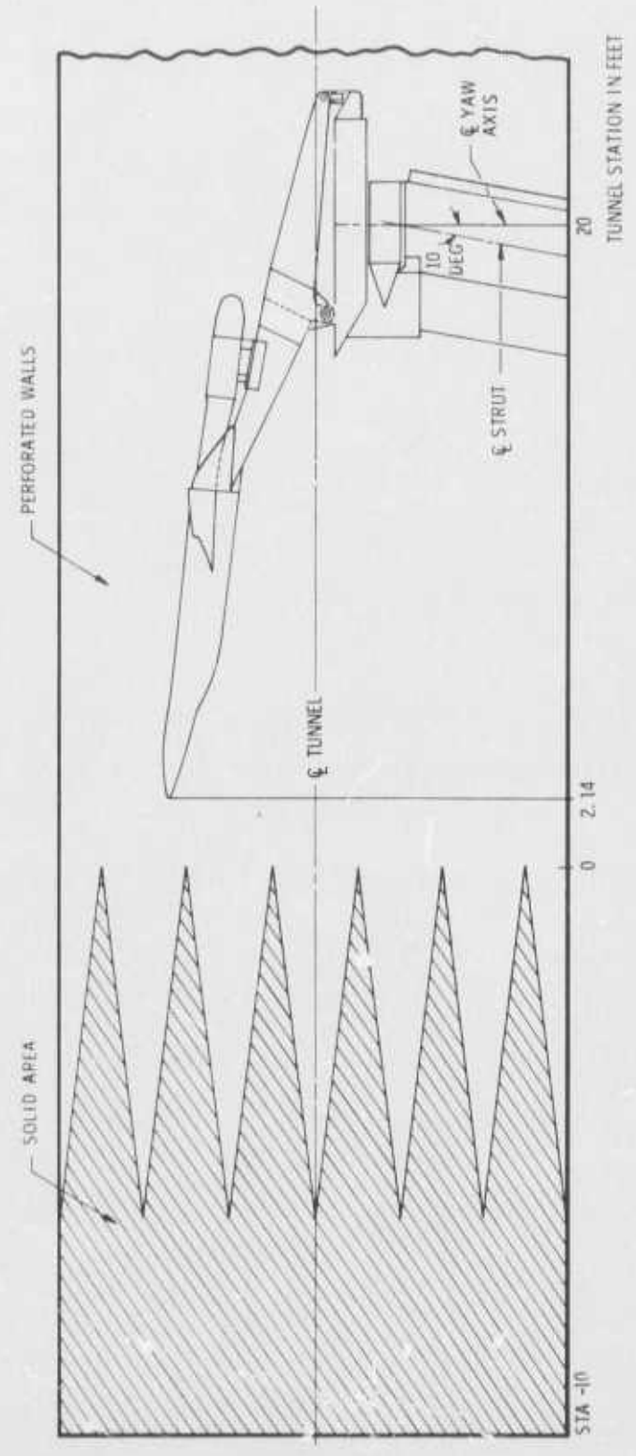

b. Location of the model in Tunnel 16T
Figure 1. Concluded.

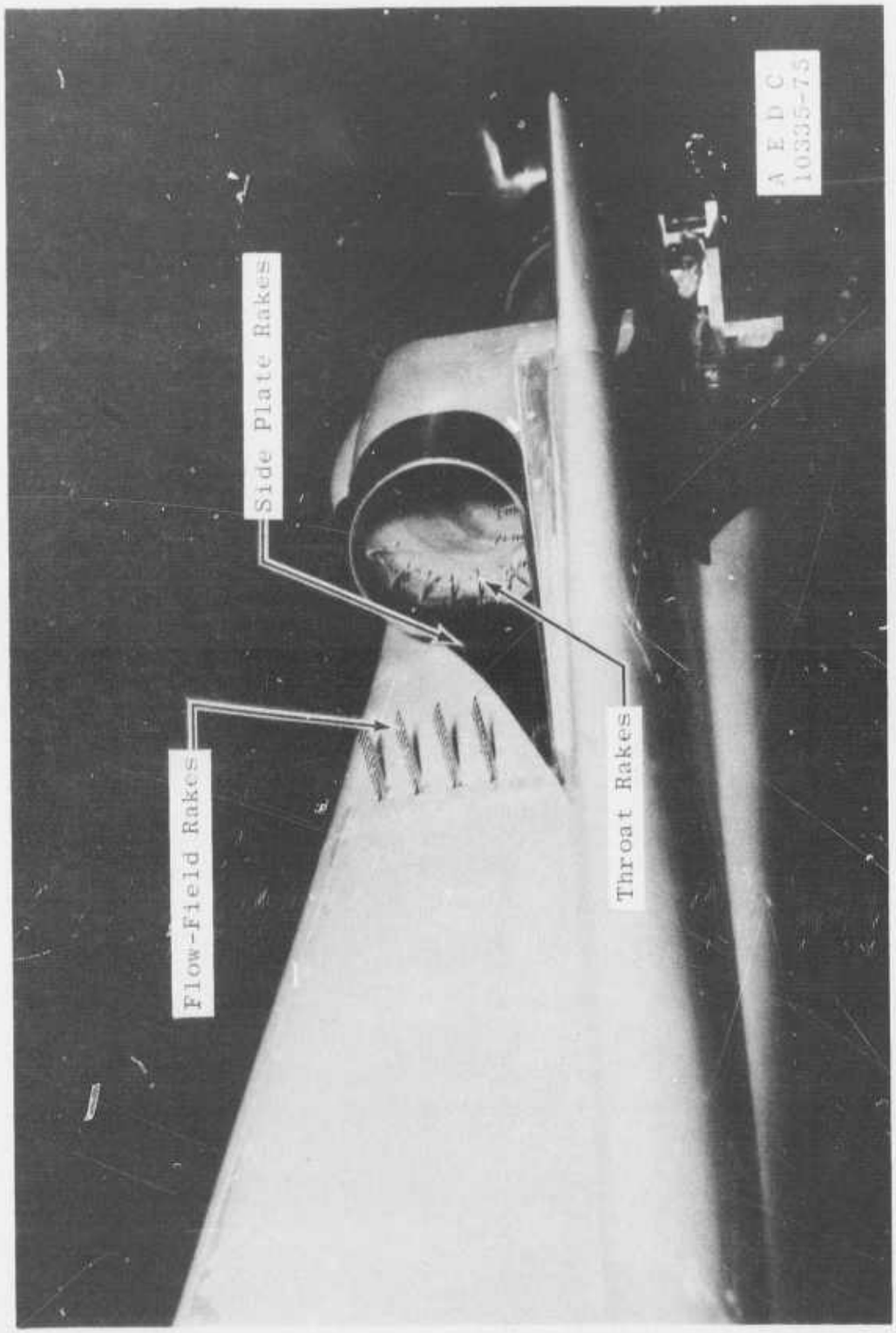

a. Right-hand inlet details

Figure 2. Inlet configuration details.

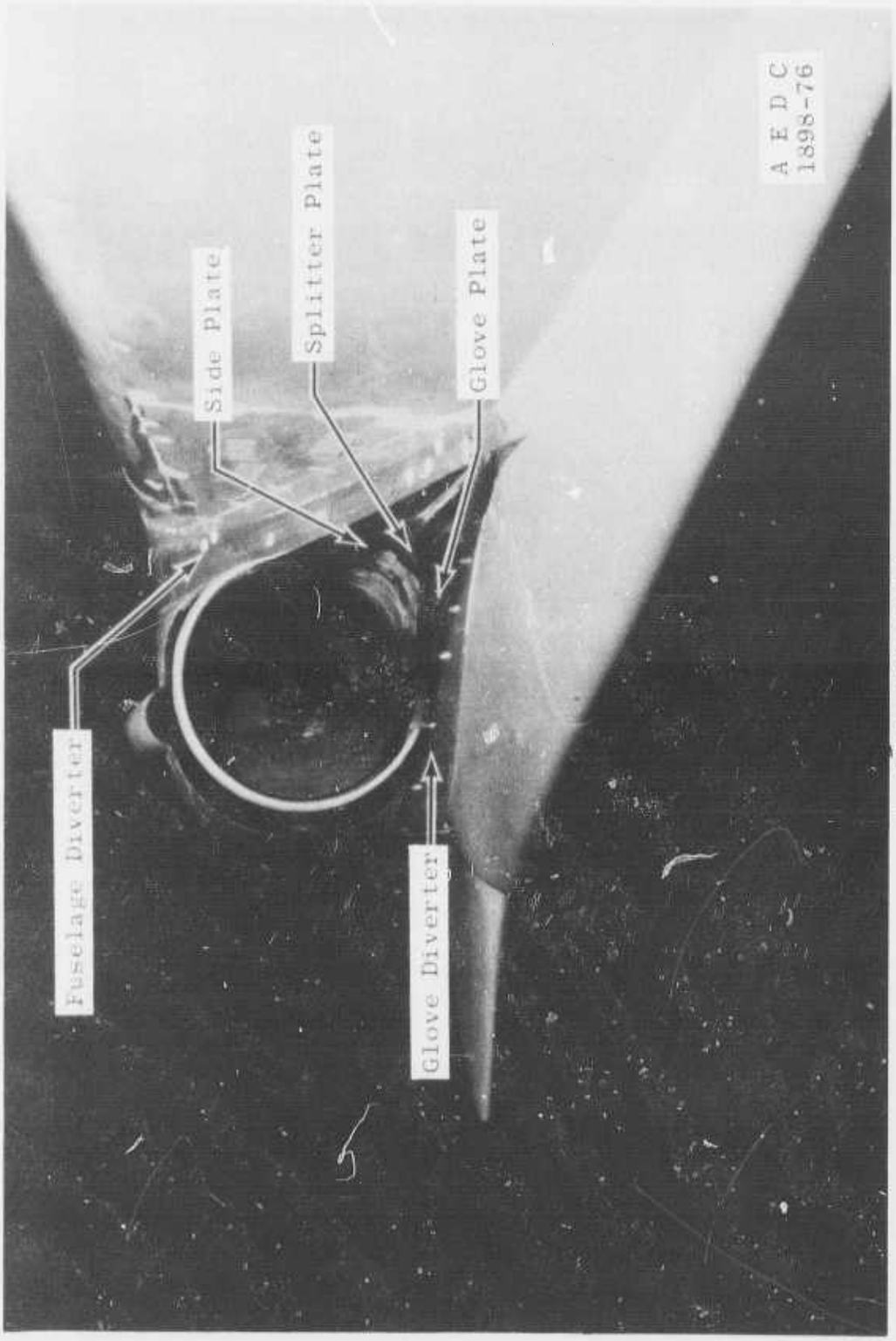

b. Left-hand inlet details
Figure 2. Continued.

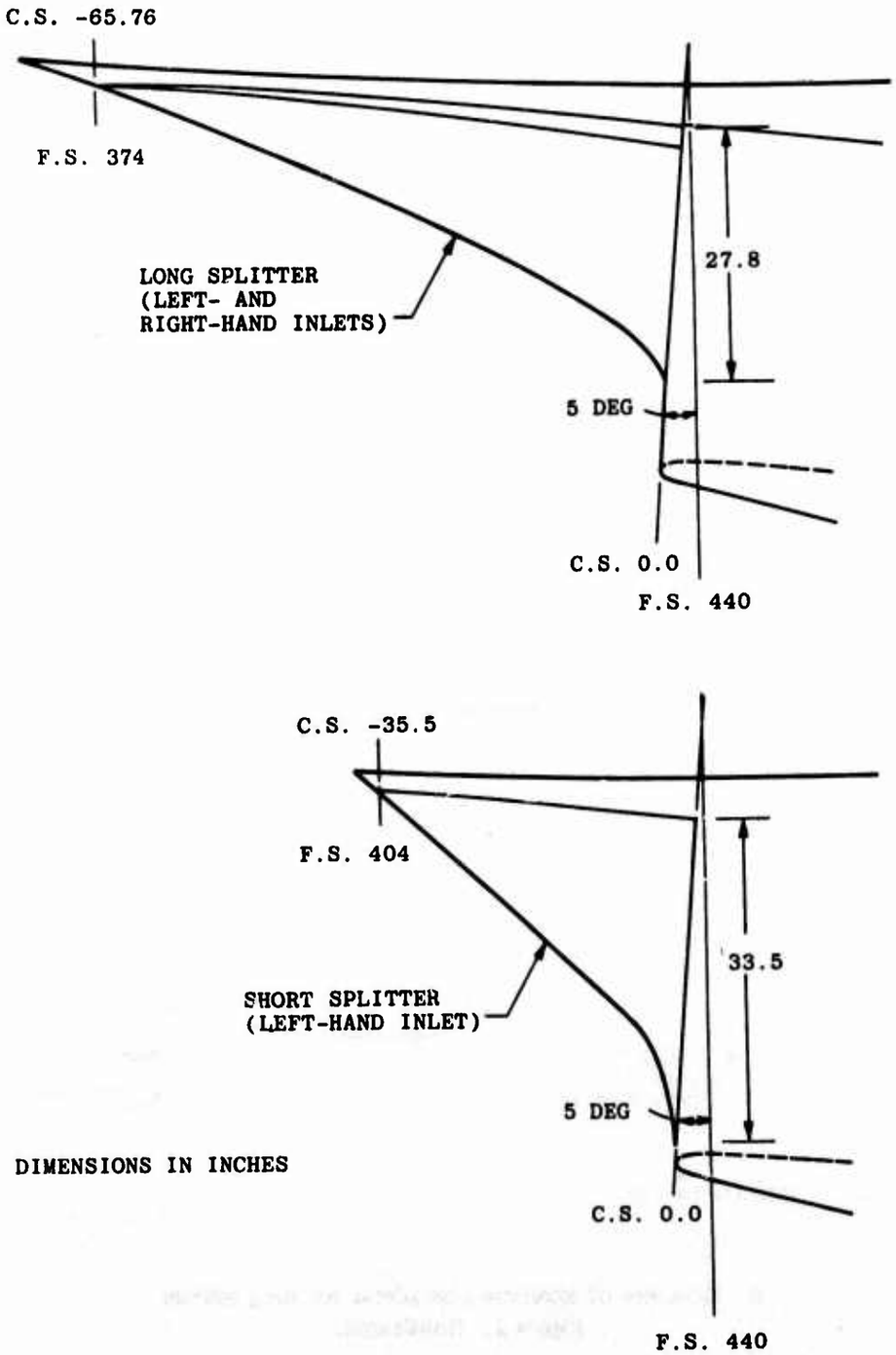

c. Sketches of short and long splitters

Figure 2. Continued.

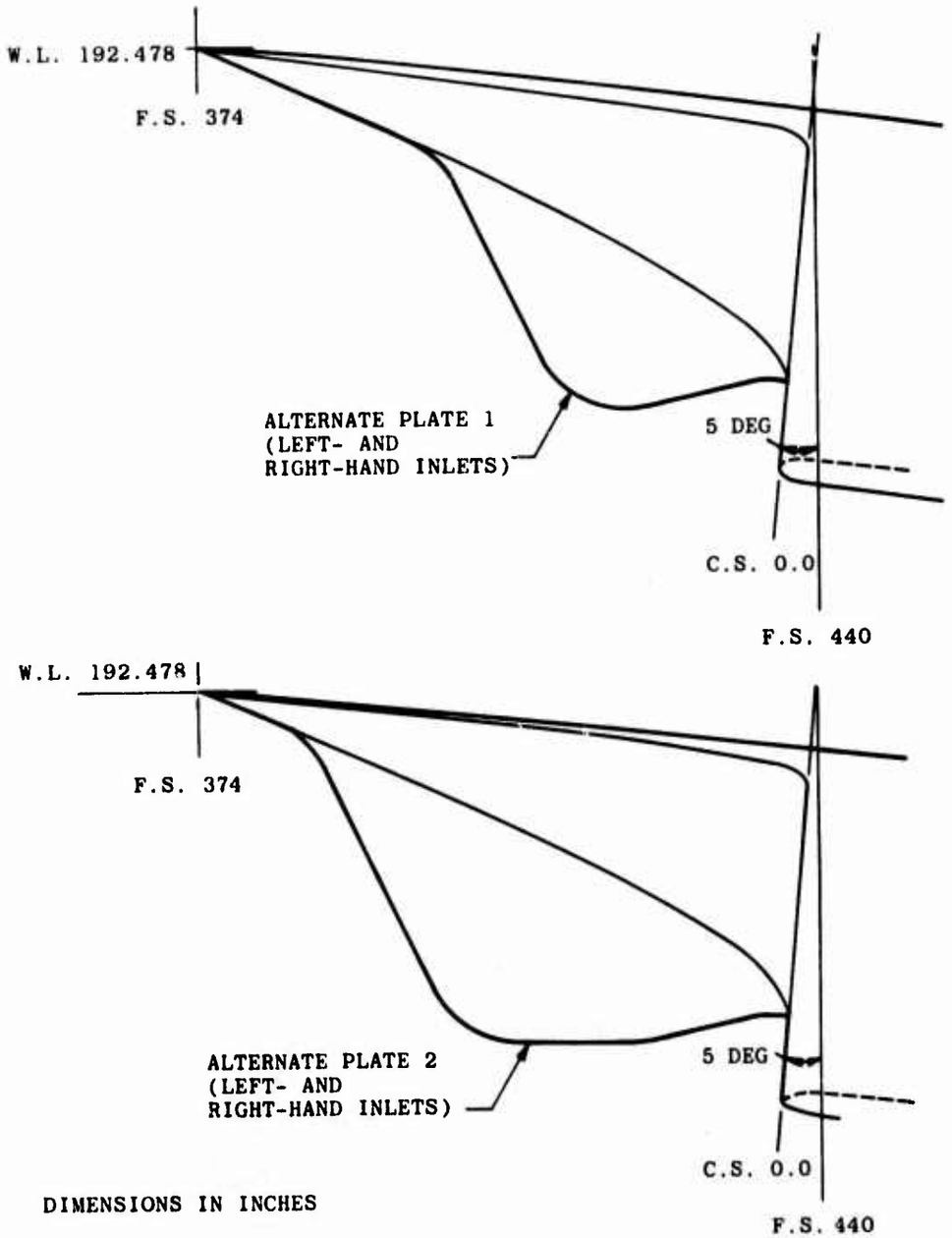

d. Sketches of alternate side plates for long splitter
Figure 2. Continued.

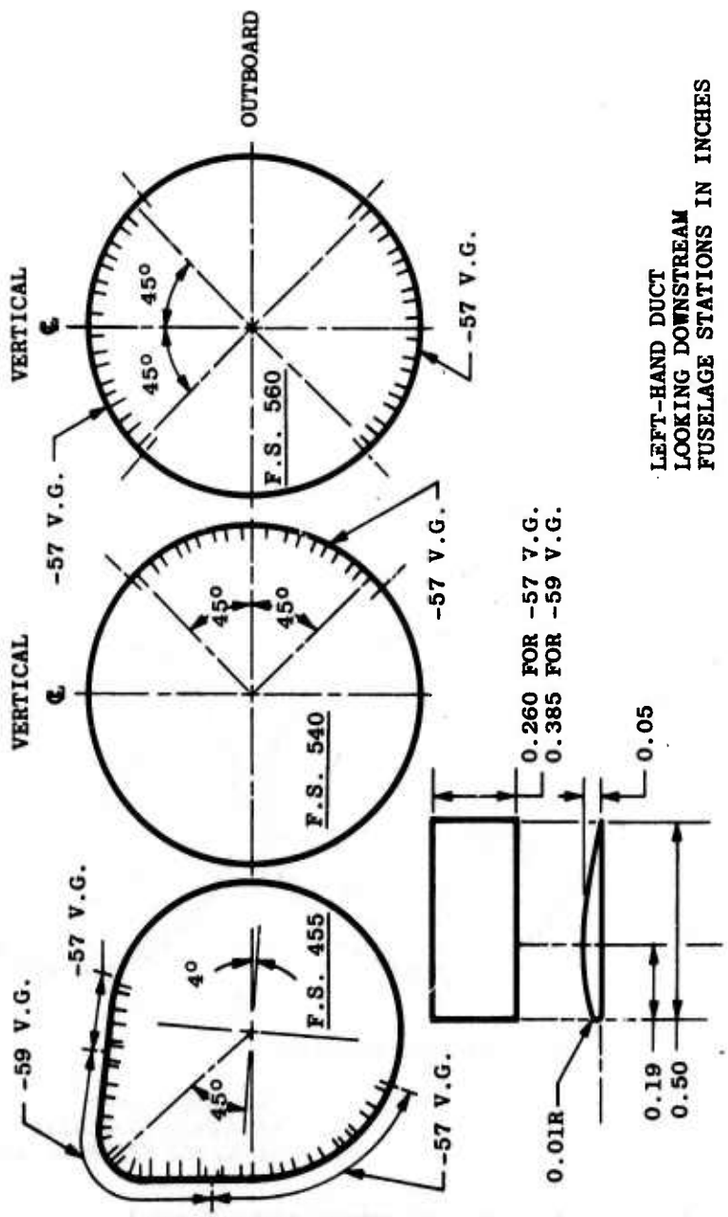

e. Sketch of vortex generator pattern 1

Figure 2. Continued.

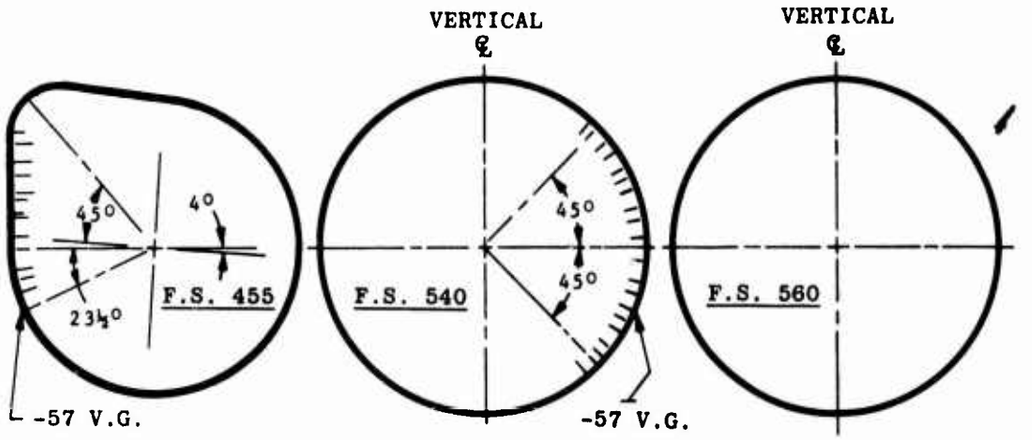

VORTEX GENERATOR PATTERN 2

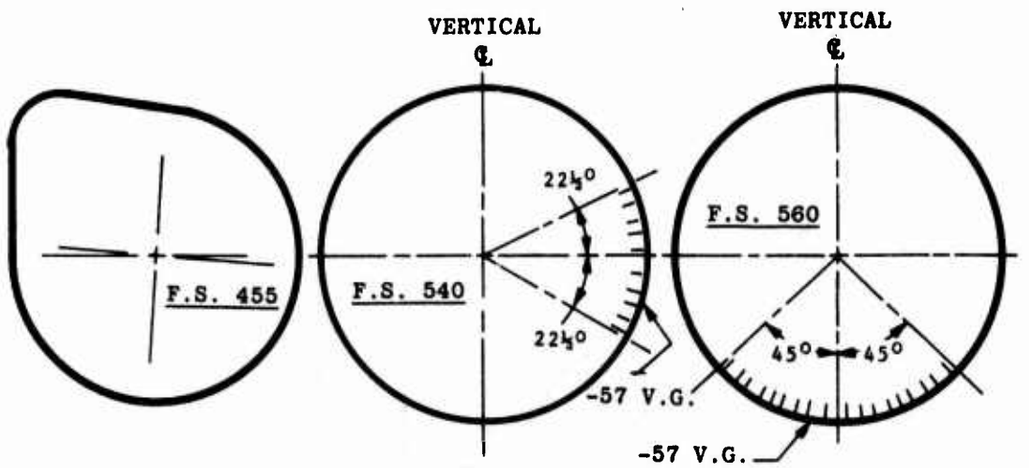

VORTEX GENERATOR PATTERN 3

LEFT-HAND DUCT
LOOKING DOWNSTREAM
FUSELAGE STATIONS IN INCHES

f. Sketch of vortex generator patterns 2 and 3
Figure 2. Concluded.

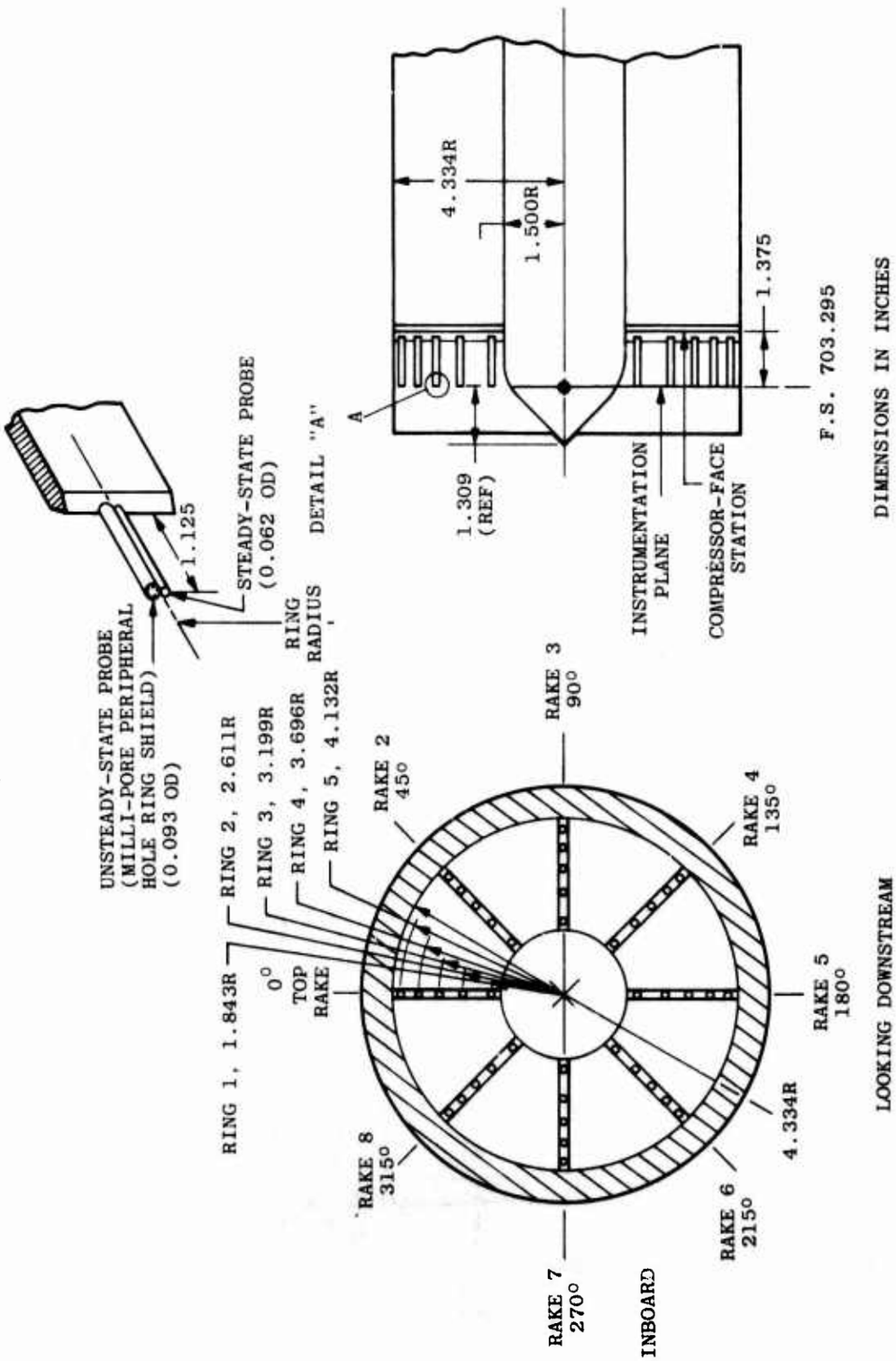

a. Left compressor-face instrumentation
Figure 3. Instrumentation drawings.

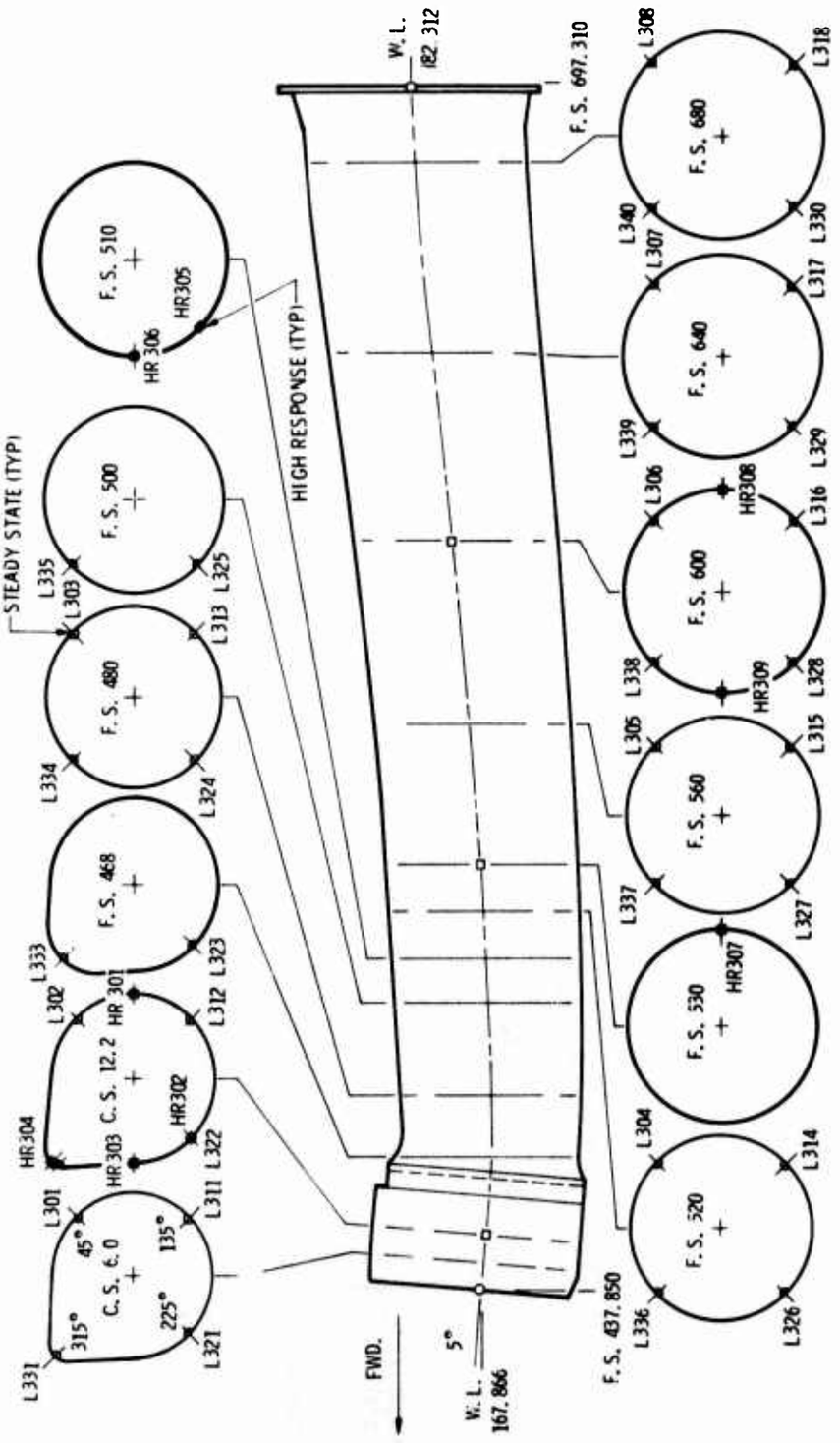

b. Left-hand primary duct instrumentation (view looking inboard)
Figure 3. Continued.

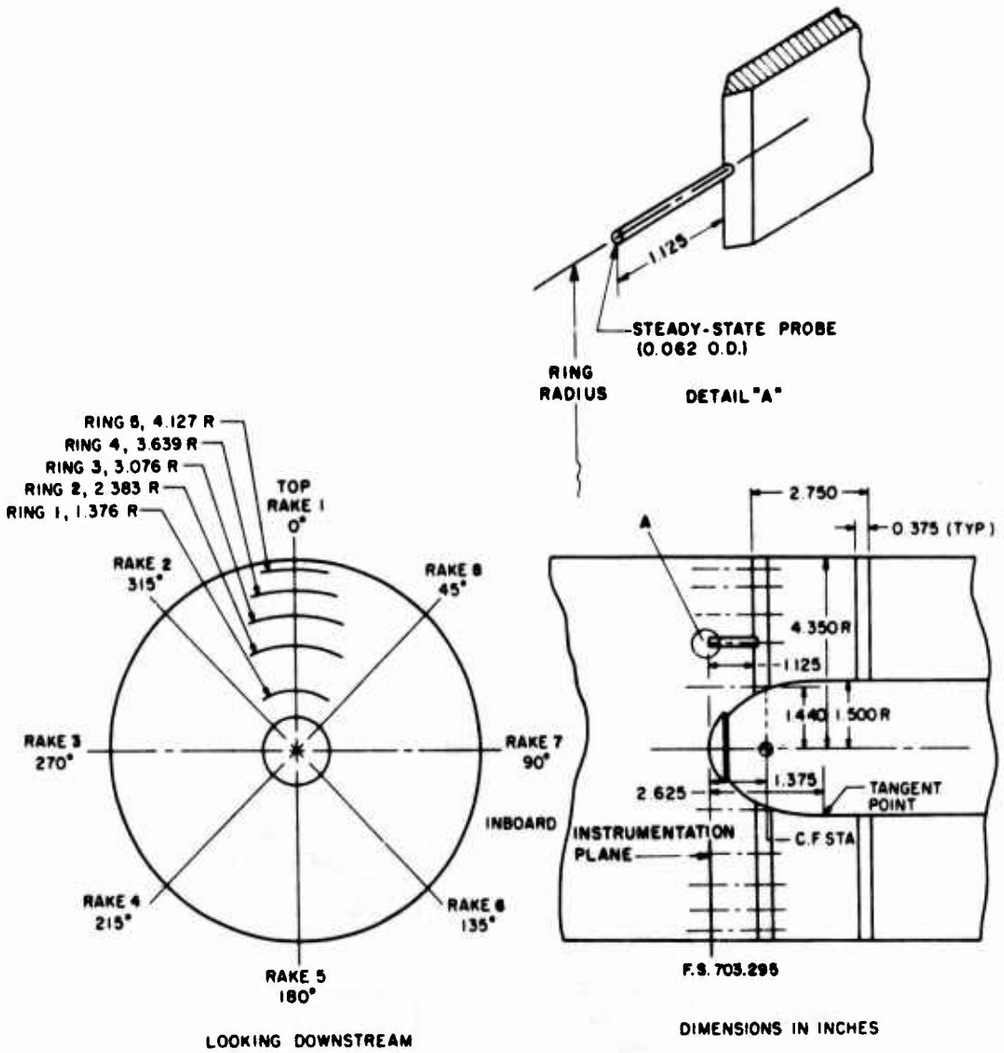

c. Right compressor-face instrumentation
Figure 3. Concluded.

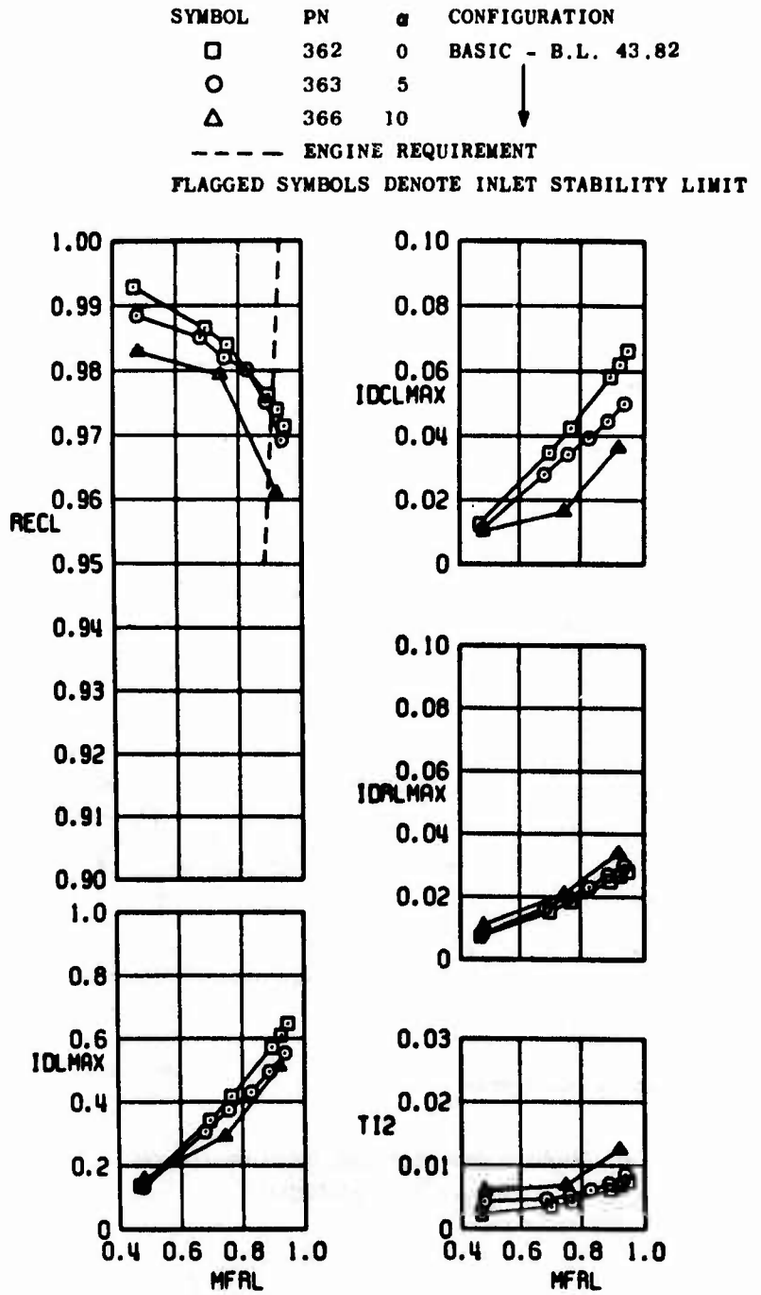

a. $M_\infty = 0.65$

Figure 4. Basic configuration performance as a function of mass-flow ratio, $\beta = 0$ deg.

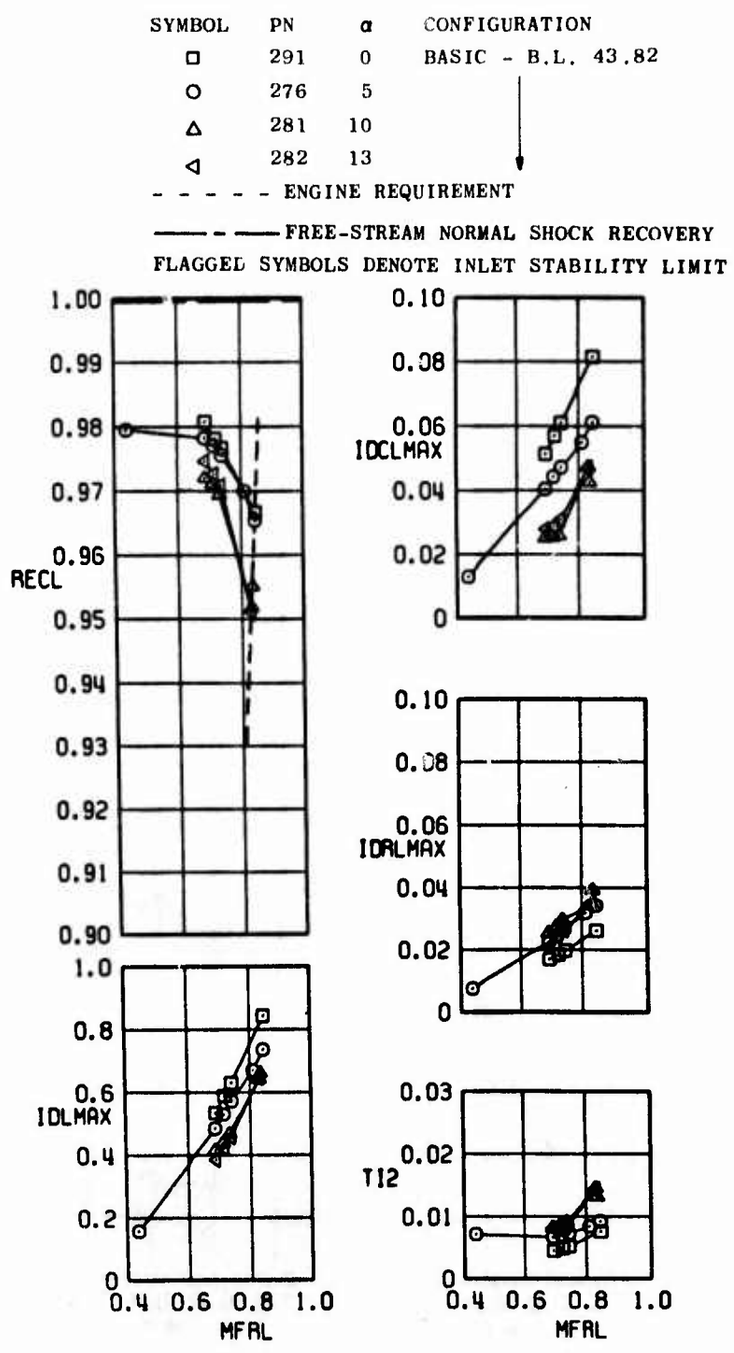

b. $M_\infty = 0.85$

Figure 4. Continued.

SYMBOL	PN	α	CONFIGURATION
□	336	0	BASIC - B.L. 43.82
○	337	5	
△	342	10	
◁	345	13	

- - - - - ENGINE REQUIREMENT

——— - ———FREE-STREAM NORMAL SHOCK RECOVERY

FLAGGED SYMBOLS DENOTE INLET STABILITY LIMIT

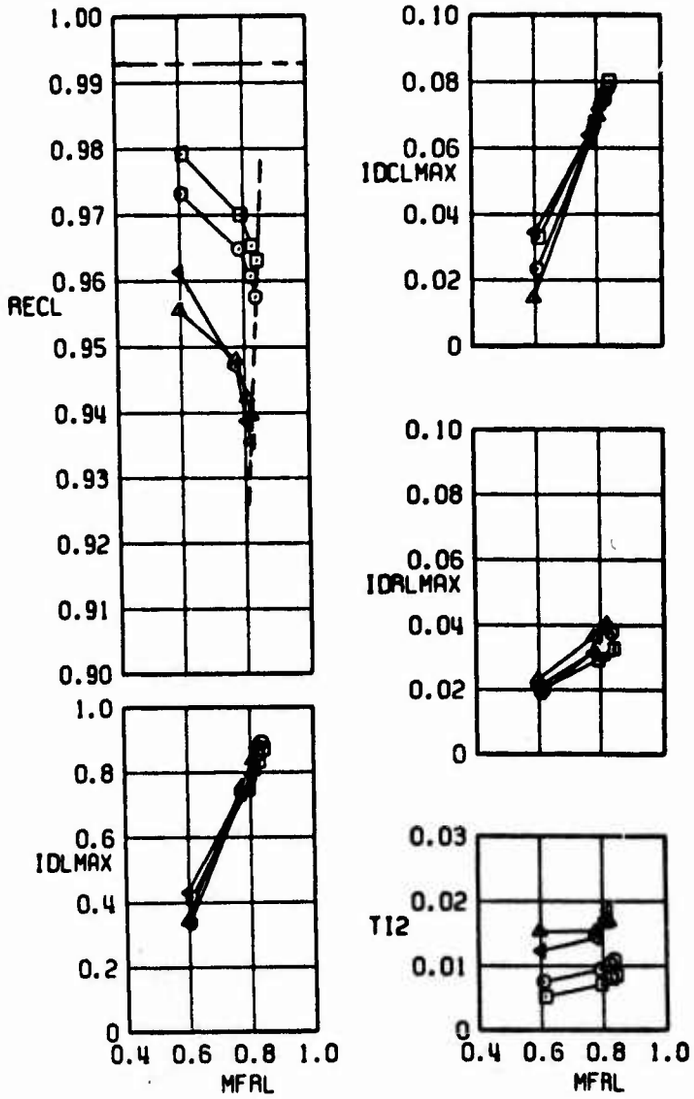

c. $M_\infty = 1.20$

Figure 4. Continued.

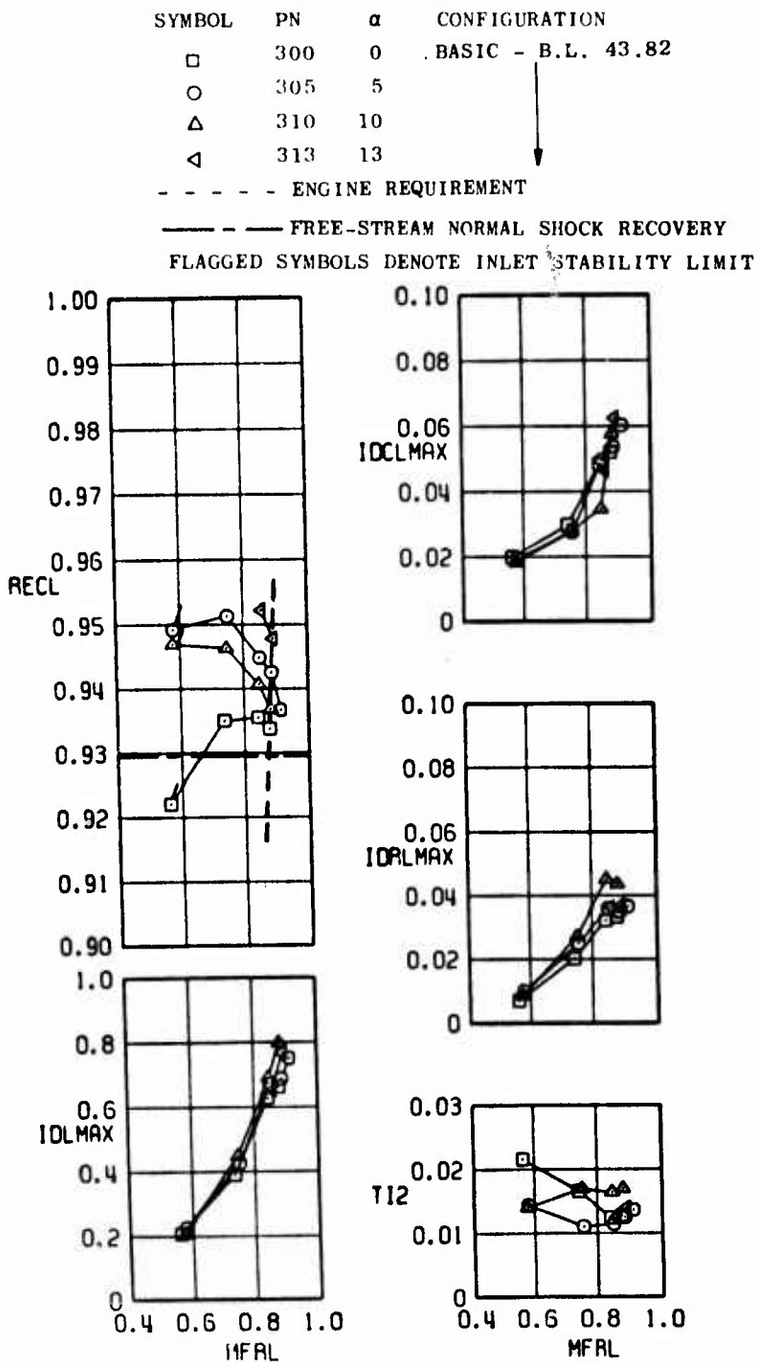

d. $M_\infty = 1.50$

Figure 4. Continued.

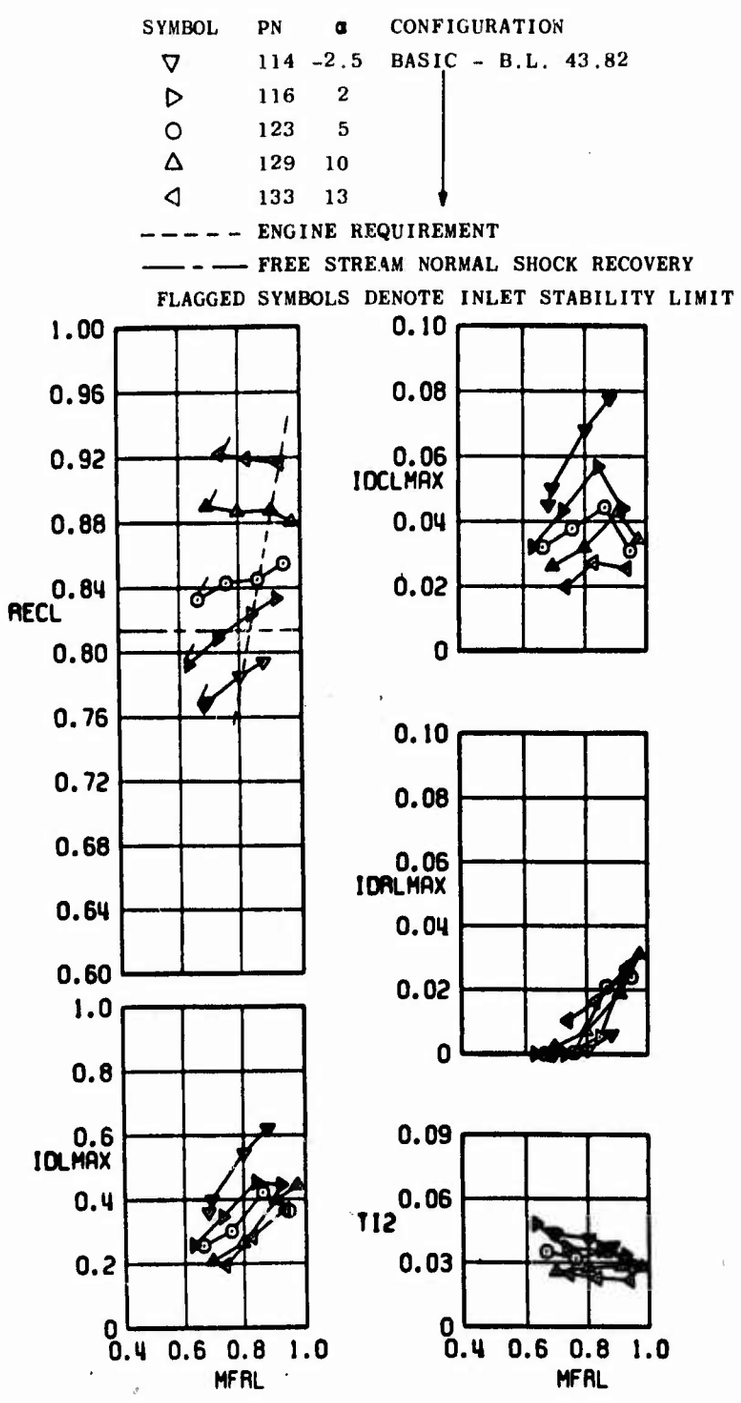

e. $M_\infty = 1.80$

Figure 4. Continued.

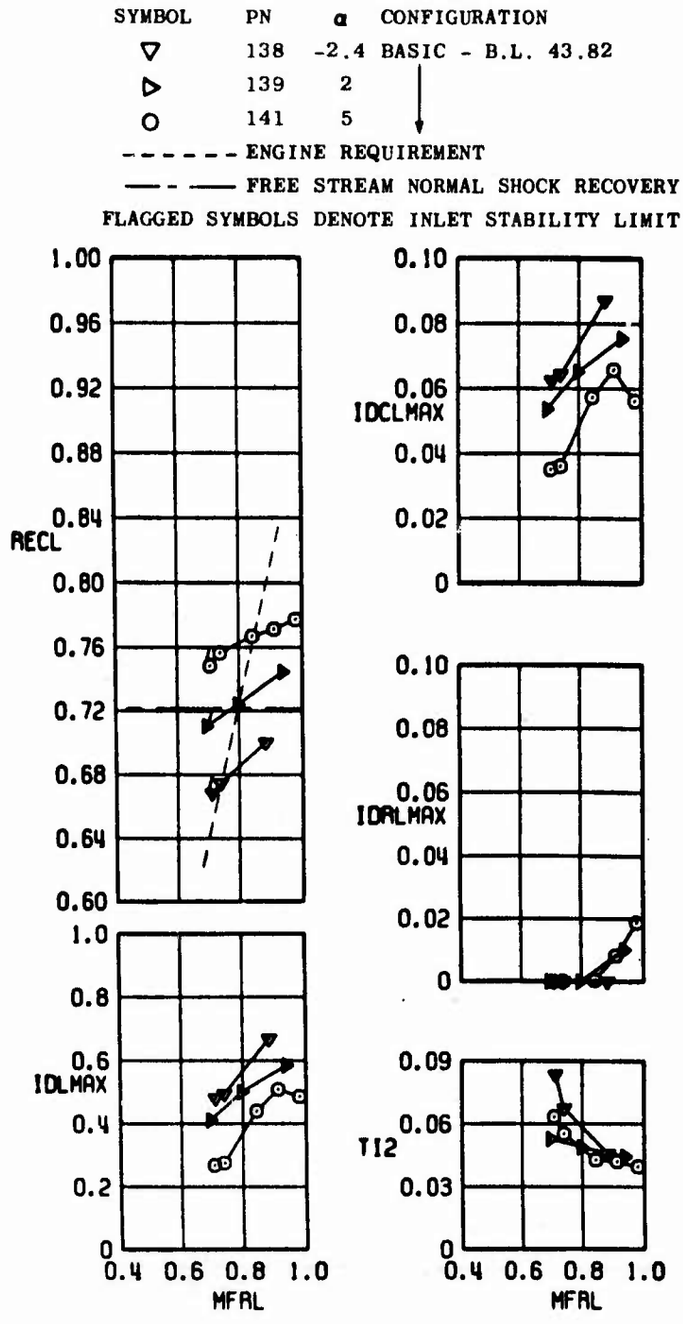

f. $M_\infty = 2.00$

Figure 4. Concluded.

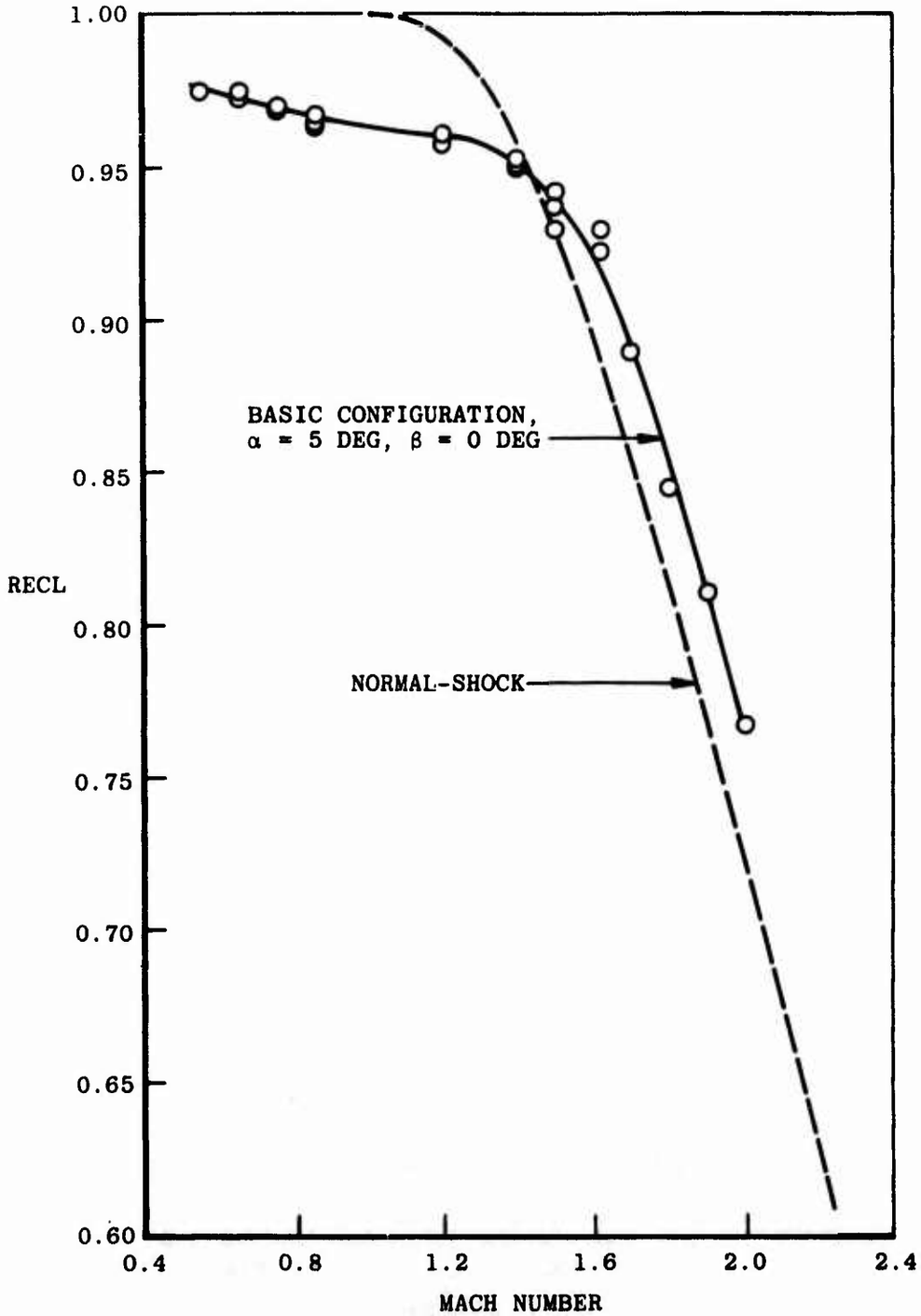

Figure 5. Comparison of basic configuration total-pressure recovery for design engine airflow with normal-shock recovery.

SYMBOL	PN	α	WPLFS	CONFIGURATION
□	362	0	337	BASIC - B.L. 43.82
○	363	5	334	↓
△	366	10	351	

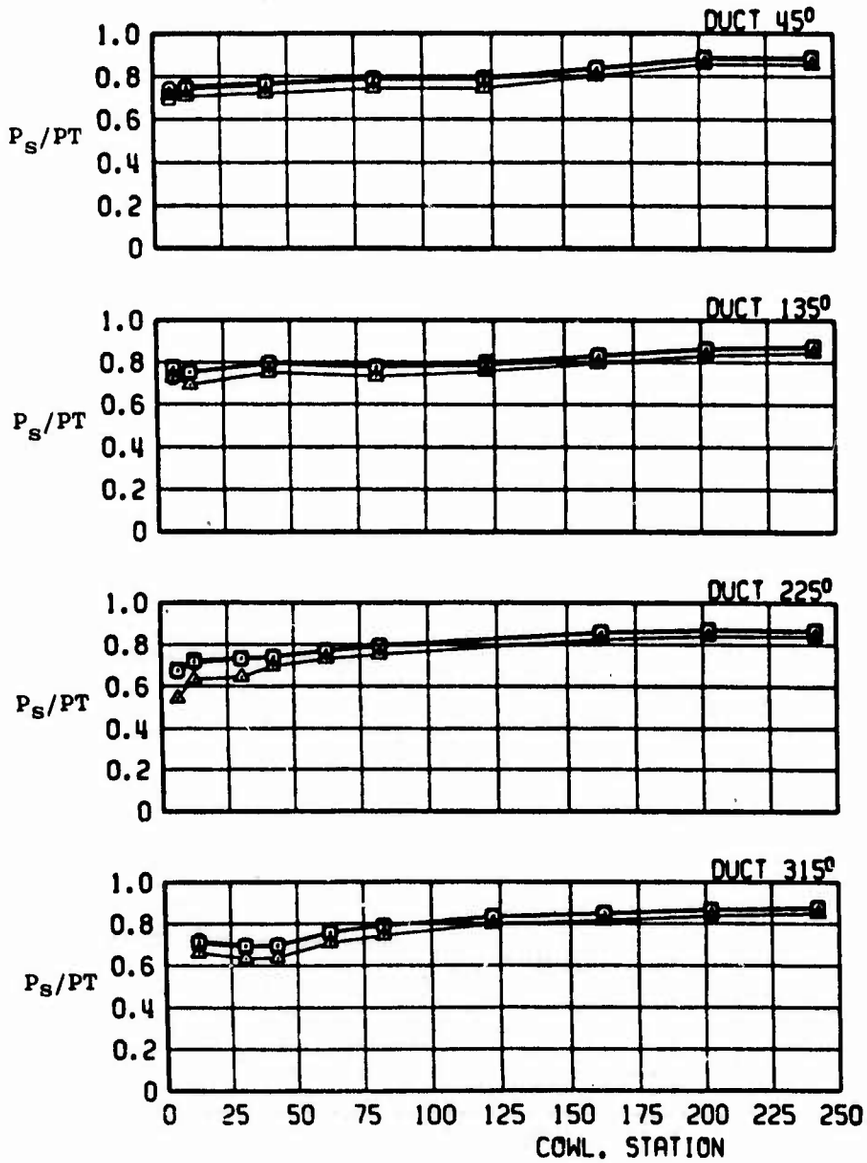

a. $M_\infty = 0.65$

Figure 6. Left-hand duct static-pressure distributions at β = 0 deg.

SYMBOL	PN	α	WPLFS	CONFIGURATION
□	291	0	355	BASIC - B.L. 43.82
○	276	5		
△	281	10		

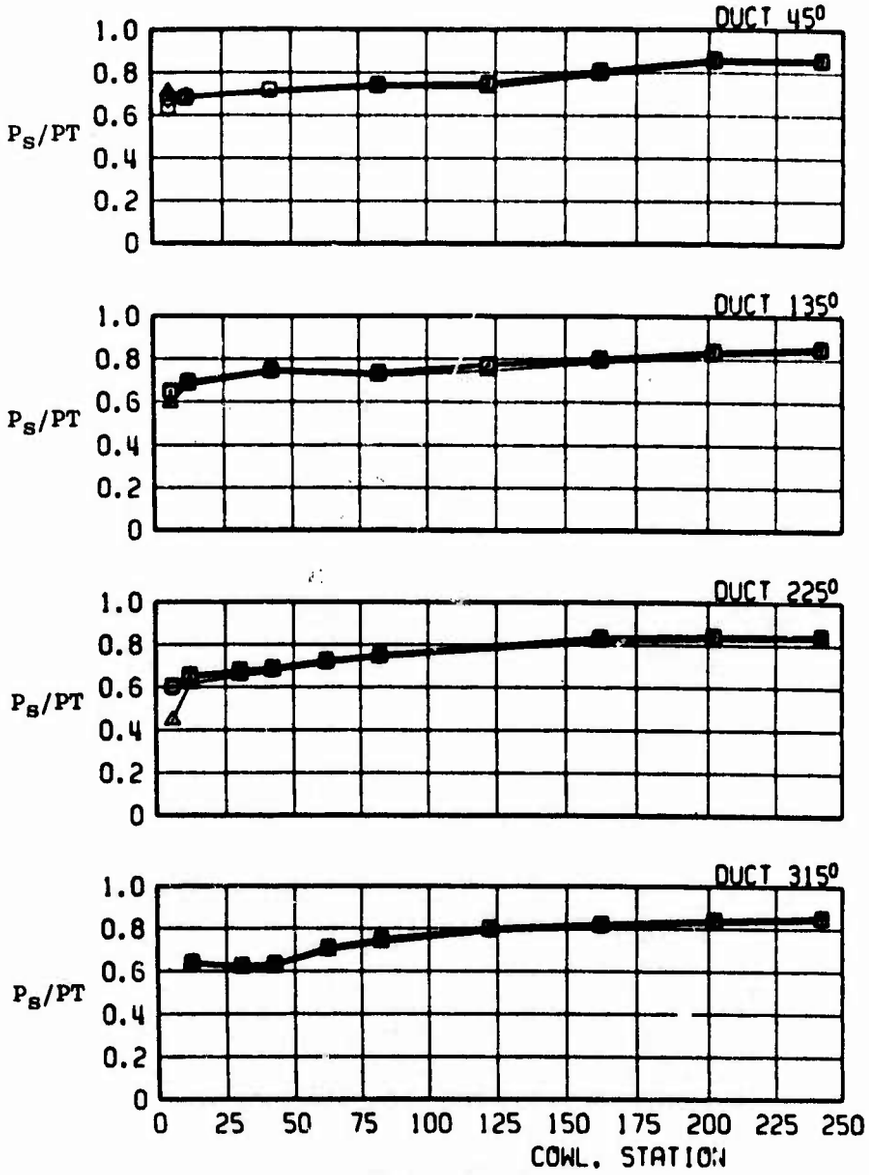

b. $M_\infty = 0.85$

Figure 6. Continued.

SYMBOL	PN	α	WPLFS	CONFIGURATION
□	333	0	353	BASIC - B.L. 43.82
○	337	5	↓	↓
△	342	10		

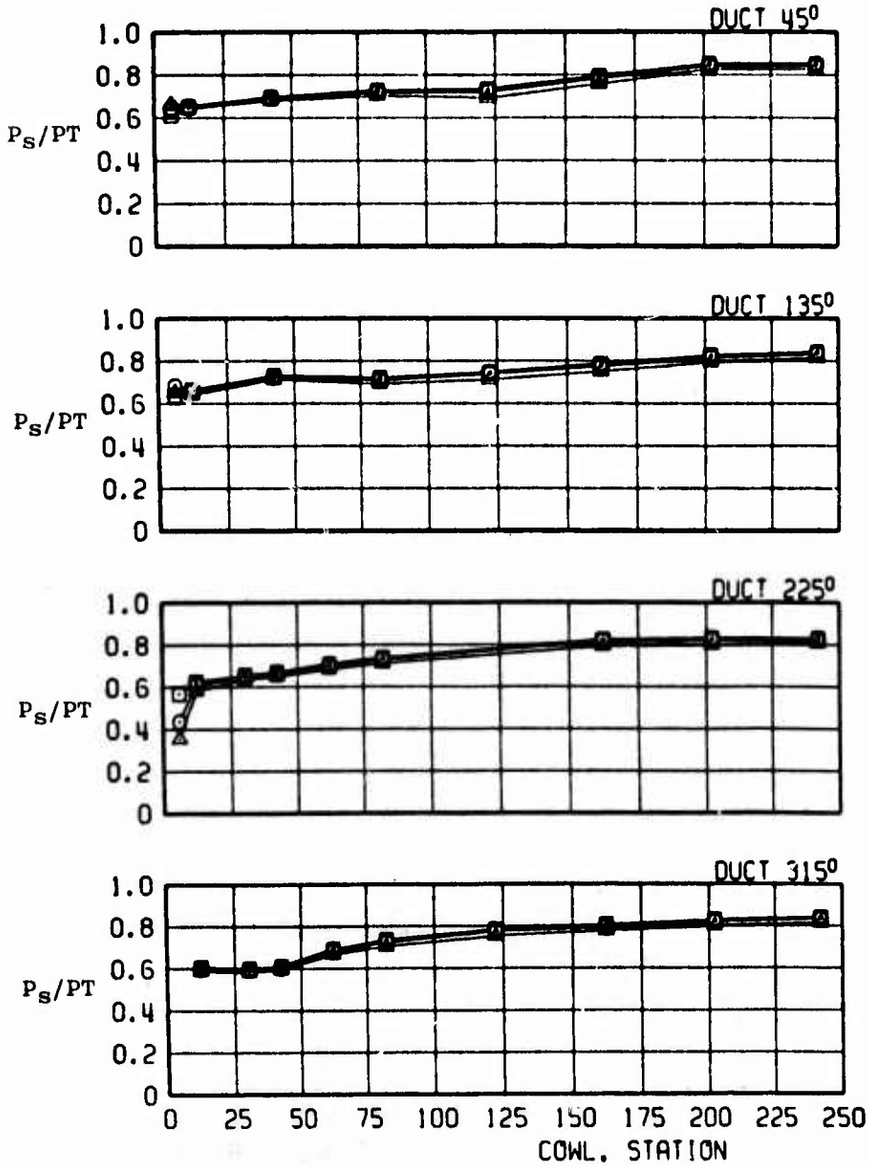

c. $M_\infty = 1.20$

Figure 6. Continued.

SYMBOL	PN	α	WPLFS	CONFIGURATION
□	300	0	333	BASIC - B.L. 43.82
○	305	5	↓	↓
△	310	10		

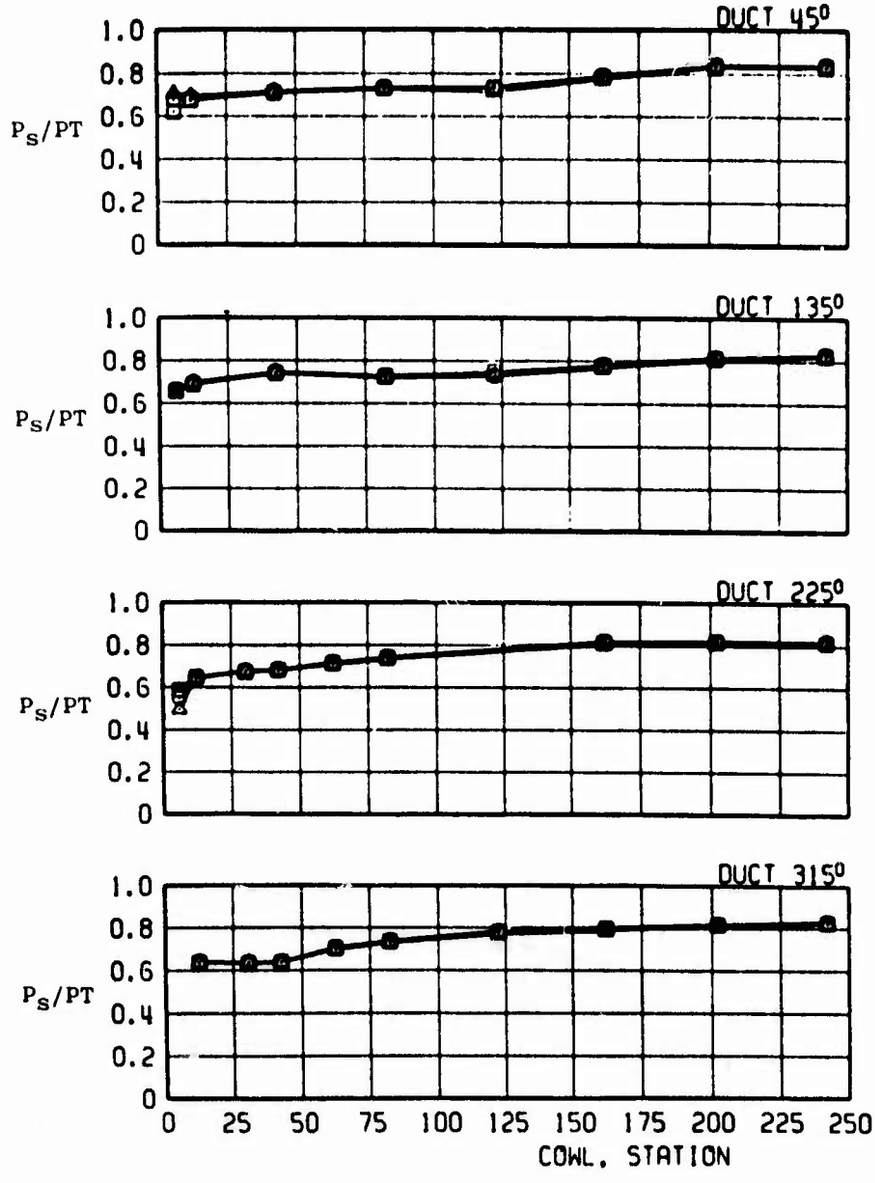

d. M_∞ = 1.50
Figure 6. Continued.

SYMBOL	PN	α	WPLFS	CONFIGURATION
▽	114	-2.5	295	BASIC - B.L. 43.82
○	123	5		
△	129	10		

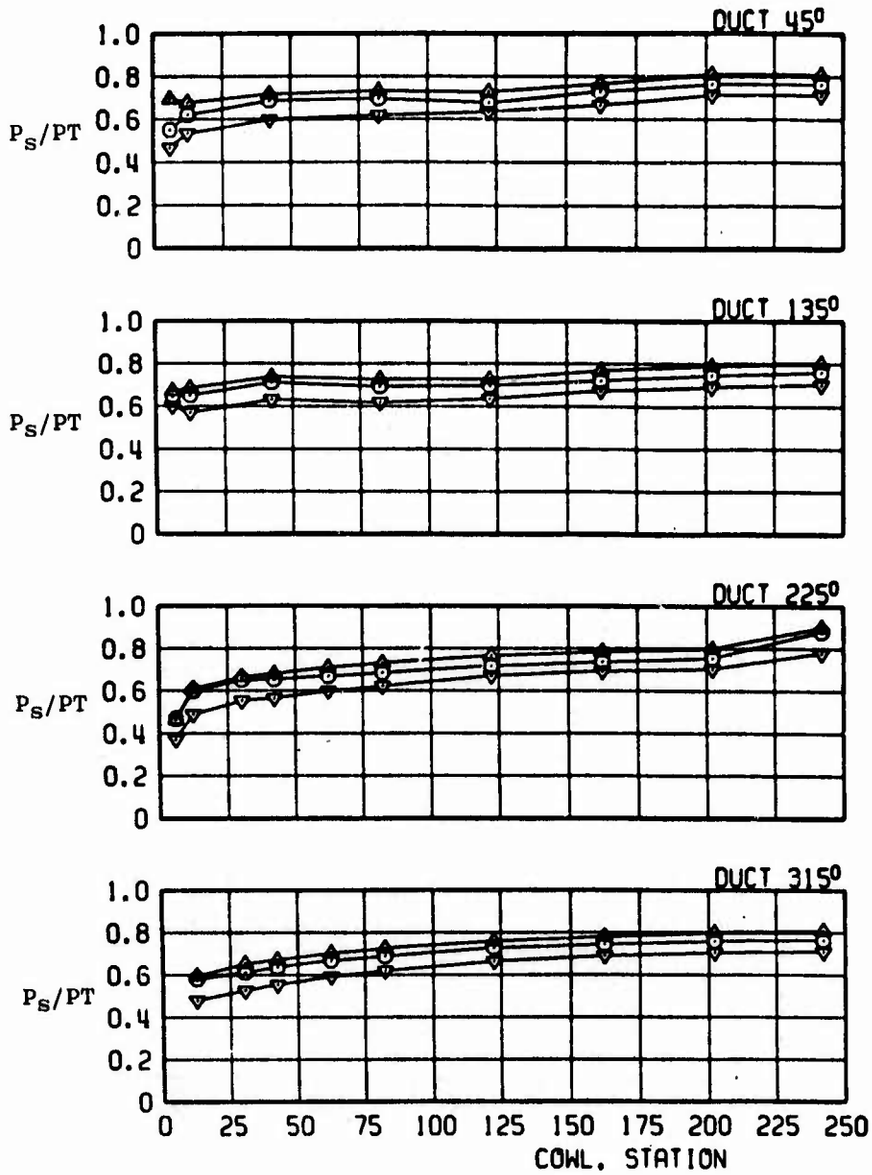

e. $M_\infty = 1.80$

Figure 6. Continued.

SYMBOL	PN	α	WPLFS	CONFIGURATION
▽	138	-2.5	270	BASIC - B.L. 43.82
▷	139	2		
⊙	141	5		

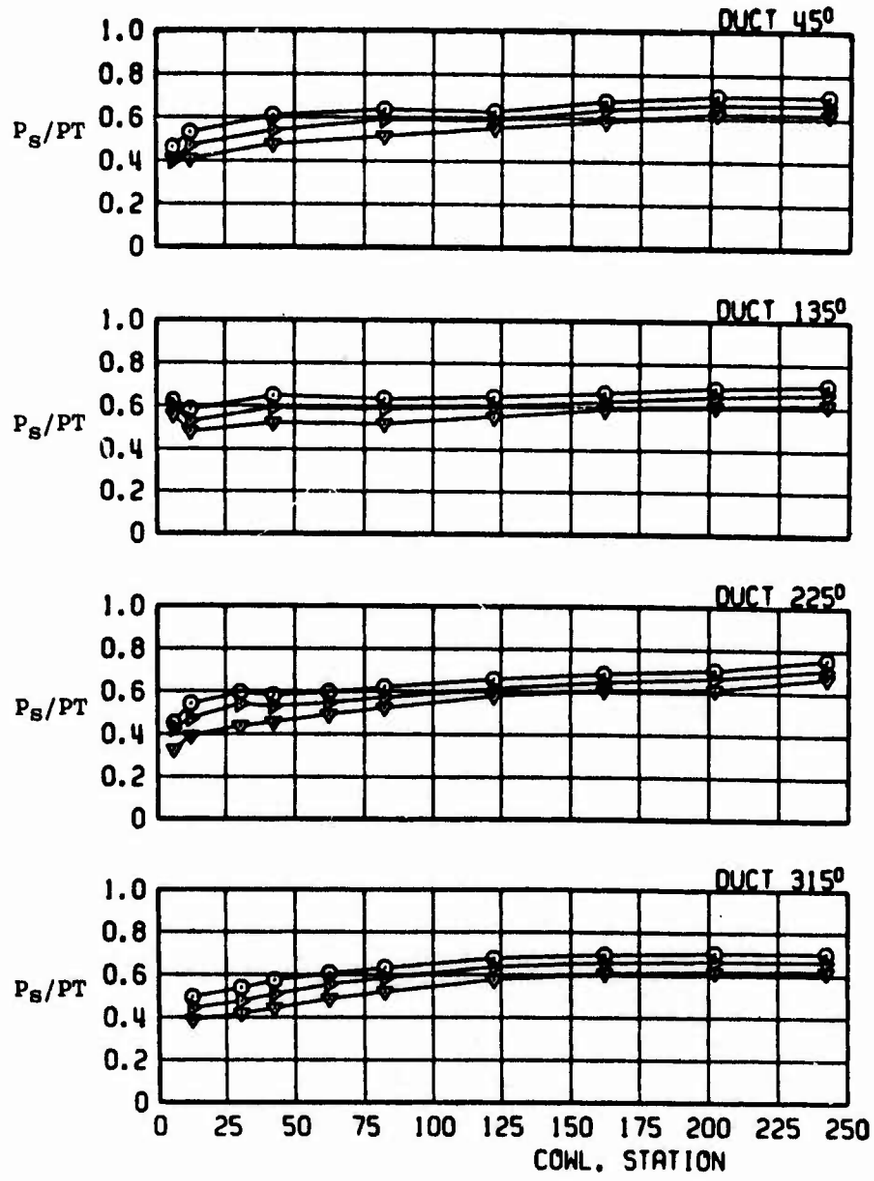

f. $M_\infty = 2.00$

Figure 6. Concluded.

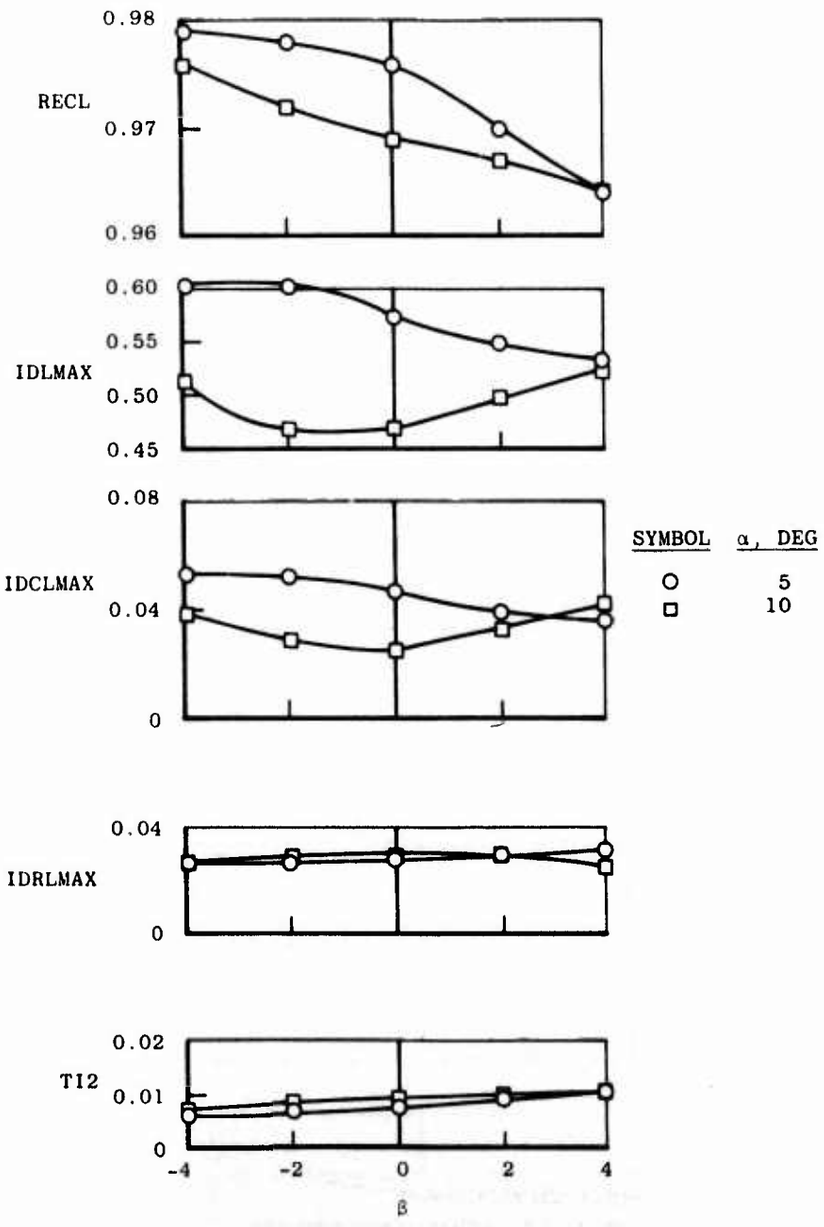

a. $M_\infty = 0.85$

Figure 7. Effect of sideslip angle on basic configuration inlet performance at design engine airflow.

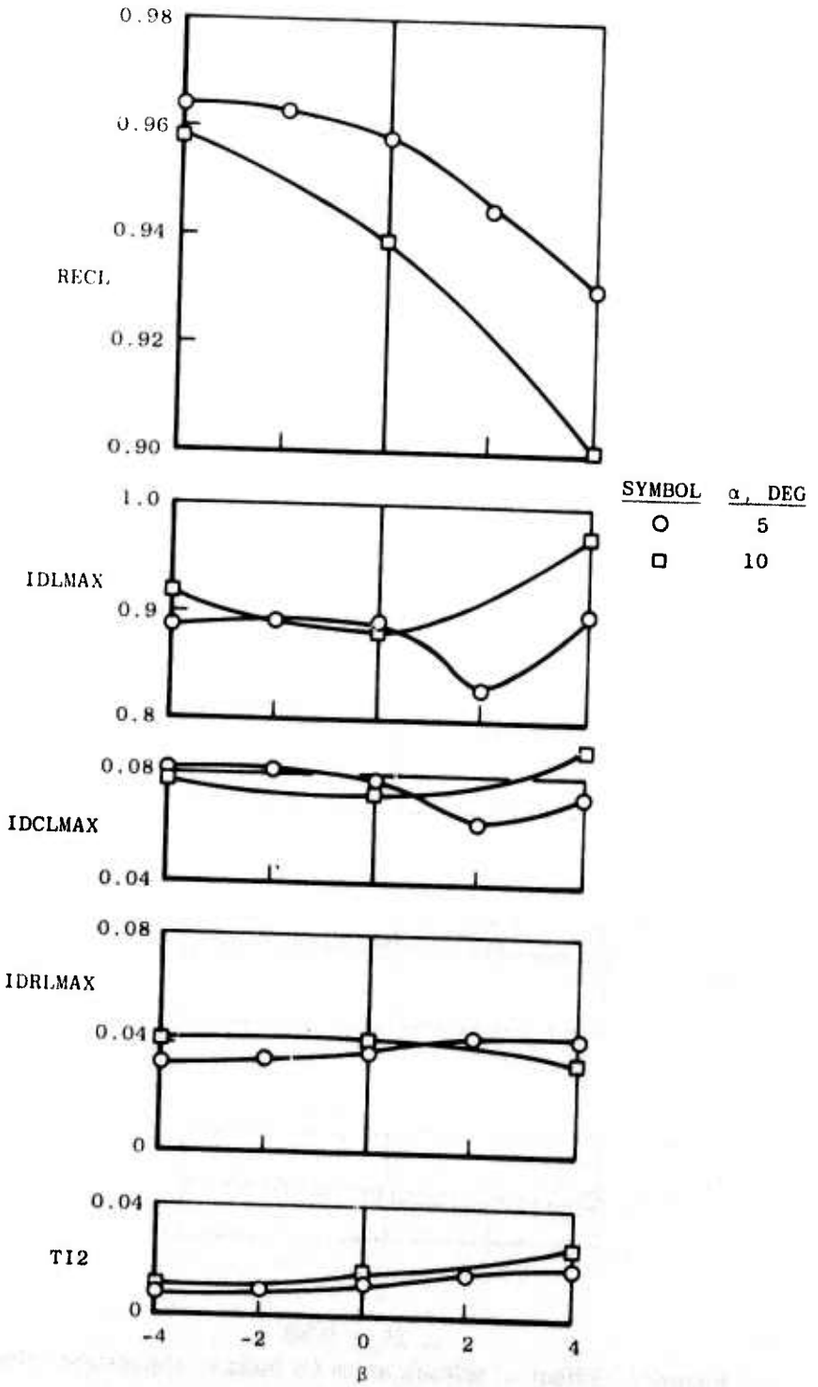

b. M_∞ = 1.20

Figure 7. Continued.

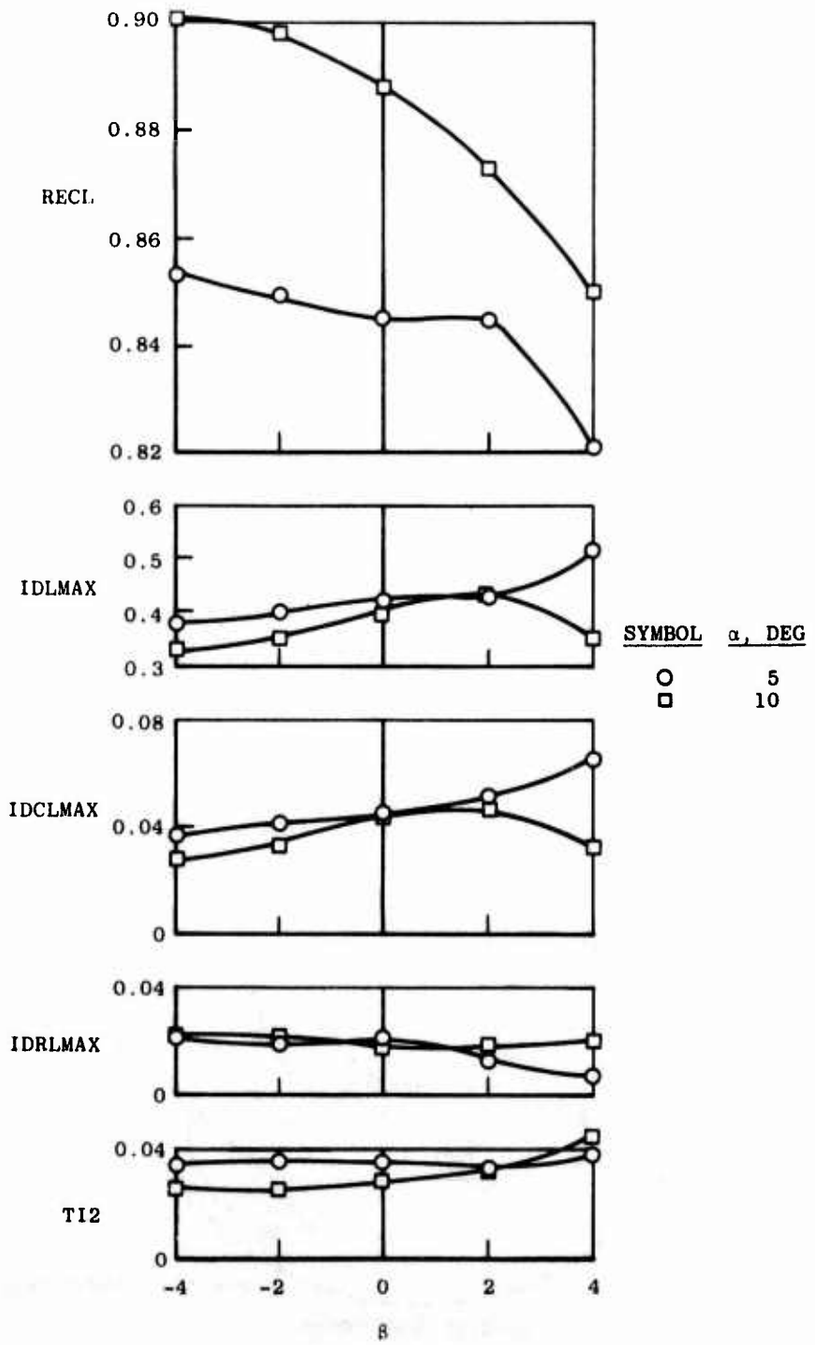

c. M_∞ = 1.80

Figure 7. Concluded.

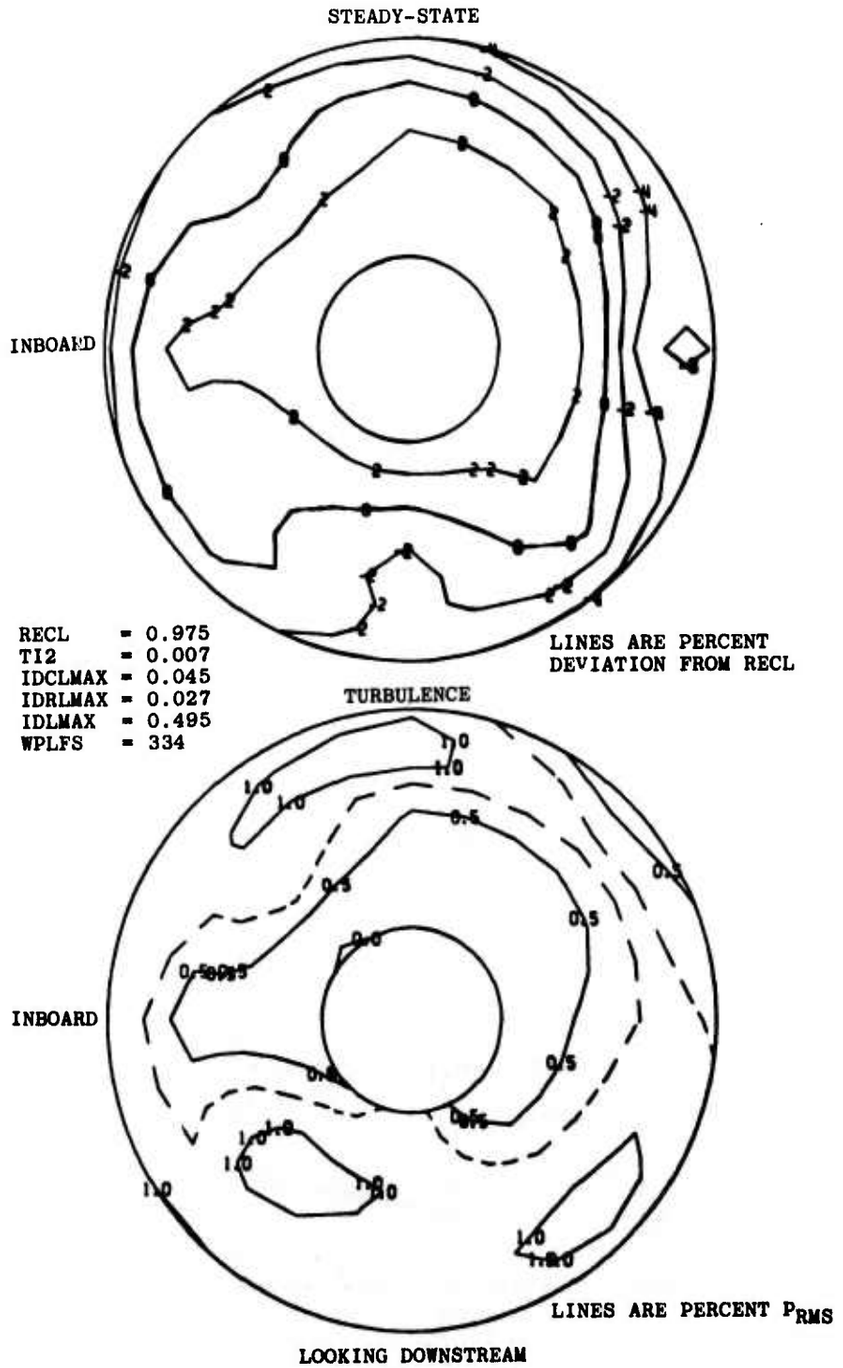

a. α = 5 deg, β = 0 deg

Figure 8. Basic configuration compressor-face pressure contours at M_∞ = 0.65.

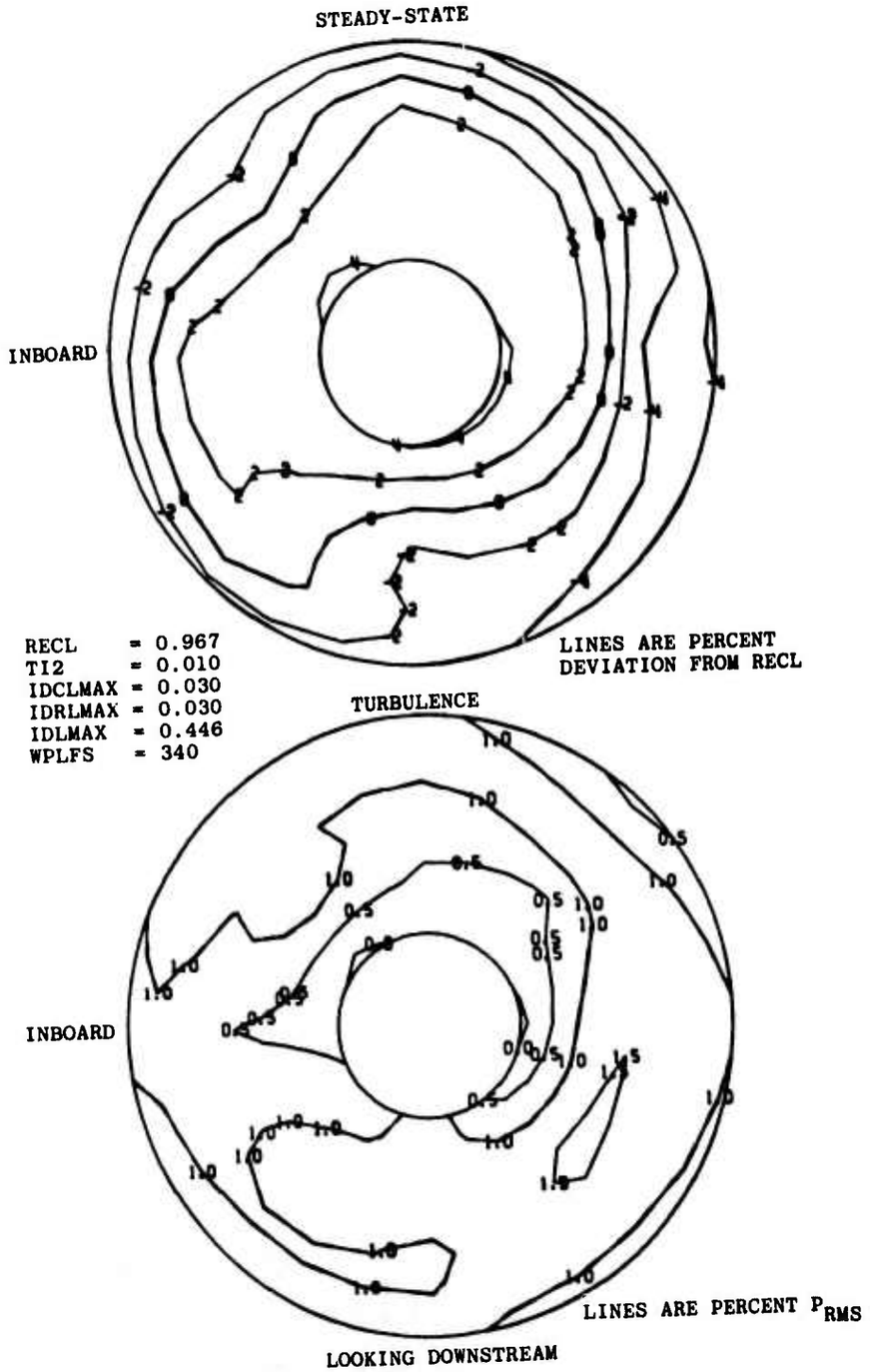

b. α = 5 deg, β = 4 deg

Figure 8. Continued.

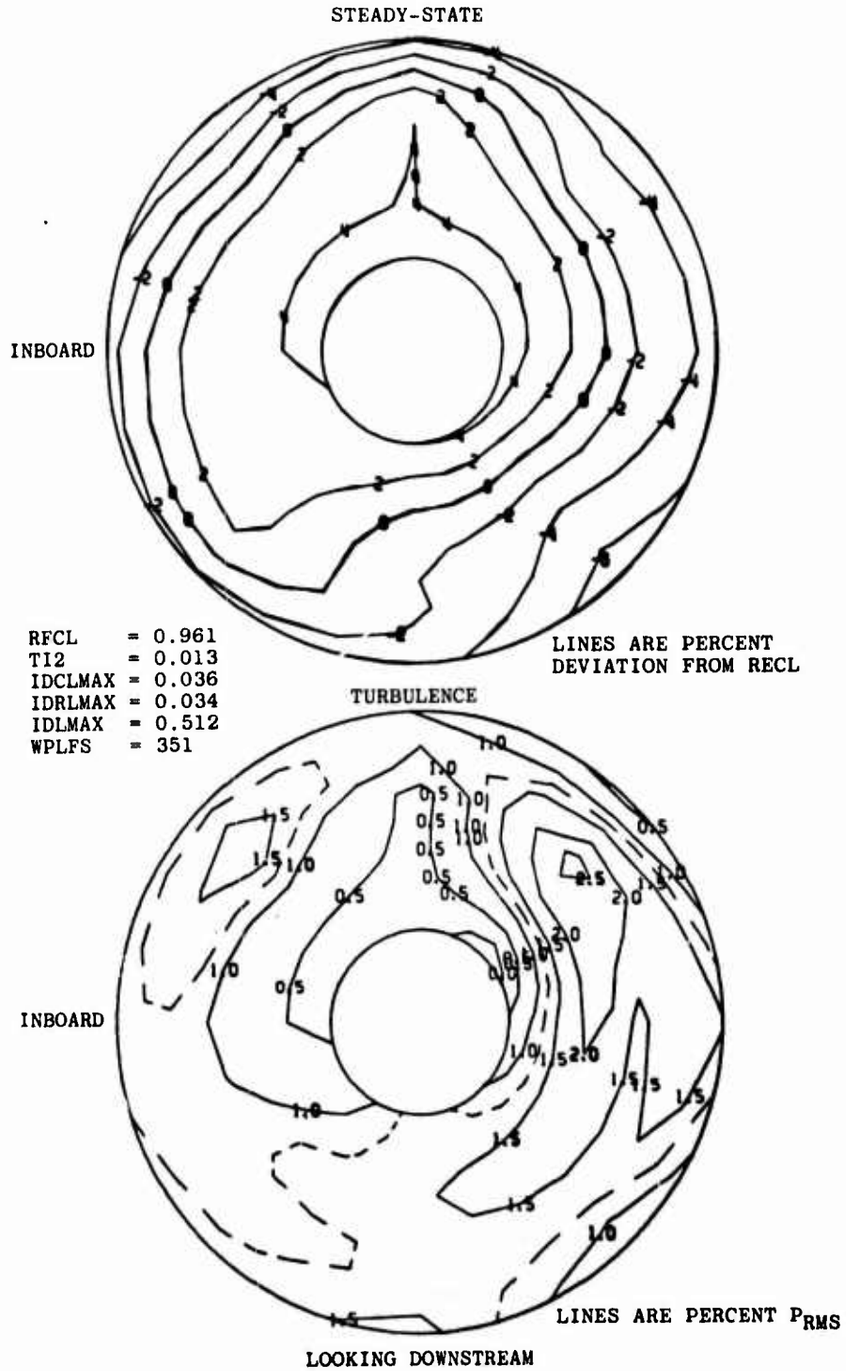

c. α = 10 deg, β = 0 deg

Figure 8. Concluded.

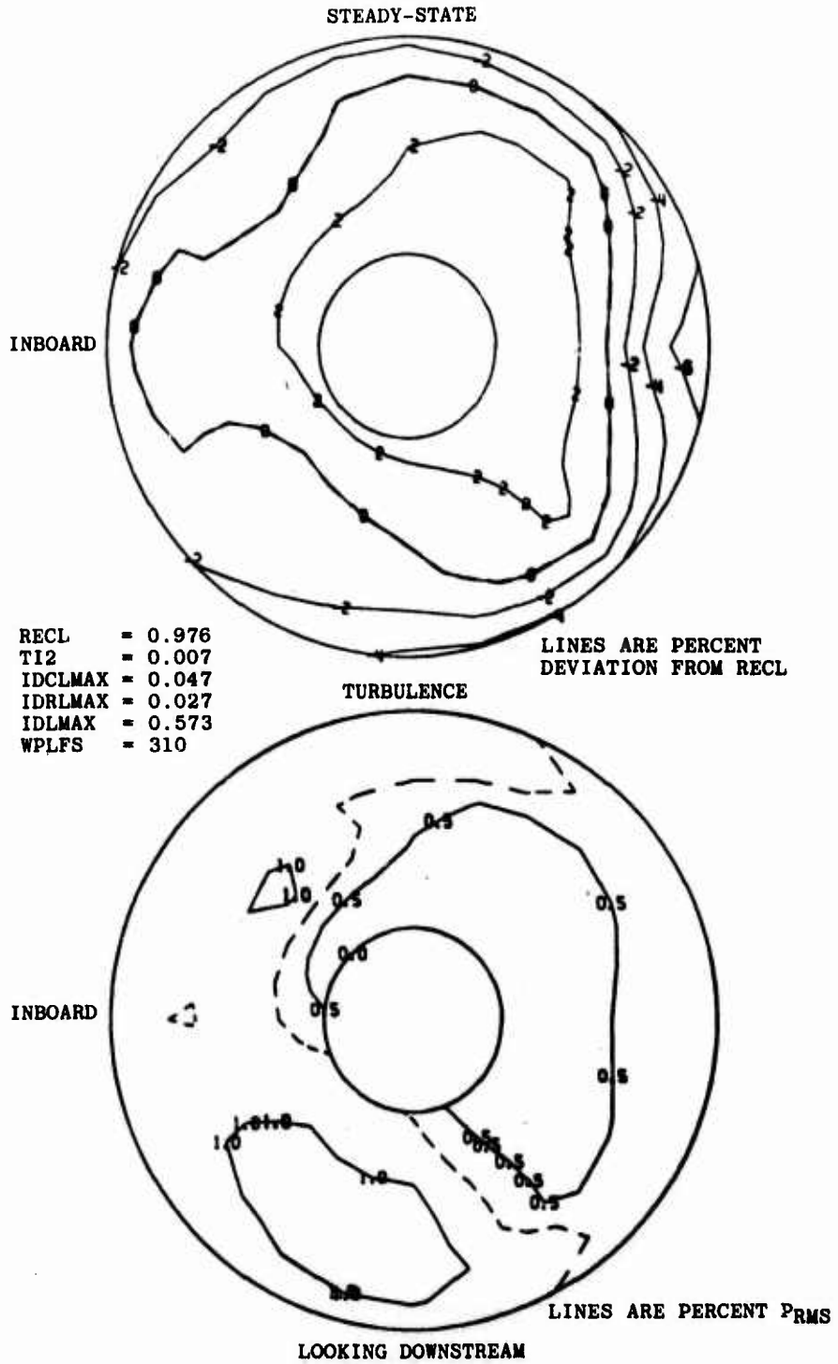

a. α = 5 deg, β = 0 deg

Figure 9. Basic configuration compressor-face pressure contours at M_∞ = 0.85.

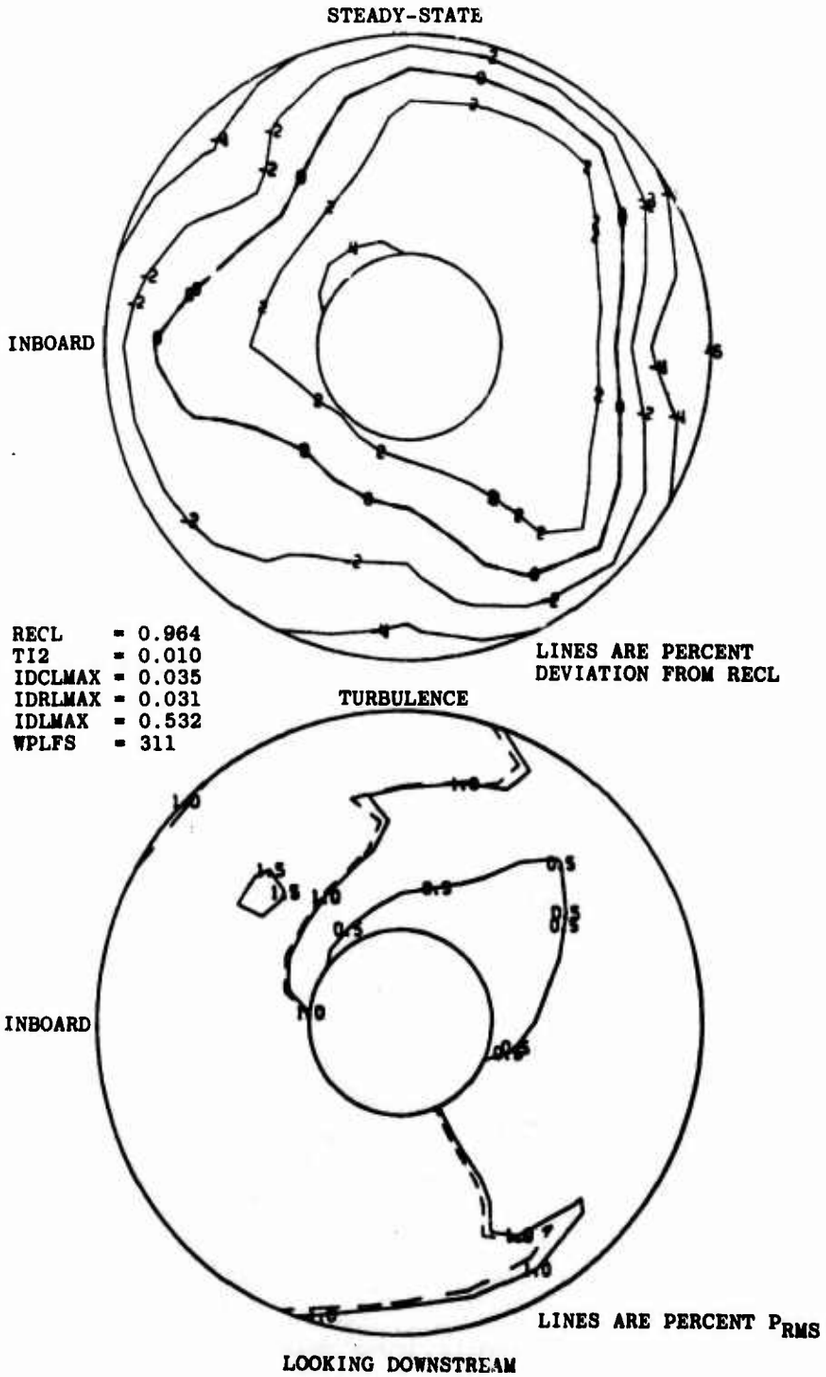

b. α = 5 deg, β = 4 deg

Figure 9. Continued.

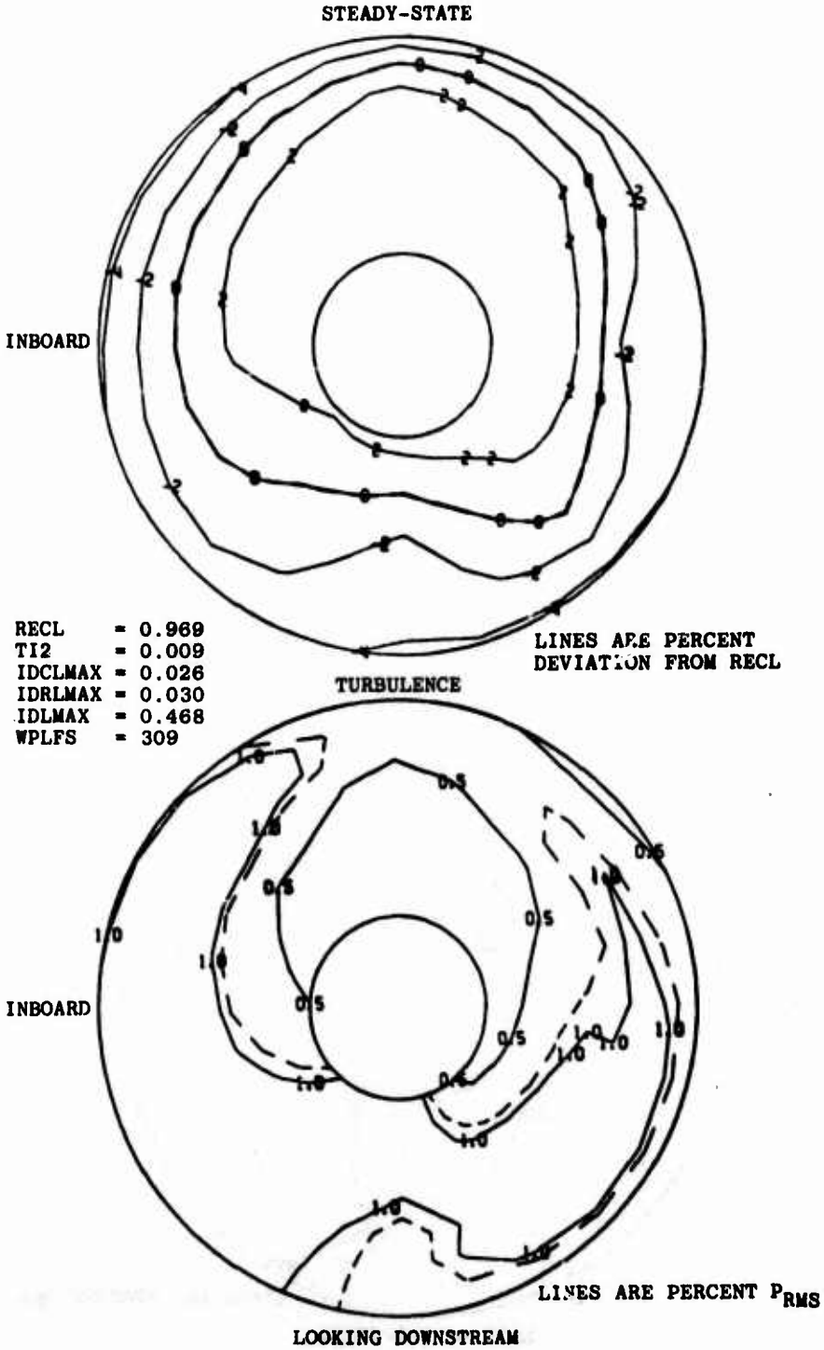

c. α = 10 deg, β = 0 deg

Figure 9. Concluded.

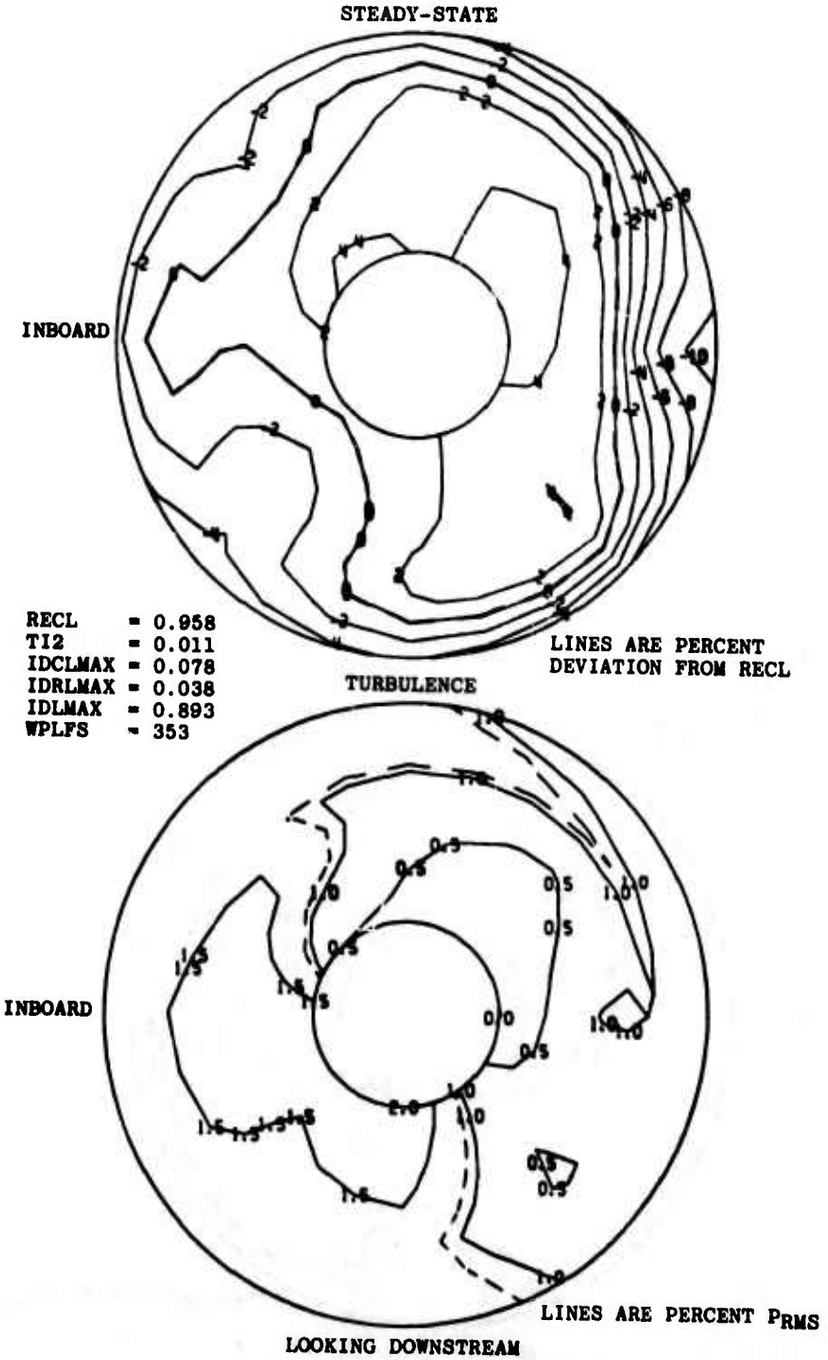

a. α = 5 deg, β = 0 deg

Figure 10. Basic configuration compressor-face pressure contours at M_∞ = 1.20.

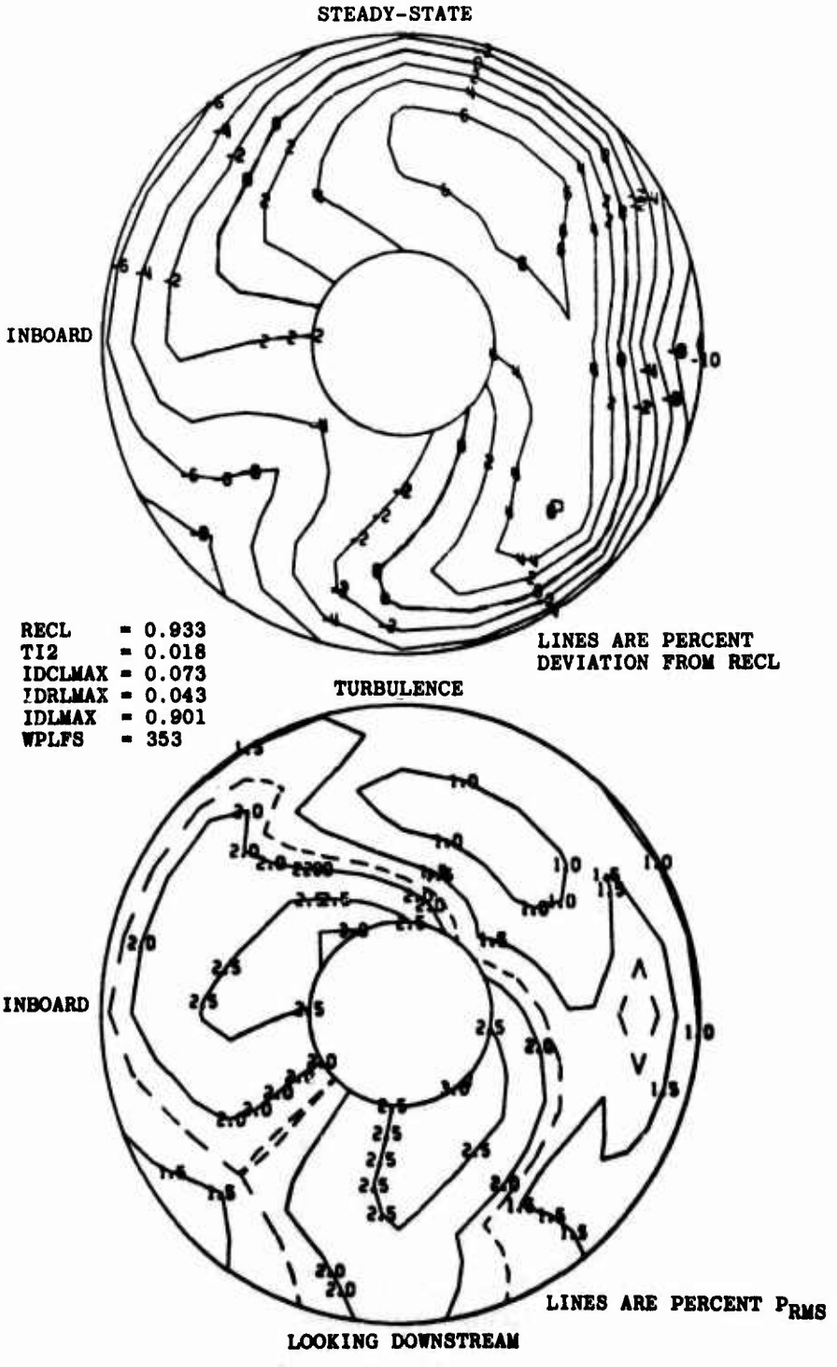

b. α = 5 deg, β = 4 deg

Figure 10. Continued.

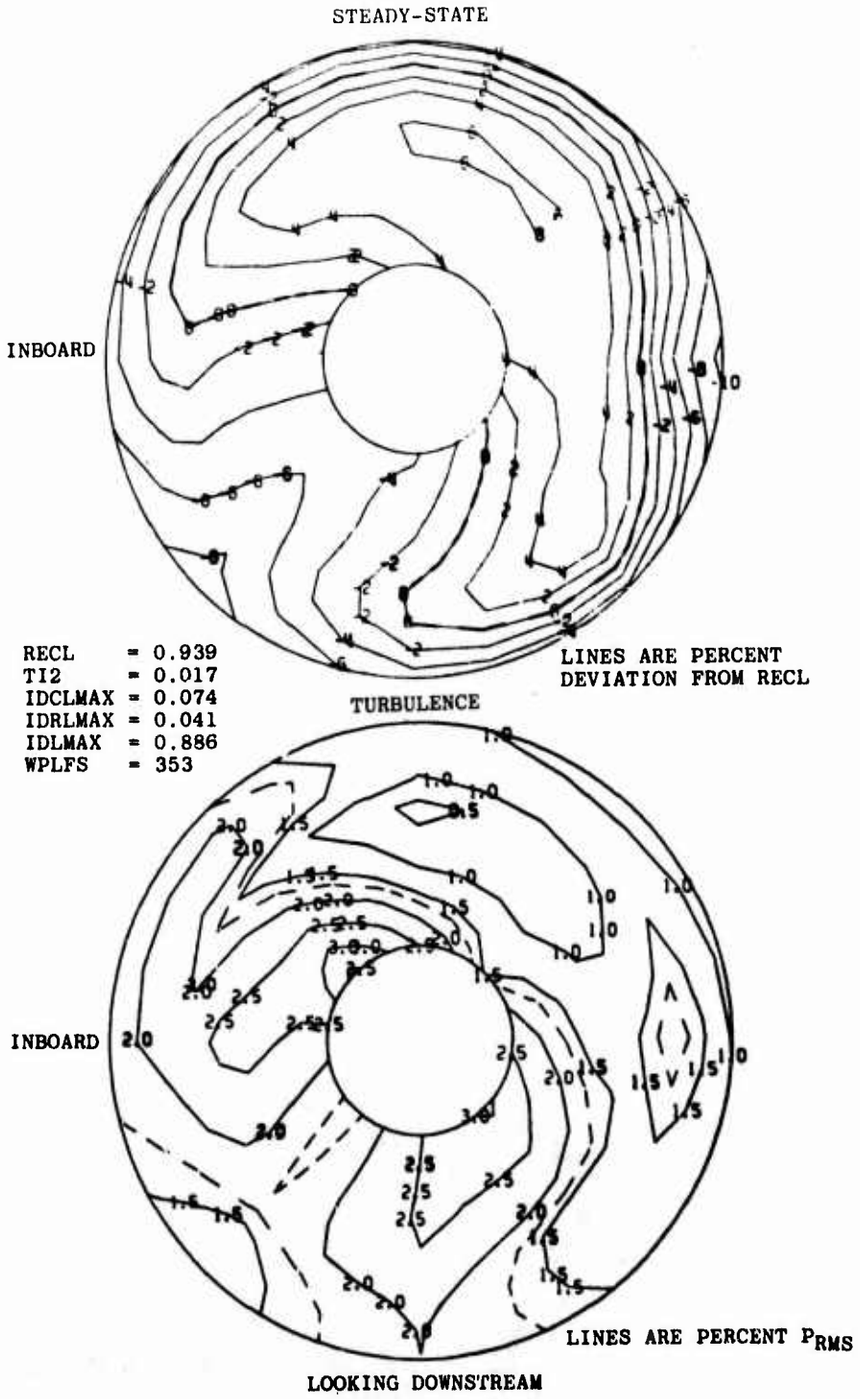

c. α = 10 deg, β = 0 deg

Figure 10. Concluded.

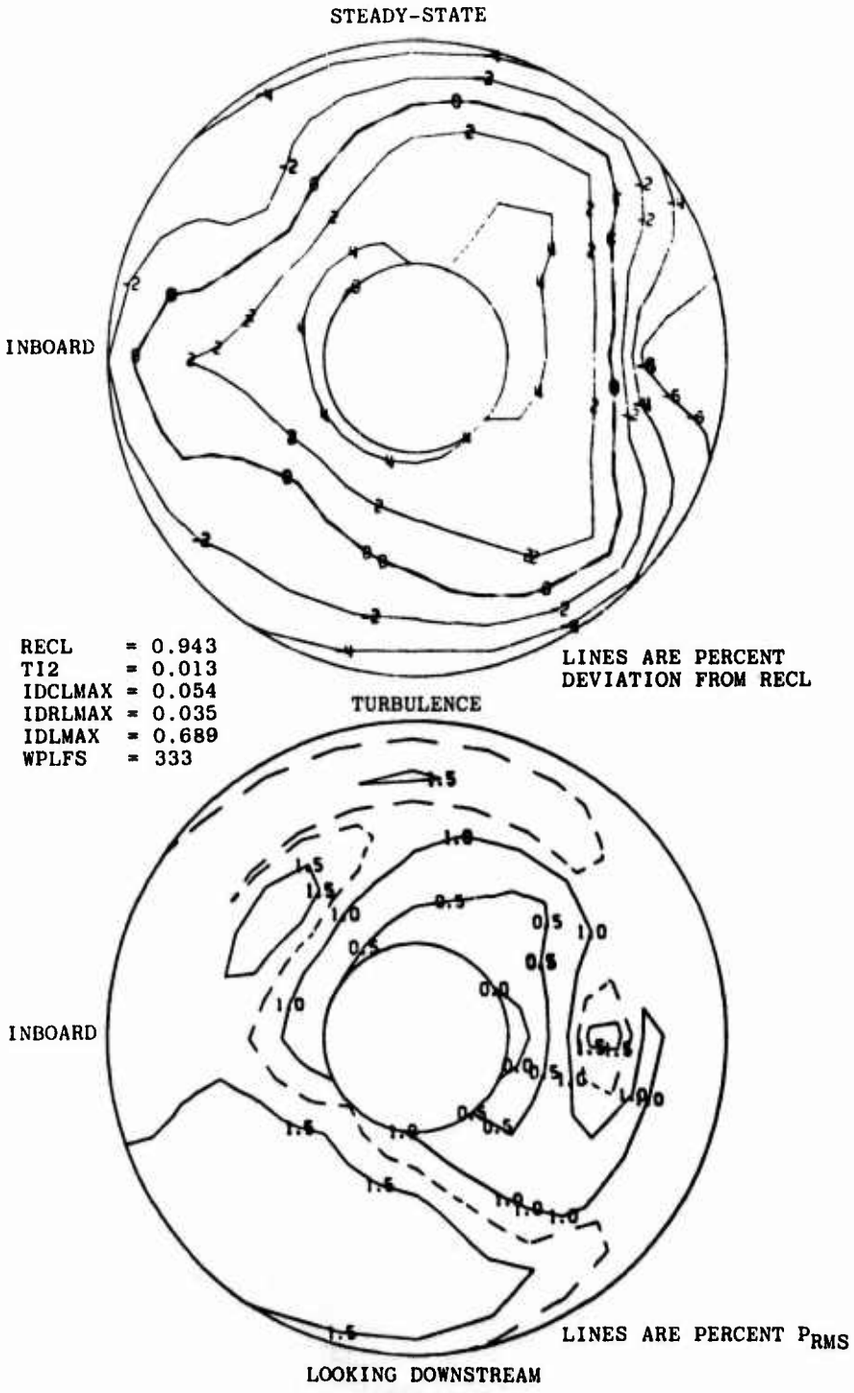

a. α = 5 deg, β = 0 deg

Figure 11. Basic configuration compressor-face pressure contours at M_∞ = 1.50.

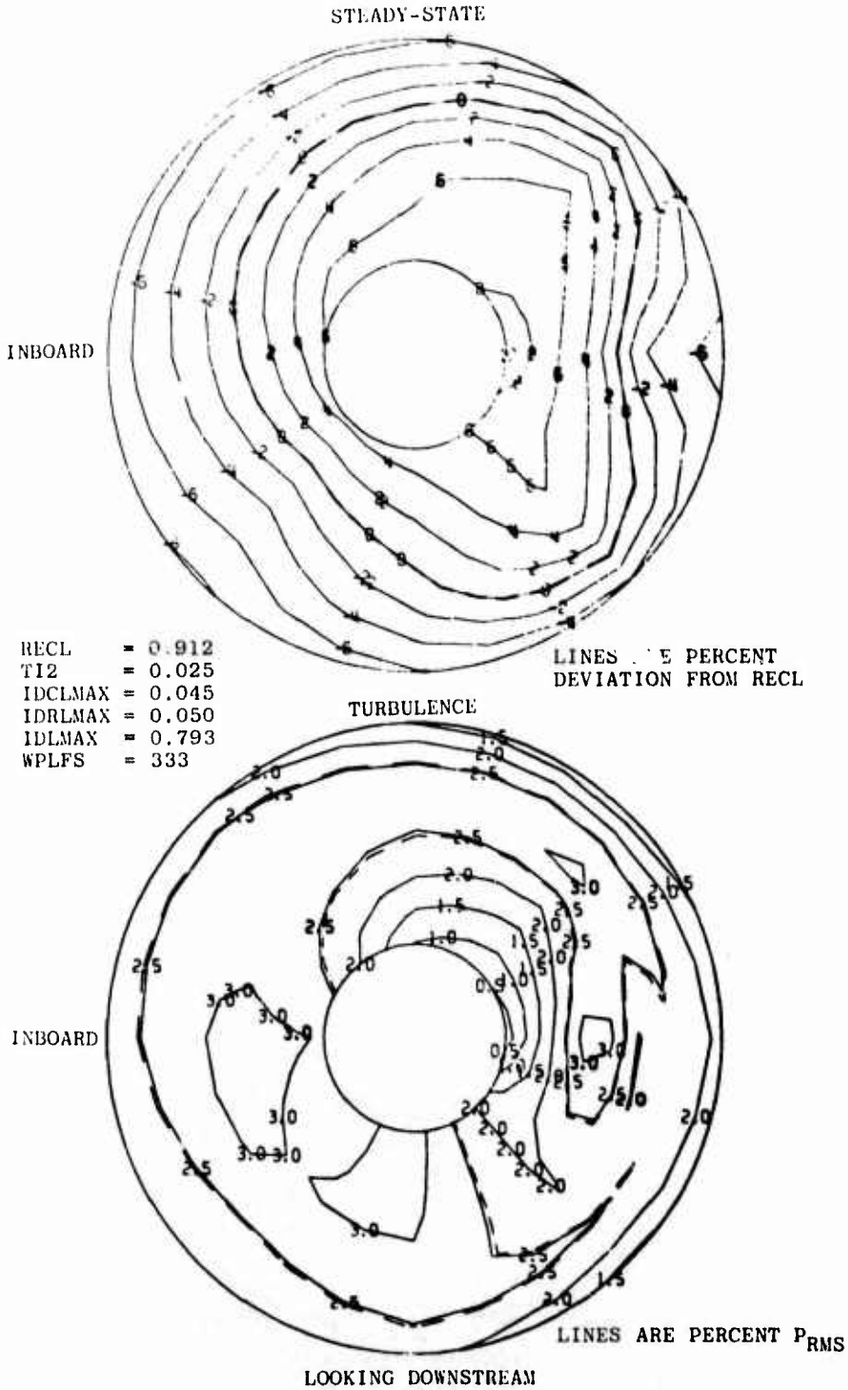

b. α = 5 deg, β = 4 deg

Figure 11. Continued.

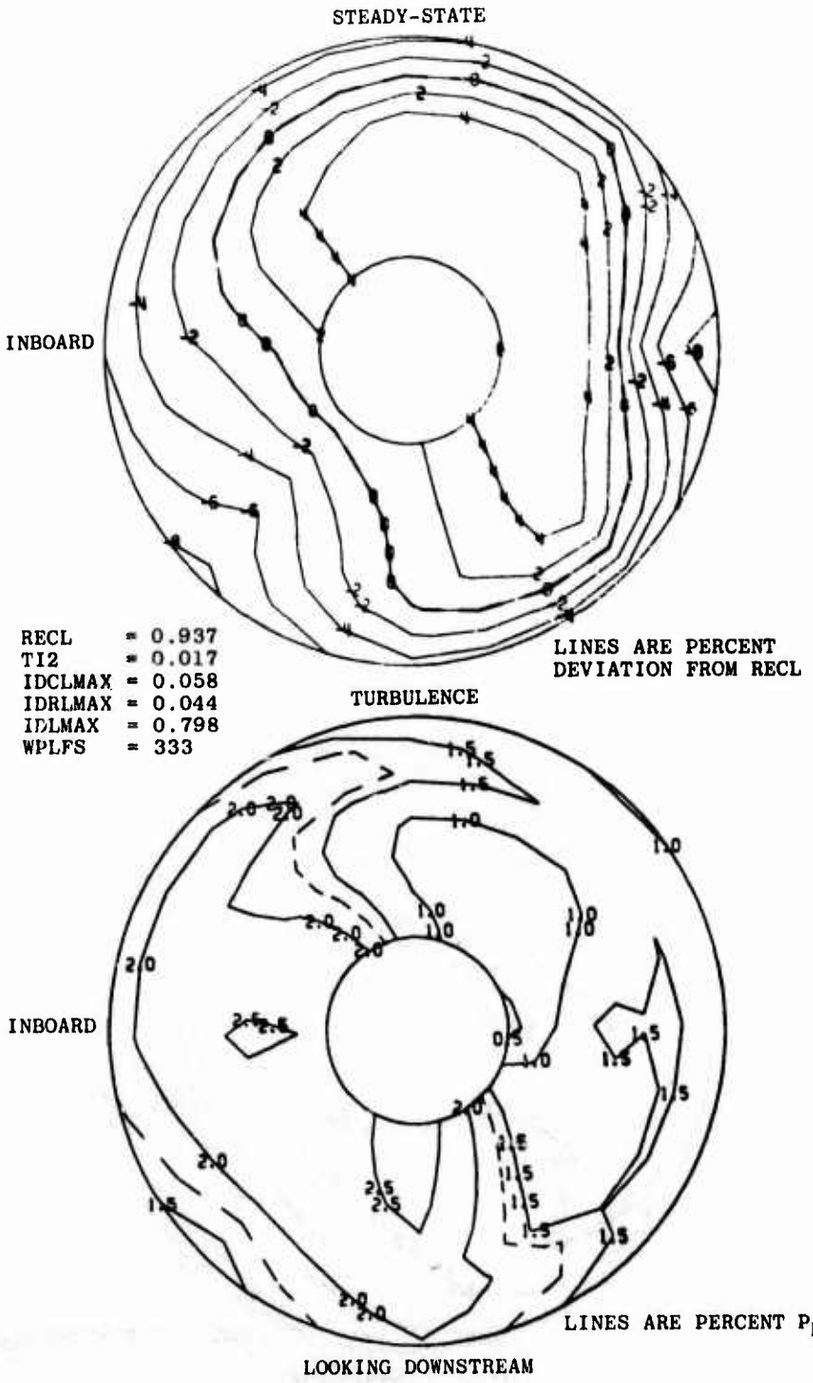

c. α = 10 deg, β = 0 deg

Figure 11. Concluded.

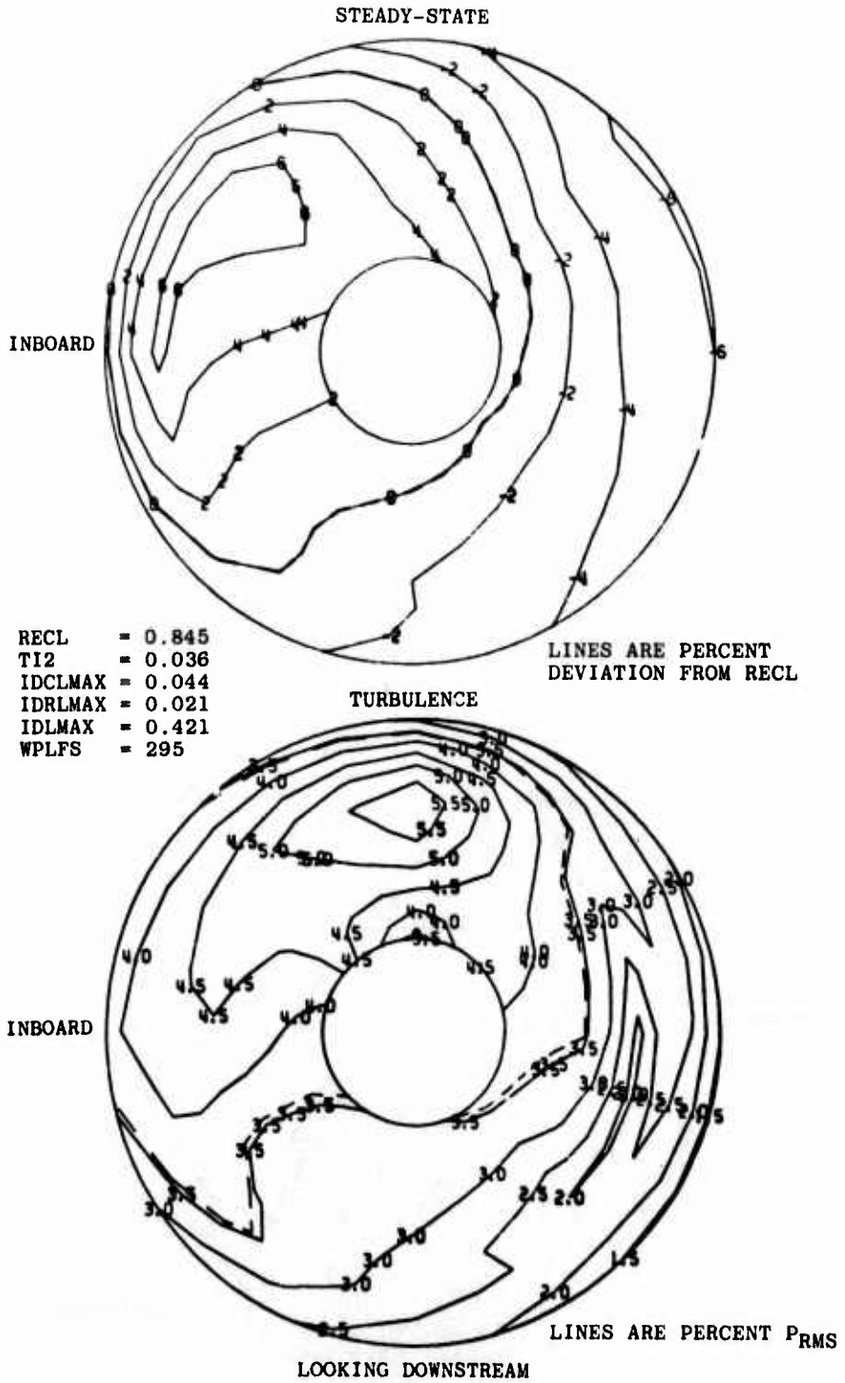

a. α = 5 deg, β = 0 deg

Figure 12. Basic configuration compressor-face pressure contours at M_∞ = 1.80.

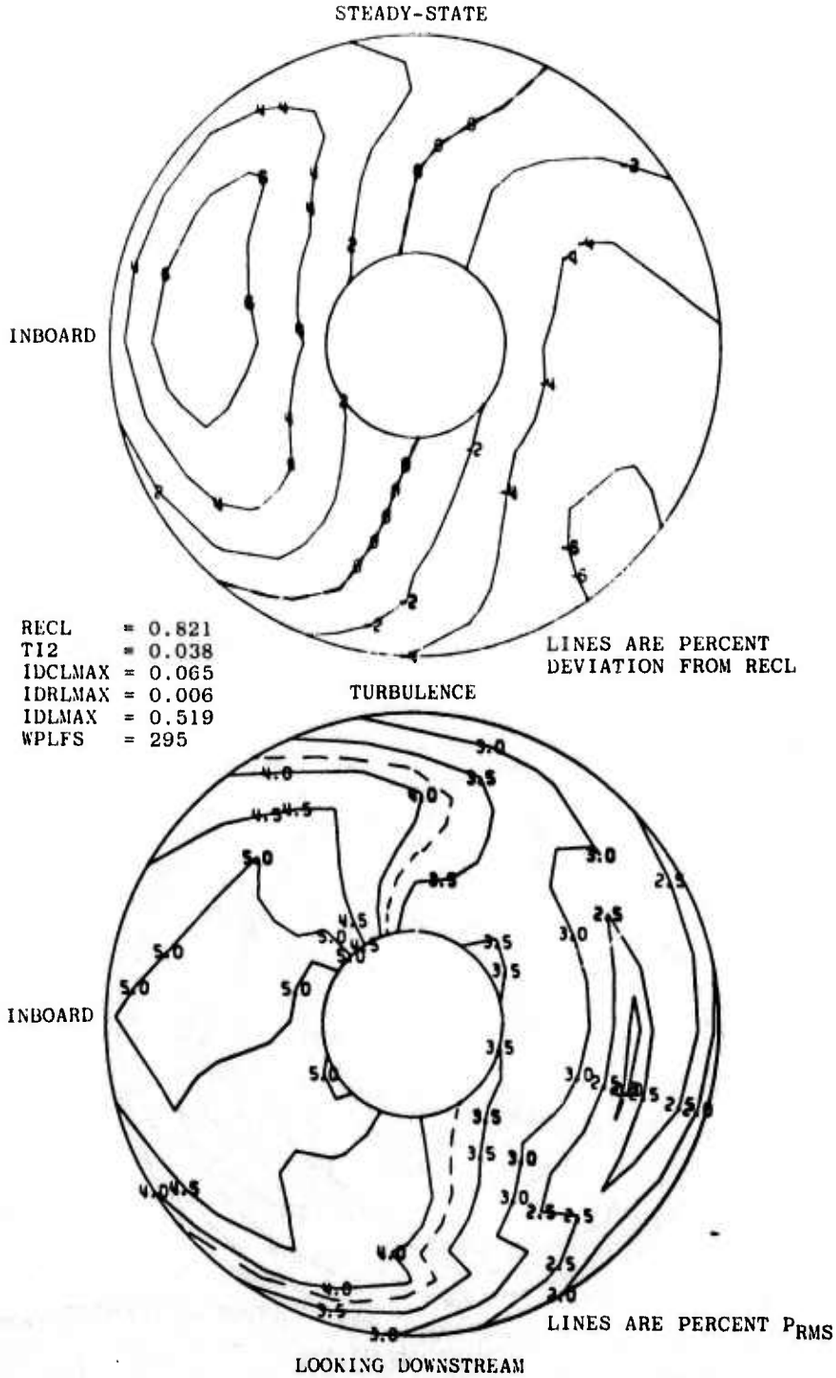

b. α = 5 deg, β = 4 deg
Figure 12. Continued.

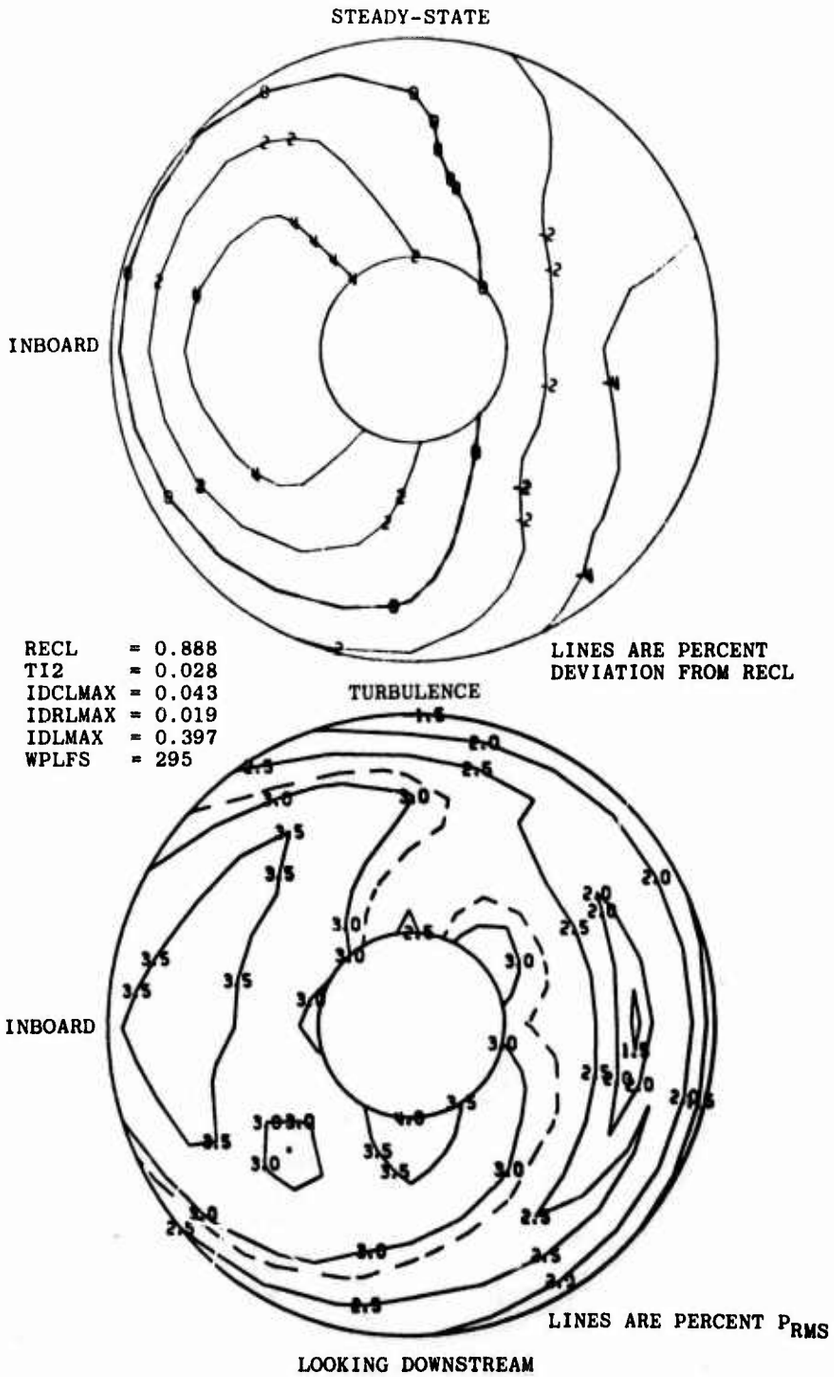

c. α = 10 deg, β = 0 deg

Figure 12. Concluded.

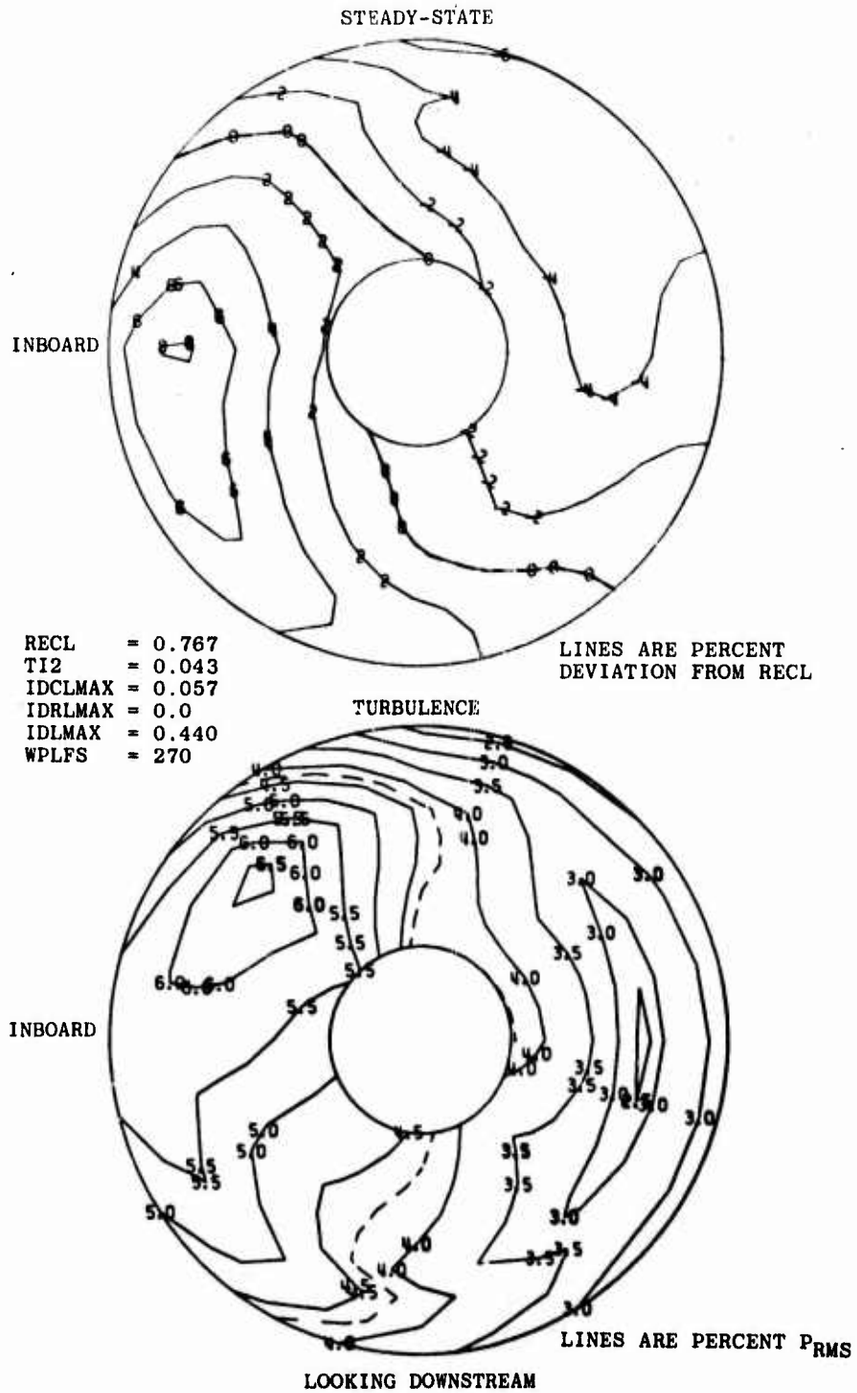

Figure 13. Basic configuration compressor-face pressure contours at M_∞ = 2.00, α = 5 deg, β = 0 deg.

SYMBOL	PN	CONFIGURATION
□	276	BASIC - B.L. 43.82
○	440	BASIC - B.L. 45.64
- - - - -		ENGINE REQUIREMENT

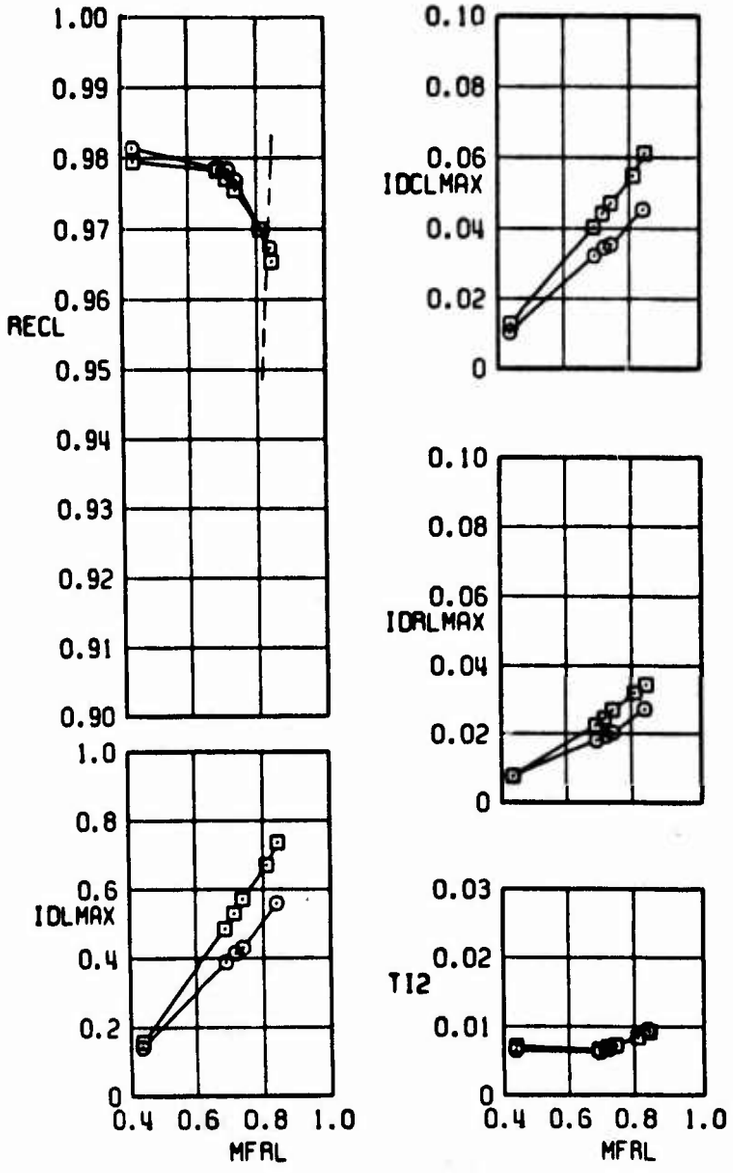

a. $M_\infty = 0.85$

Figure 14. Effect of inlet buttock-line position on inlet performance, α = 5 deg, β = 0 deg.

SYMBOL	PN	CONFIGURATION
□	320	BASIC - B.L. 43.82
○	471	BASIC - B.L. 45.64

- - - - - ENGINE REQUIREMENT

——— - - ——— FREE-STREAM NORMAL SHOCK RECOVERY

FLAGGED SYMBOLS DENOTE INLET STABILITY LIMIT

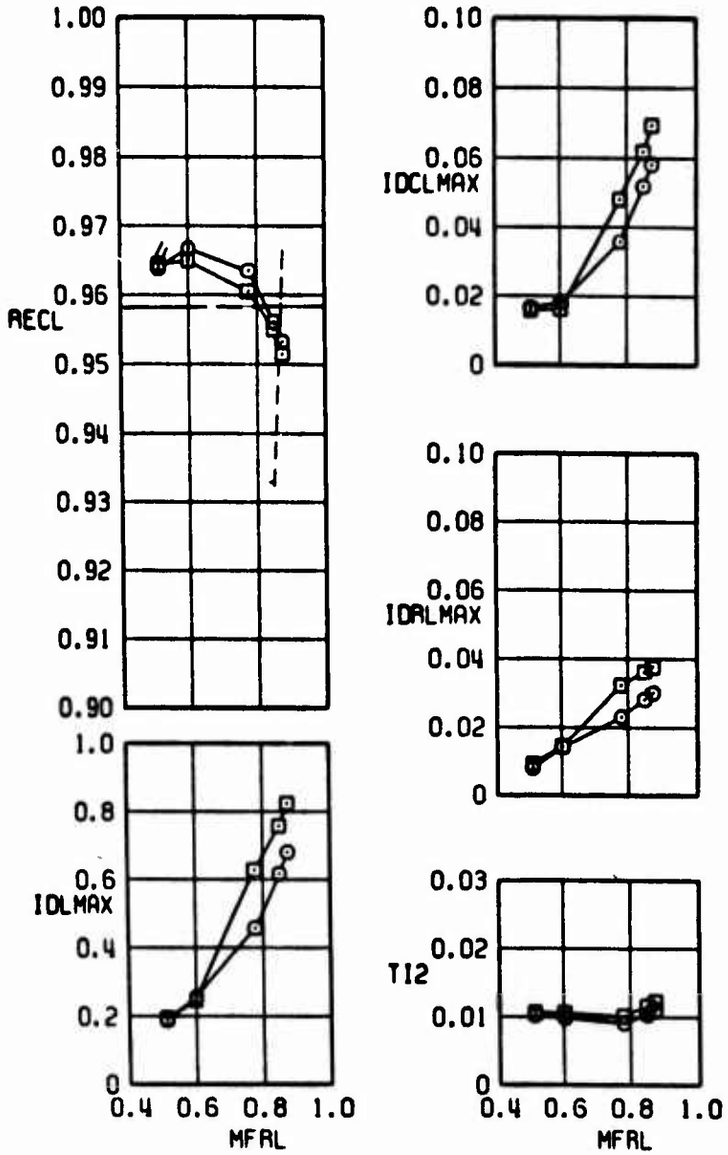

b. $M_\infty = 1.40$

Figure 14. Concluded.

SYMBOL	PN	CONFIGURATION
□	20	BASIC - B.L. 43.82
○	41	BASIC - B.L. 47.45

- - - - - ENGINE REQUIREMENT

——— — — FREE-STREAM NORMAL SHOCK RECOVERY

FLAGGED SYMBOLS DENOTE INLET STABILITY LIMIT

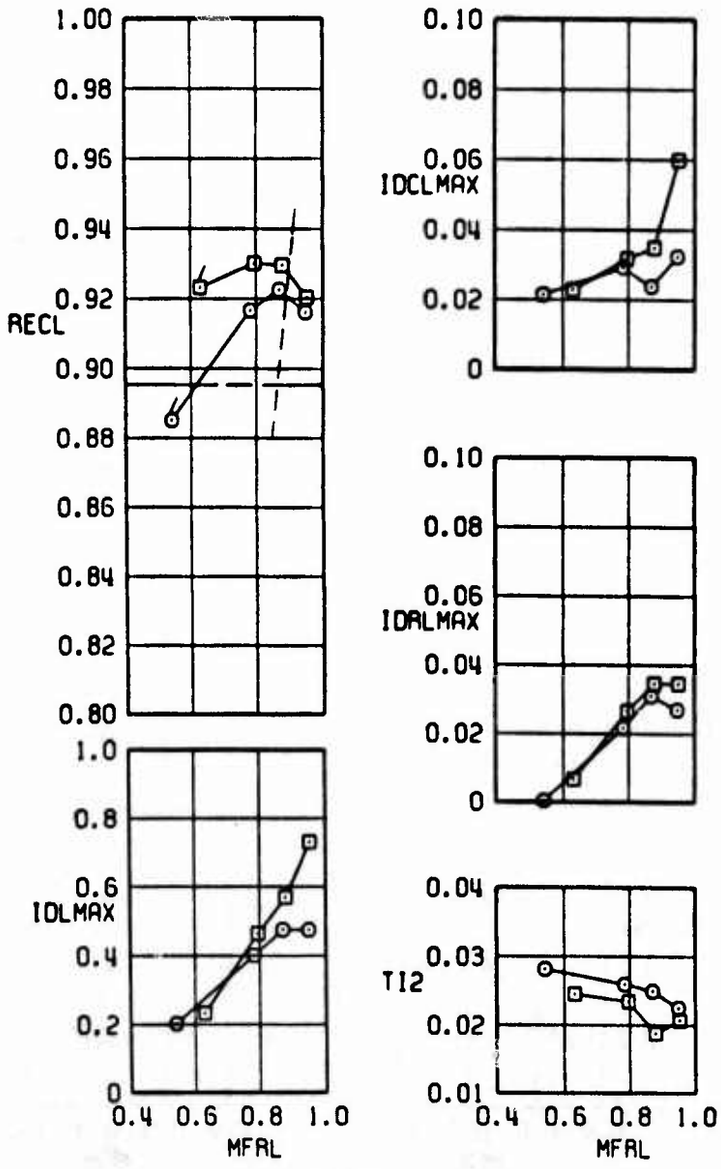

a. α = 5 deg, β = 0 deg

Figure 15. Effect of inlet buttock-line position on inlet performance at M_∞ = 1.62.

SYMBOL	PN	CONFIGURATION
□	25	BASIC - B.L. 43.82
O	46	BASIC - B.L. 47.45

- - - - - ENGINE REQUIREMENT

——— - ——FREE-STREAM NORMAL SHOCK RECOVERY

FLAGGED SYMBOLS DENOTE INLET STABILITY LIMIT

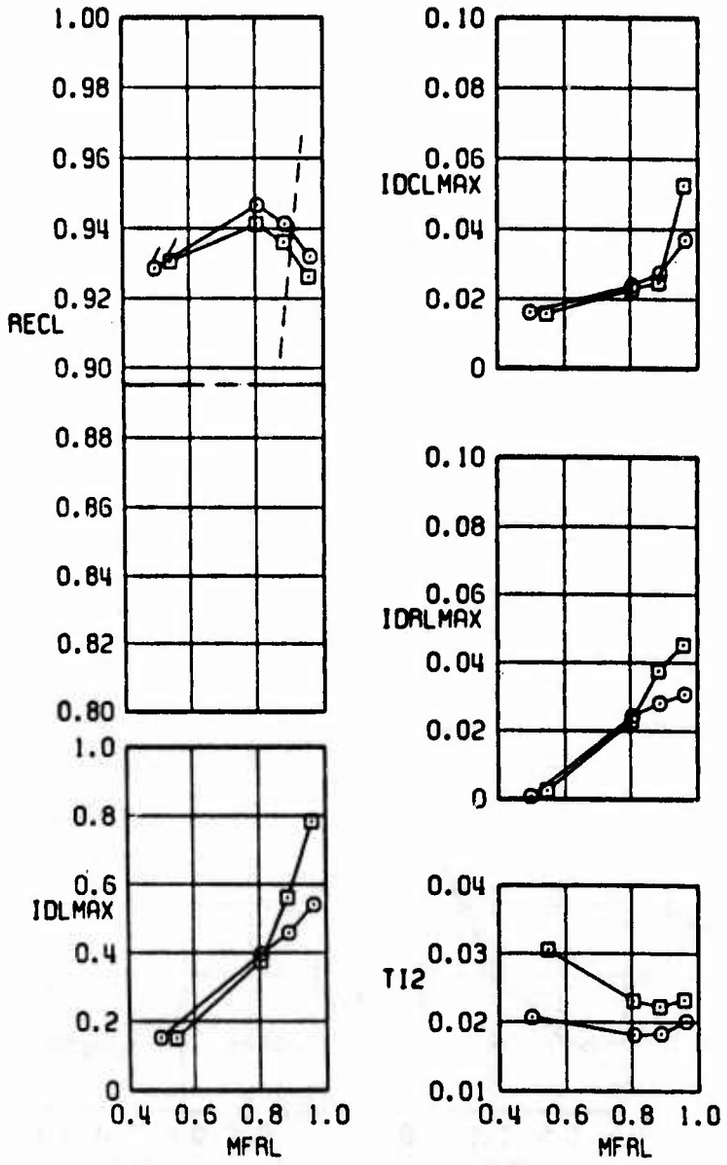

b. α = 10 deg, β = 0 deg

Figure 15. Concluded.

SYMBOL	PN	CONFIGURATION
□	20	LONG SPLITTER
O	63	SHORT SPLITTER

- - - - - - ENGINE REQUIREMENT

——— - - ——— FREE-STREAM NORMAL SHOCK RECOVERY

FLAGGED SYMBOLS DENOTE INLET STABILITY LIMIT

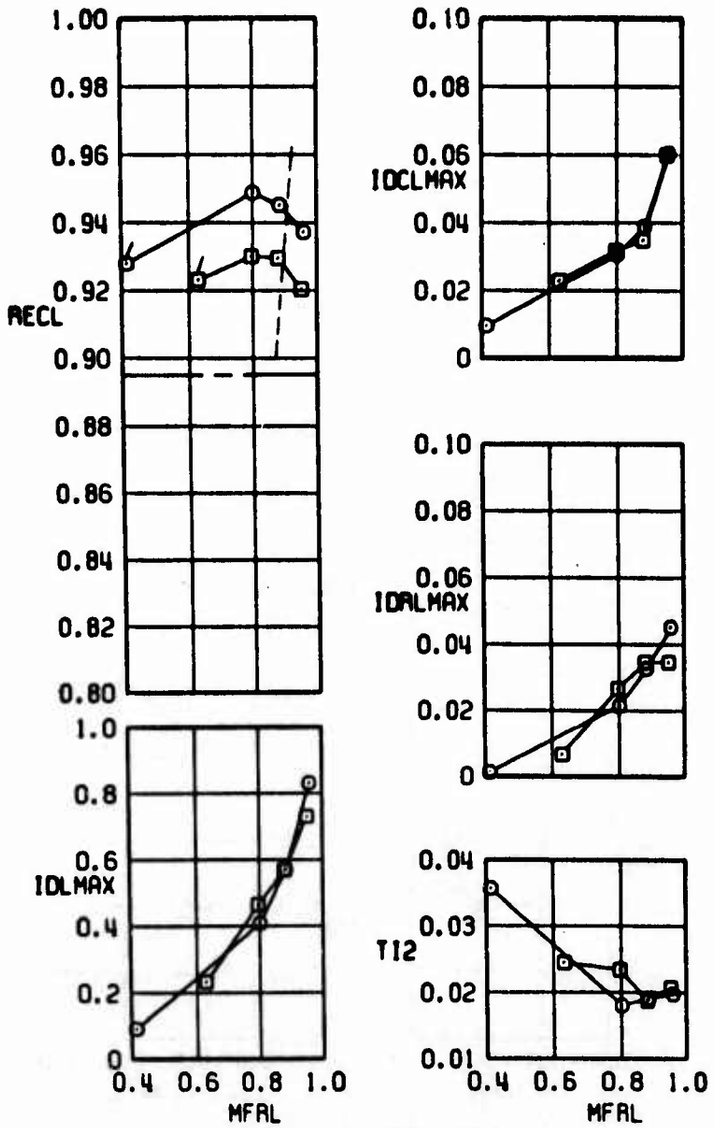

a. α = 5 deg, β = 0 deg

Figure 16. Comparison of long splitter and short splitter inlet performance at M_∞ = 1.60.

SYMBOL	PN	CONFIGURATION
□	25	BASIC SPLITTER
○	69	SHORT SPLITTER

- - - - - ENGINE REQUIREMENT

——— - - —— FREE-STREAM NORMAL SHOCK RECOVERY

FLAGGED SYMBOLS DENOTE INLET STABILITY LIMIT

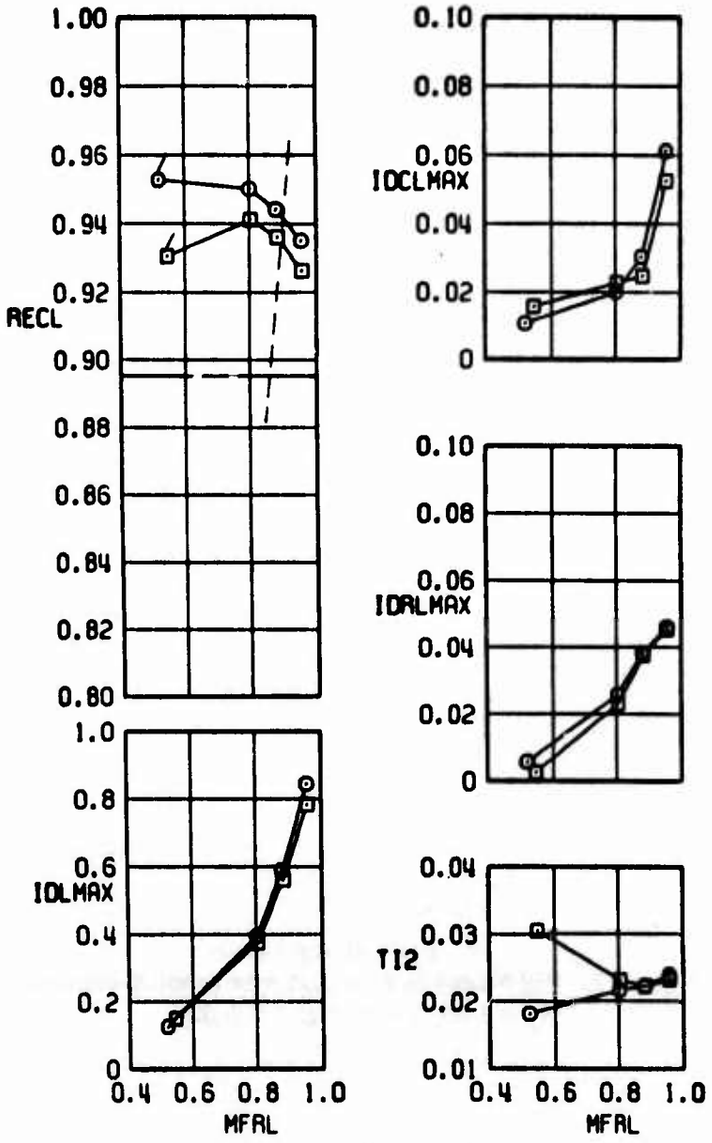

b. α = 10 deg, β = 0 deg

Figure 16. Concluded.

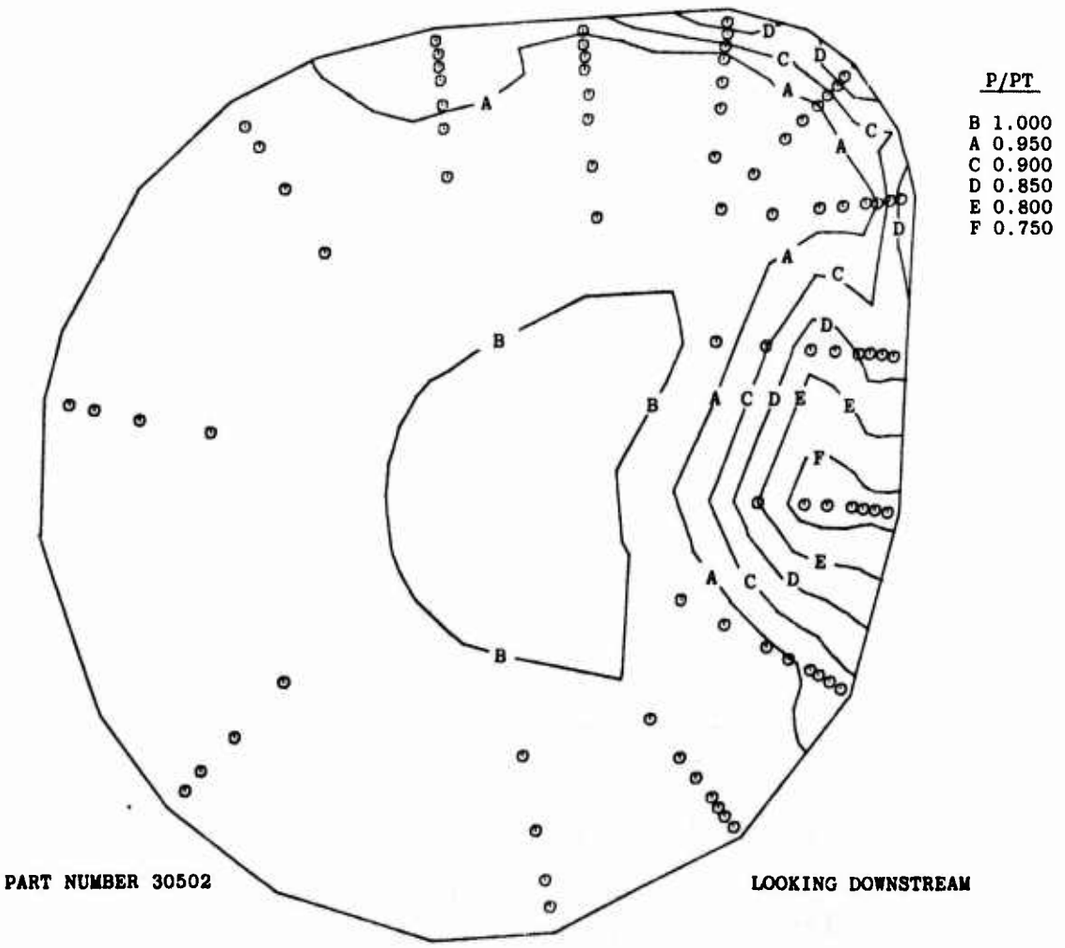

a. Basic configuration

Figure 17. Right-hand inlet throat rake pressure contours at M_∞ = 1.50, α = 5 deg, β = 0 deg.

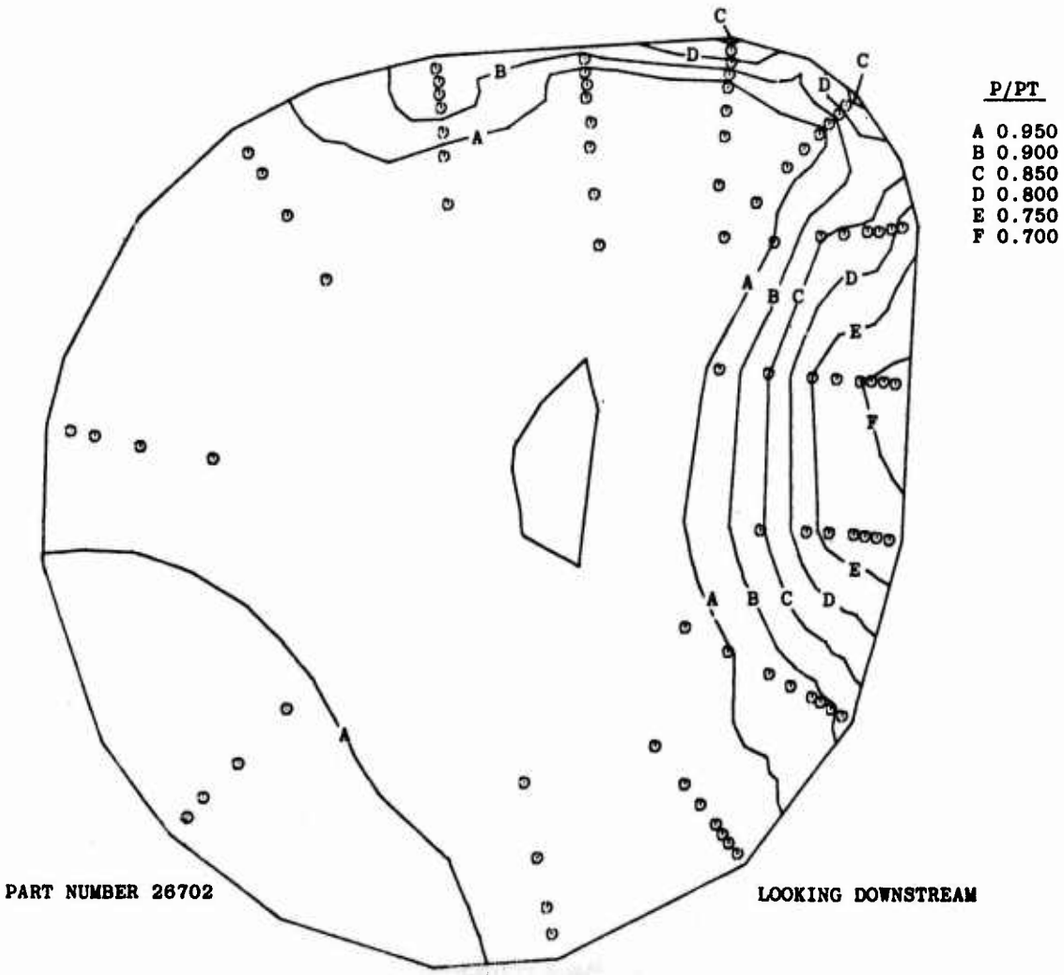

b. Alternate side plate 2
Figure 17. Concluded.

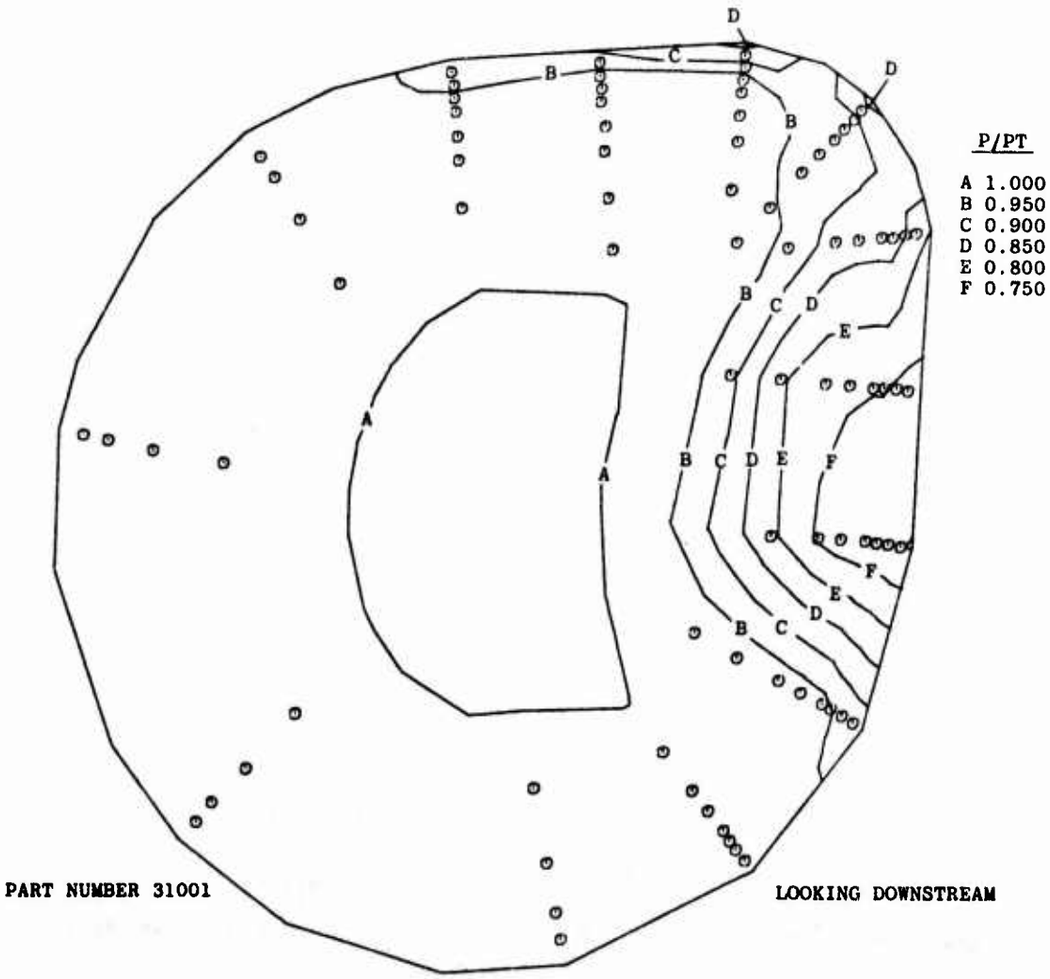

a. Basic configuration

Figure 18. Right-hand inlet throat rake pressure contours at M_∞ = 1.50, α = 10 deg, β = 0 deg.

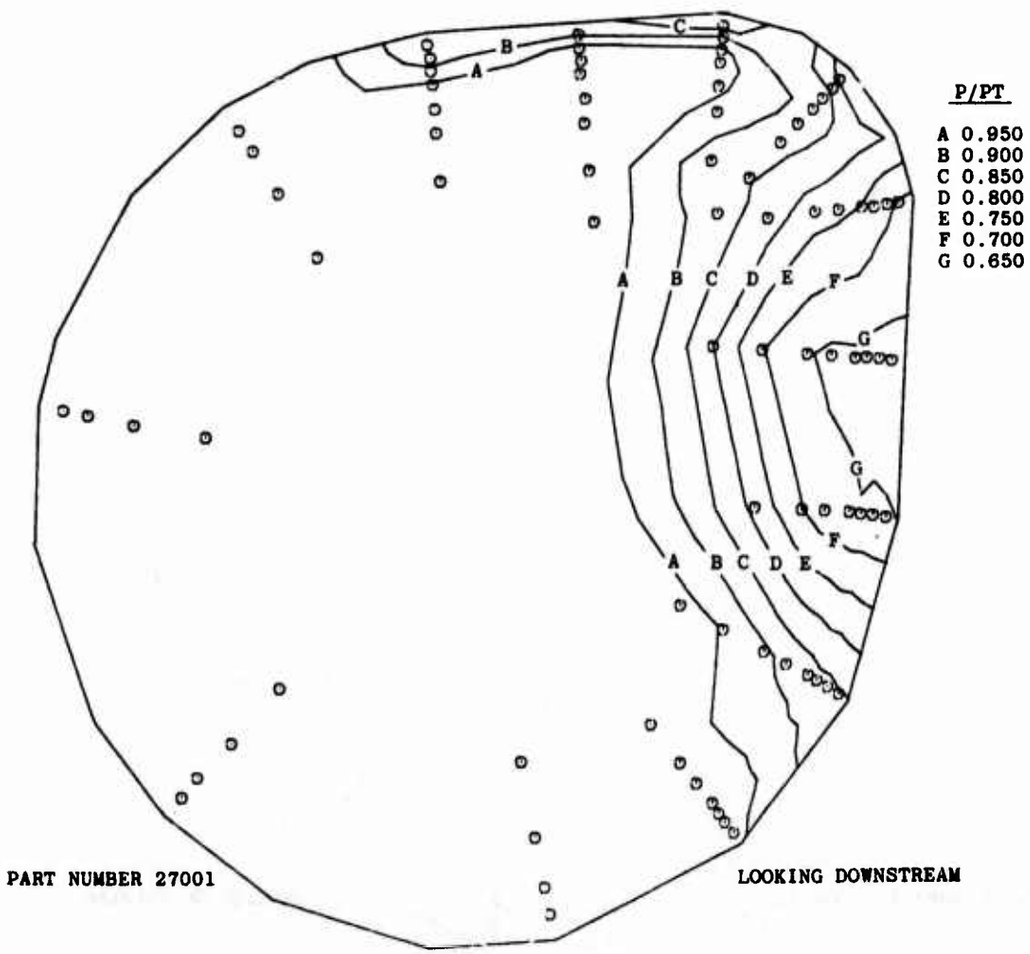

b. Alternate side plate 2
Figure 18. Concluded.

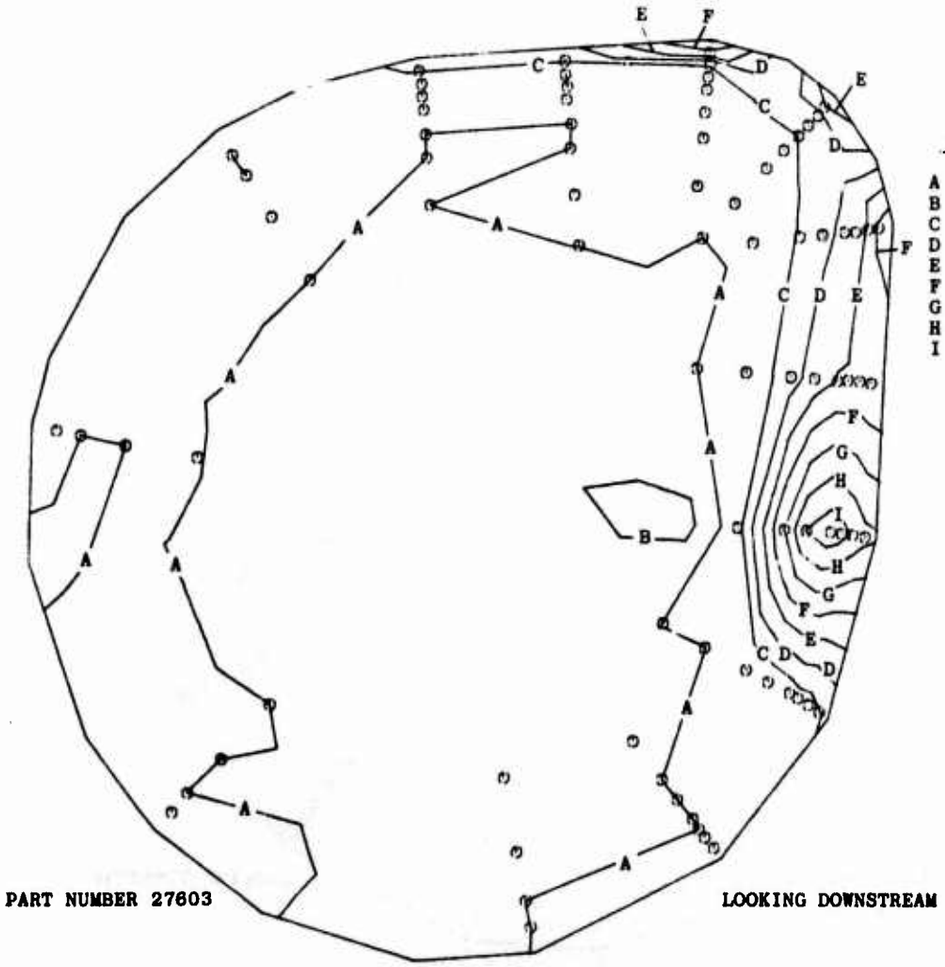

a. Basic configuration

Figure 19. Right-hand inlet throat rake pressure contours at M_∞ = 0.85, α = 5 deg, β = 0 deg.

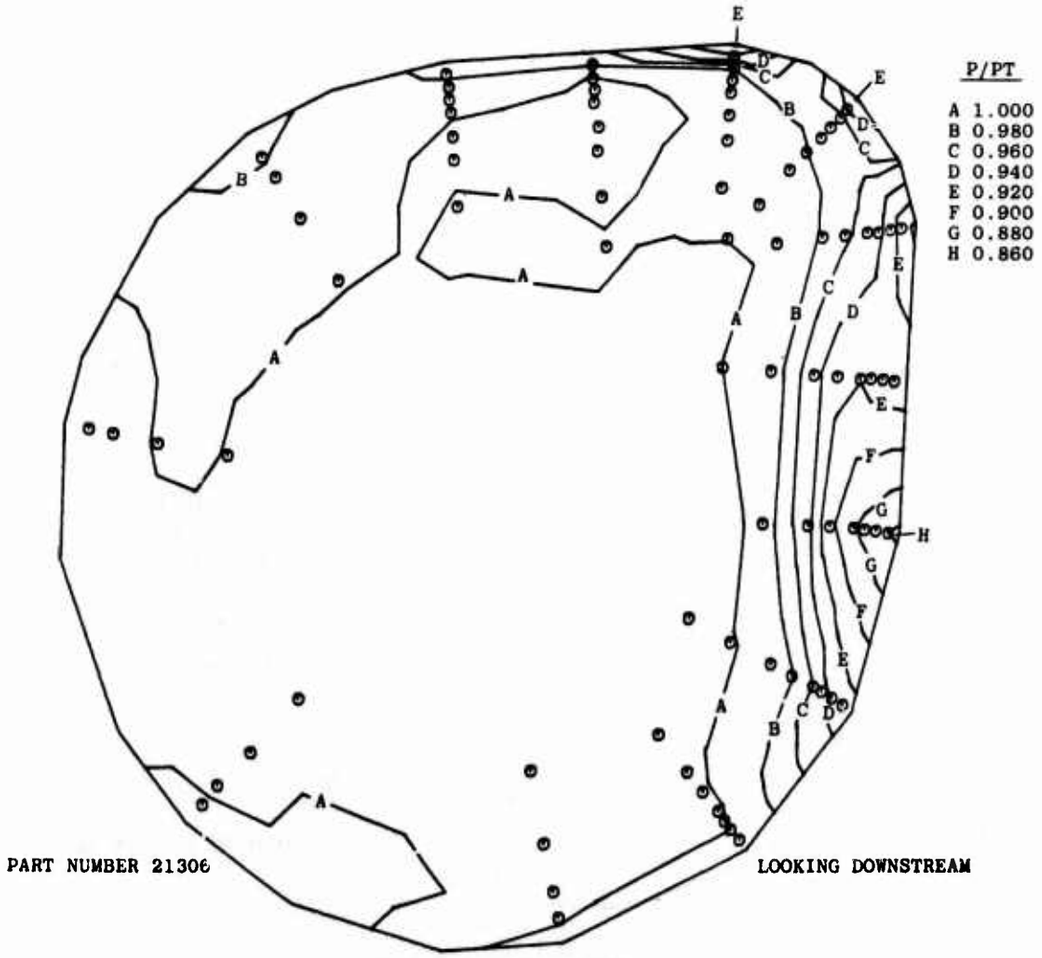

b. Alternate side plate 1
Figure 19. Continued.

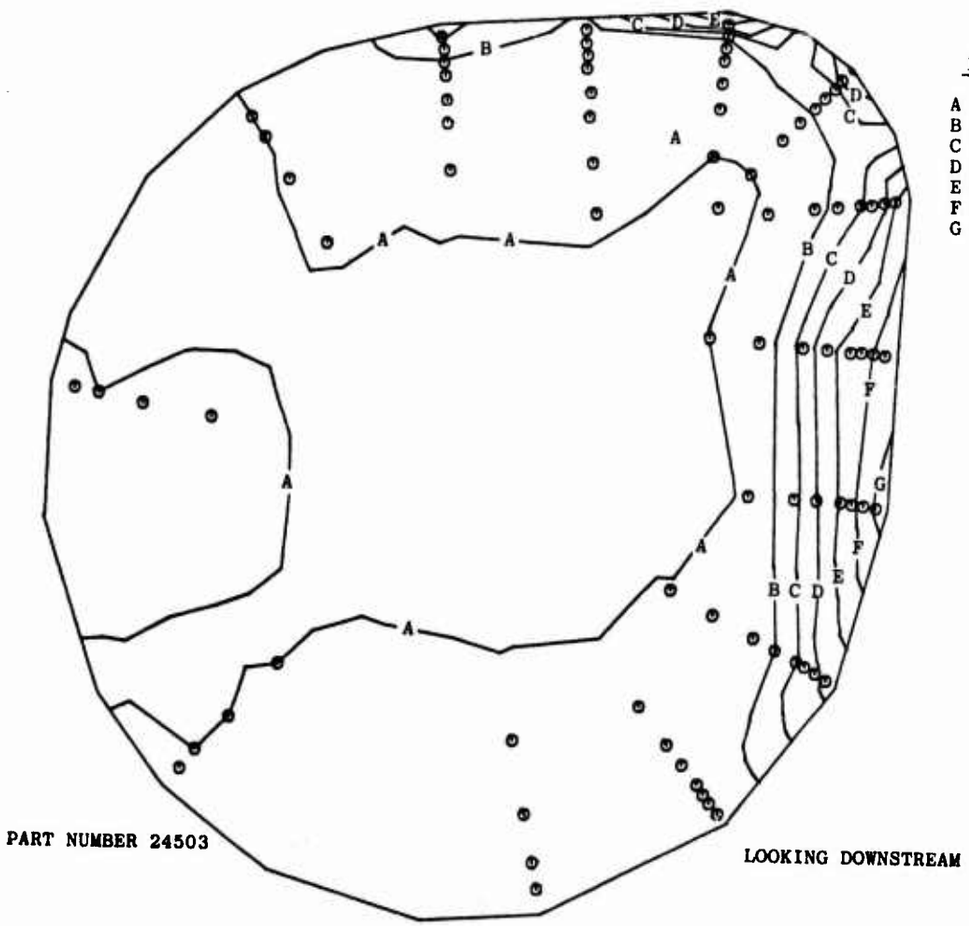

c. Alternate side plate 2
Figure 19. Concluded.

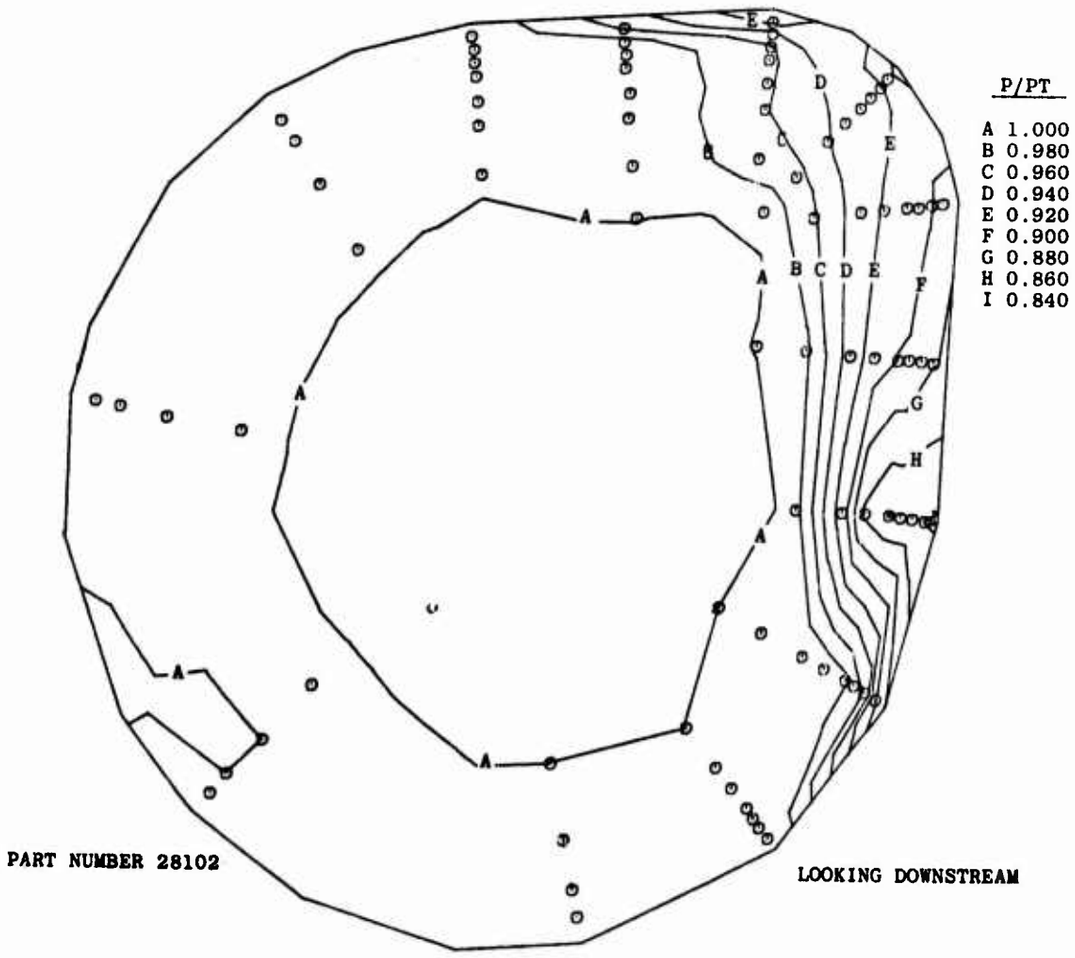

a. Basic configuration

Figure 20. Right-hand inlet throat rake pressure contours at M_∞ = 0.85, α = 10 deg, β = 0 deg.

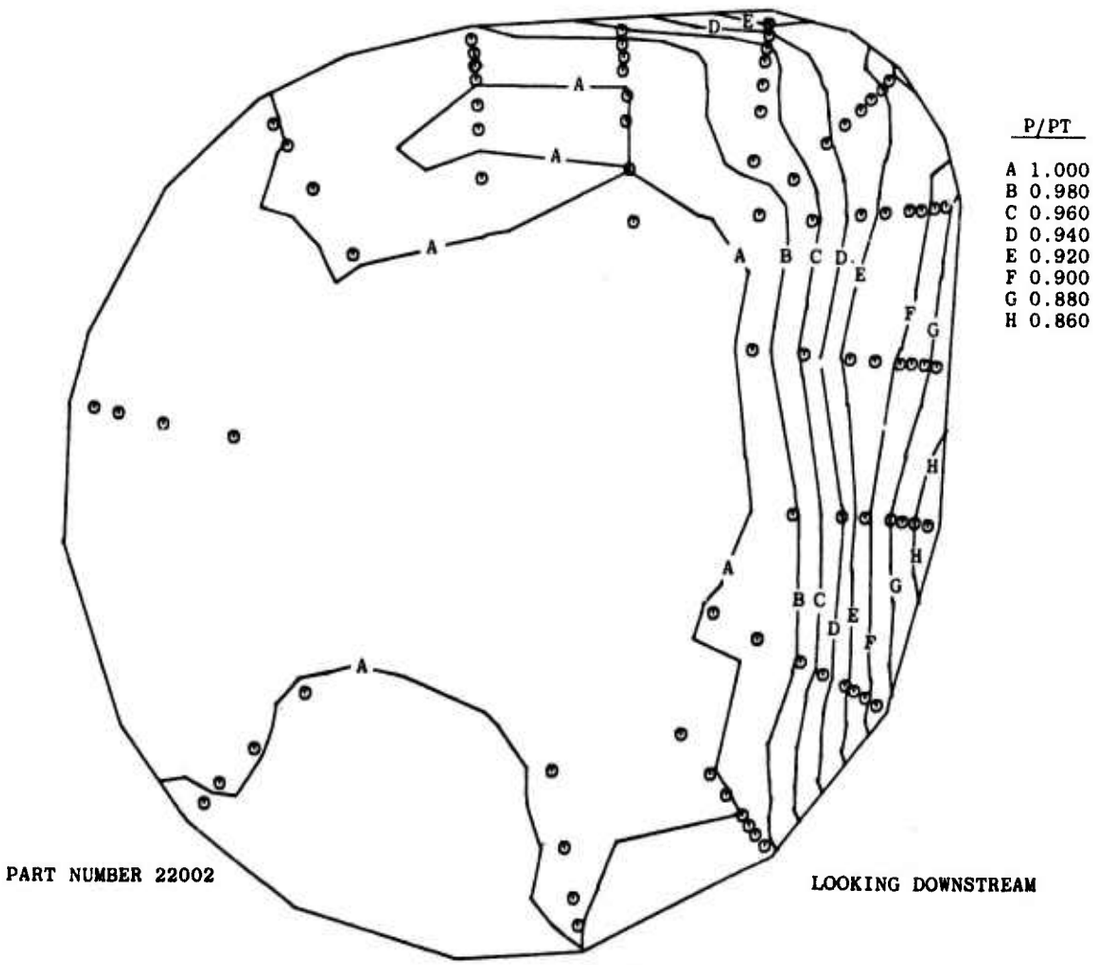

b. Alternate side plate 1
Figure 20. Continued.

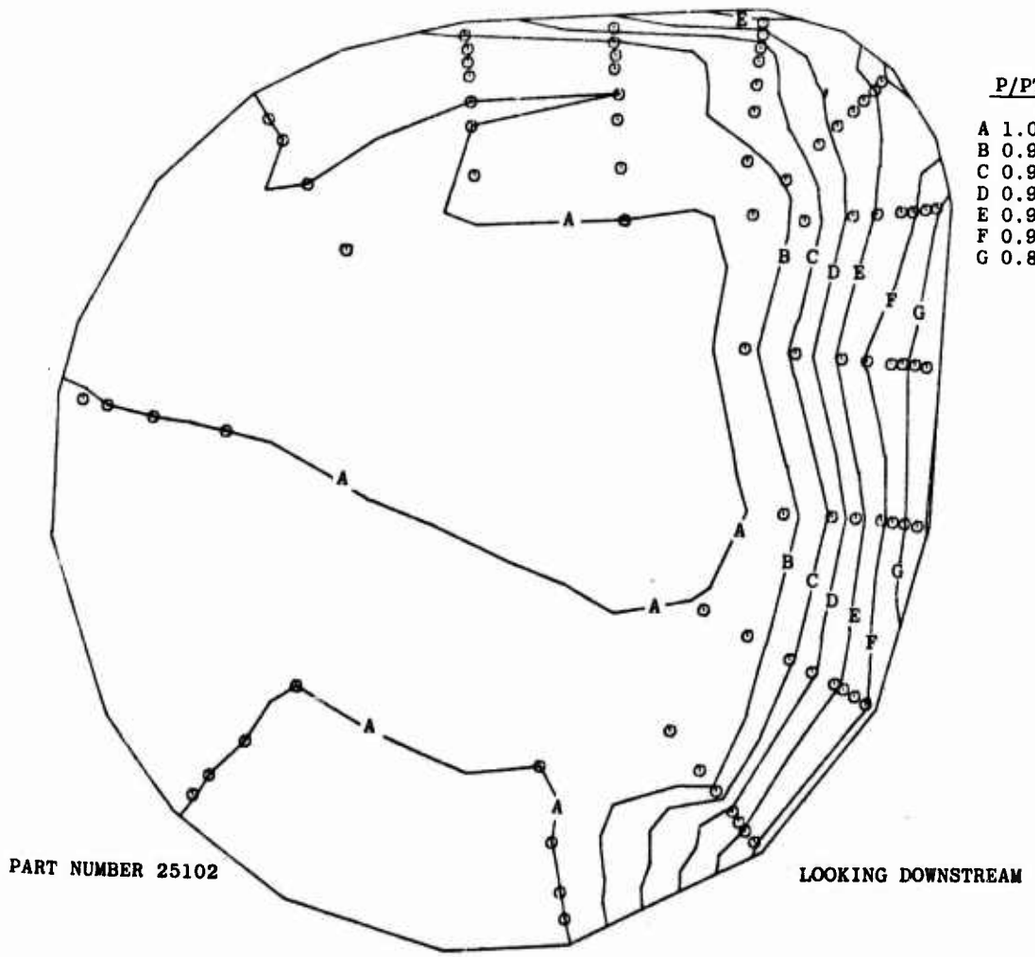

c. Alternate side plate 2

Figure 20. Concluded.

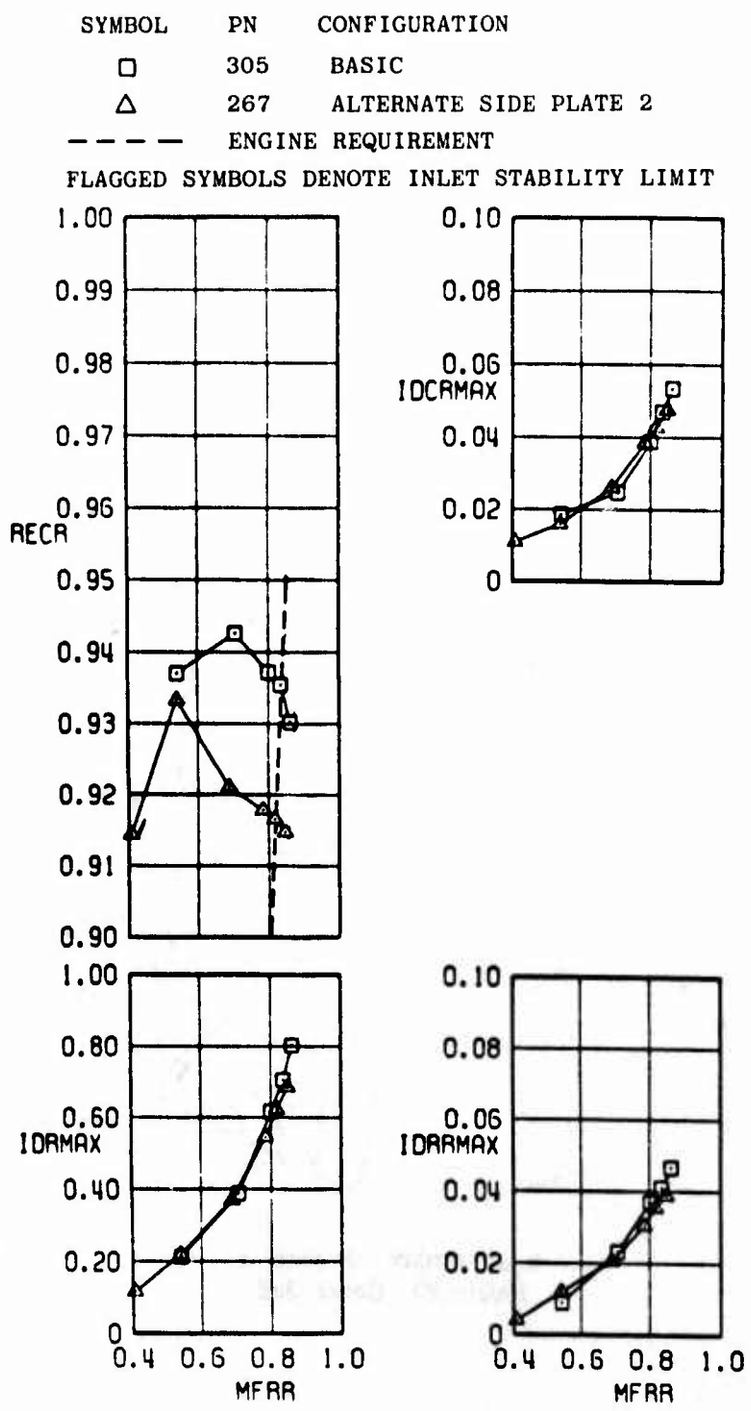

Figure 21. Effect of alternate side plate 2 on inlet performance at M_∞ = 1.50, α = 5 deg, β = 0 deg.

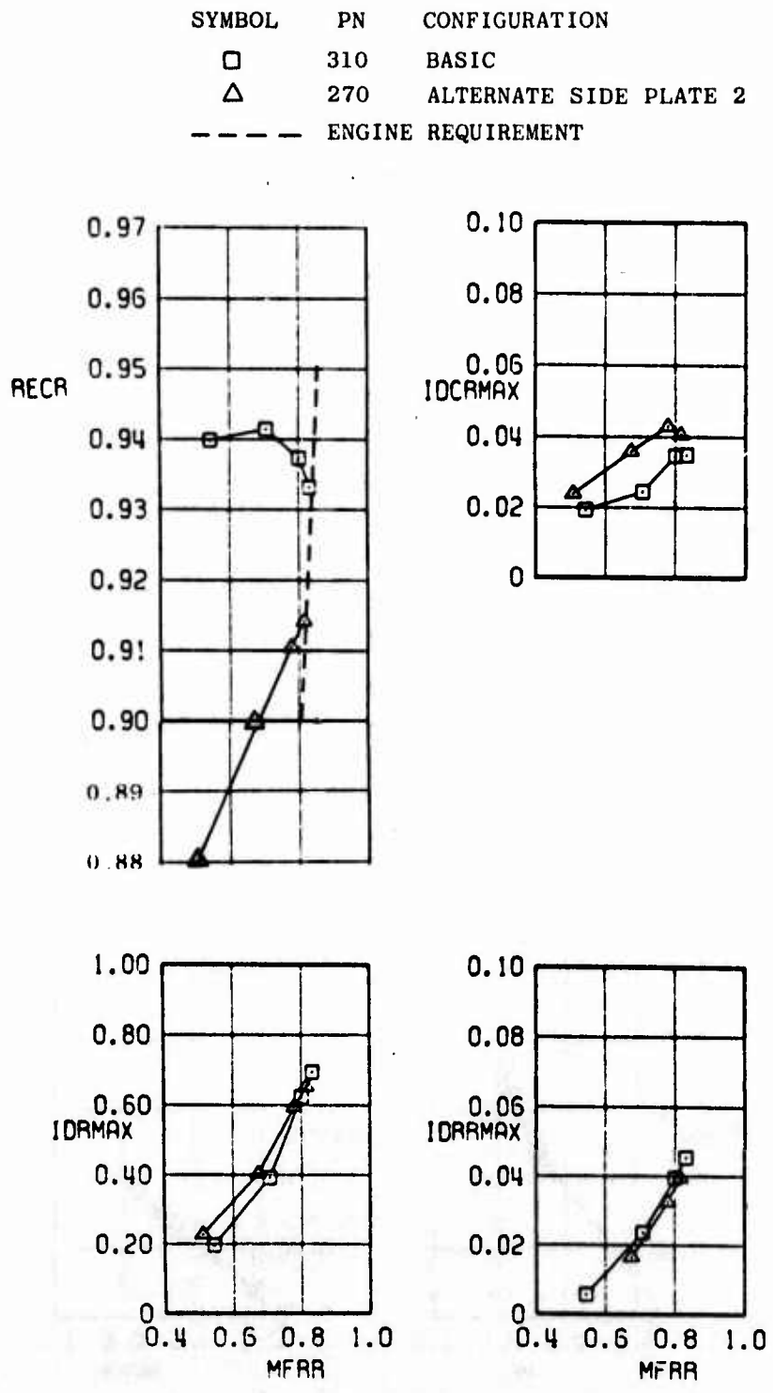

Figure 22. Effect of alternate side plate 2 on inlet performance at M_∞ = 1.50, α = 10 deg, β = 0 deg.

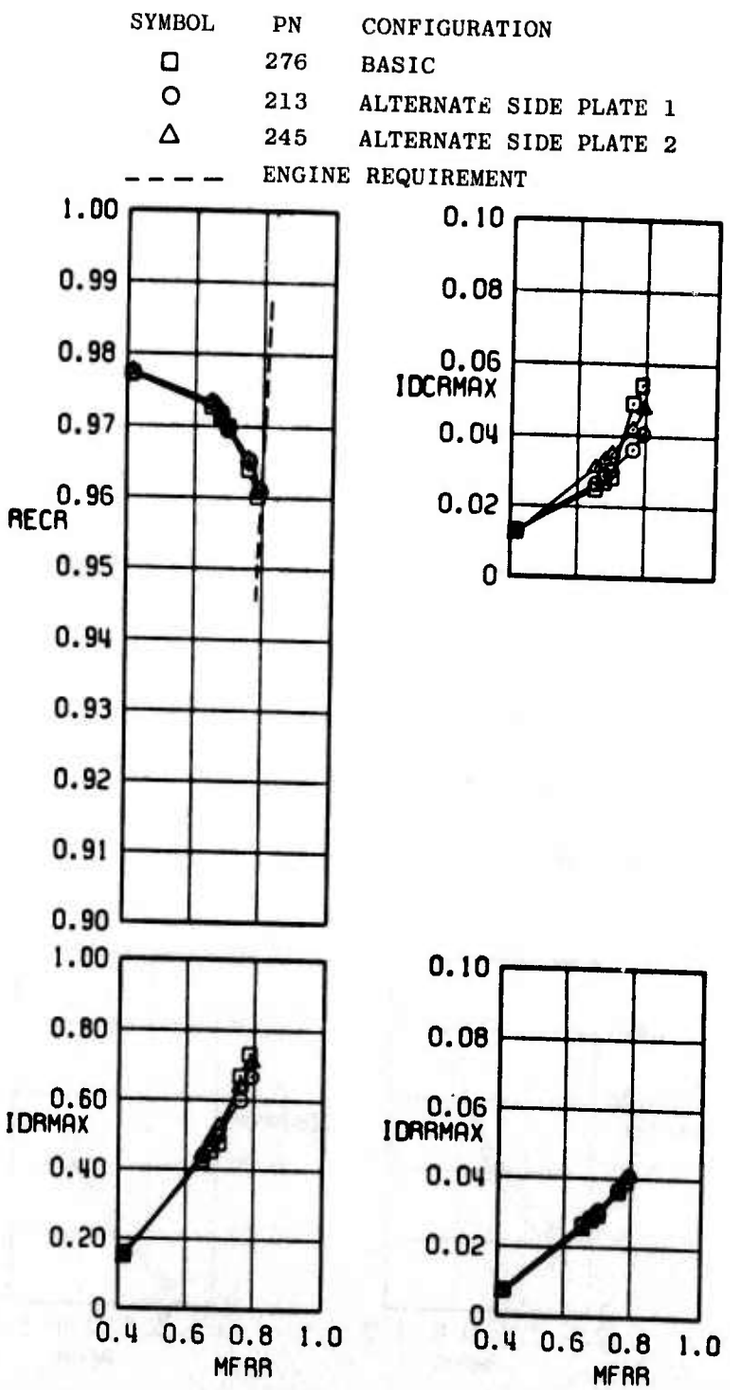

Figure 23. Effect of alternate side plates 1 and 2 on inlet performance at M_∞ = 0.85, α = 5 deg, β = 0 deg.

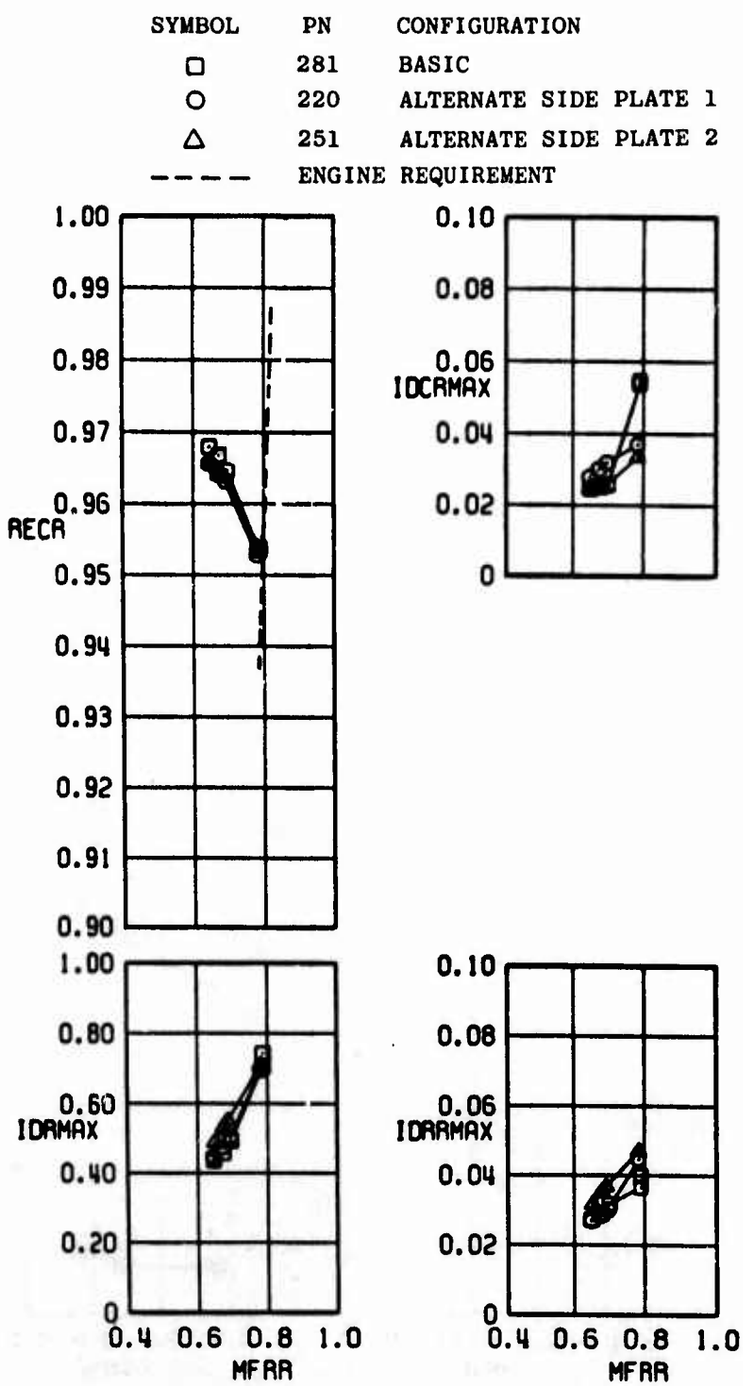

Figure 24. Effect of alternate side plates 1 and 2 on inlet performance at M_∞ = 0.85, α = 10 deg, β = 0 deg.

SYMBOL	PN	CONFIGURATION
□	276	BASIC
○	213	V.G. PATTERN 1
- - - - -		ENGINE REQUIREMENT

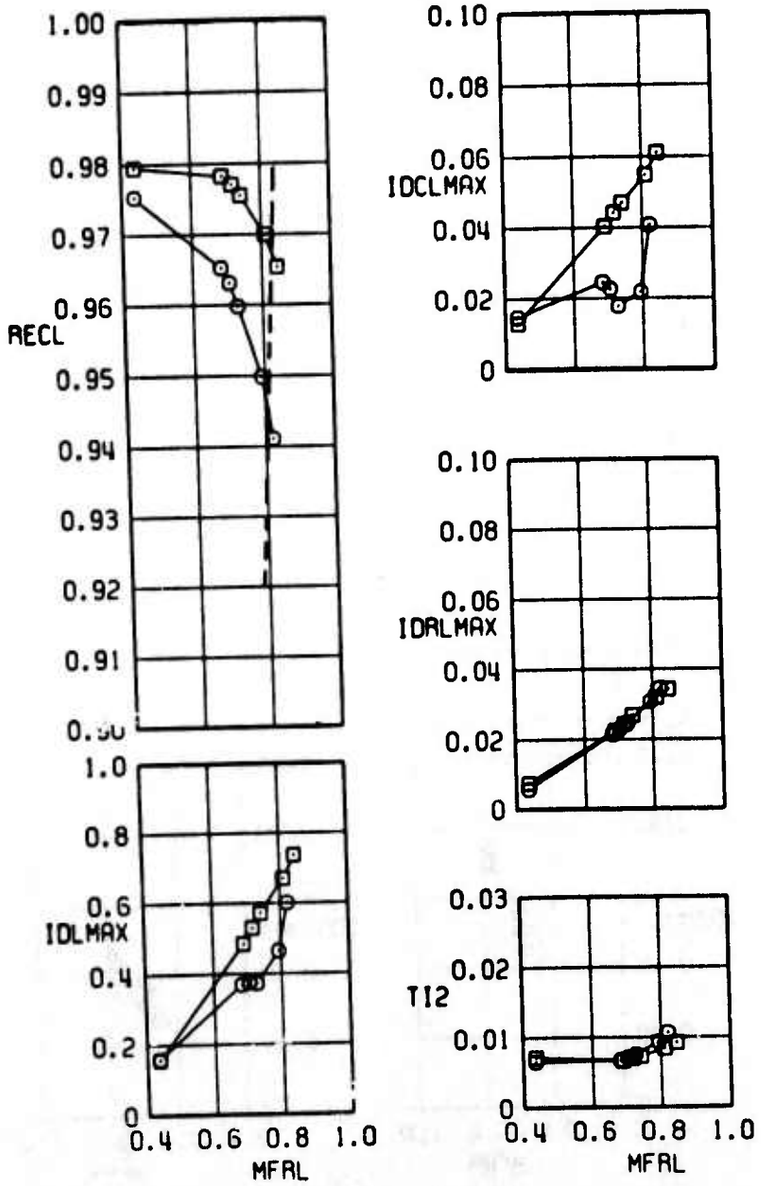

a. α = 5 deg, β = 0 deg

Figure 25. Effect of vortex generator pattern 1 on inlet performance at M_∞ = 0.85.

SYMBOL	PN	CONFIGURATION
□	281	BASIC
○	220	V.G. PATTERN 1
- - - - -		ENGINE REQUIREMENT

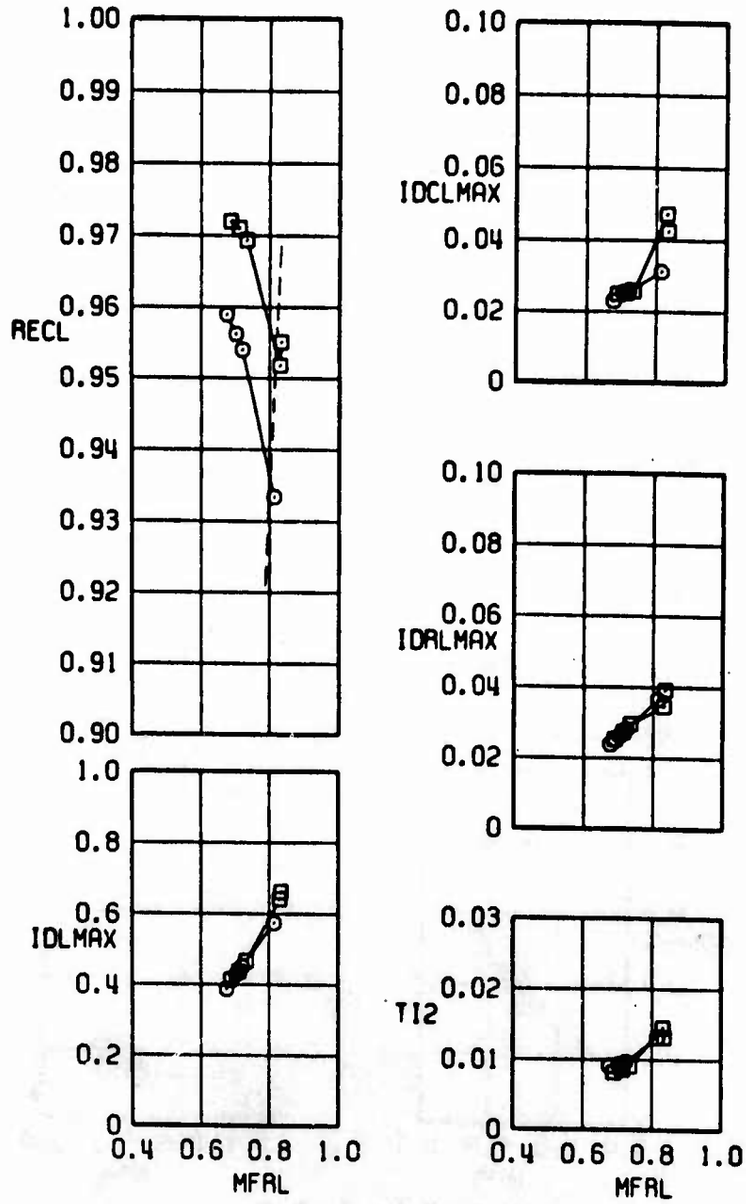

b. α = 10 deg, β = 0 deg

Figure 25. Concluded.

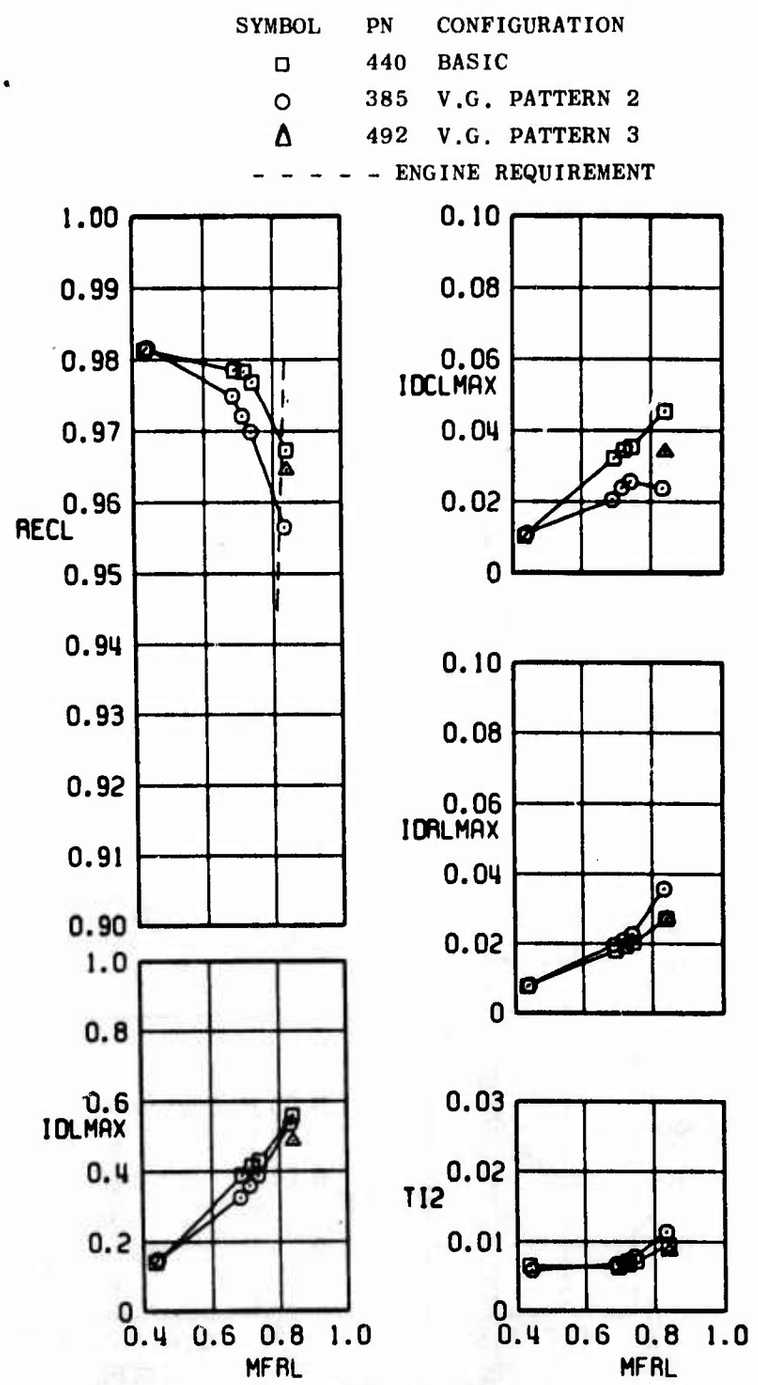

a. α = 5 deg, β = 0 deg

Figure 26. Effect of vortex generator patterns 2 and 3 on inlet performance at M_∞ = 0.85.

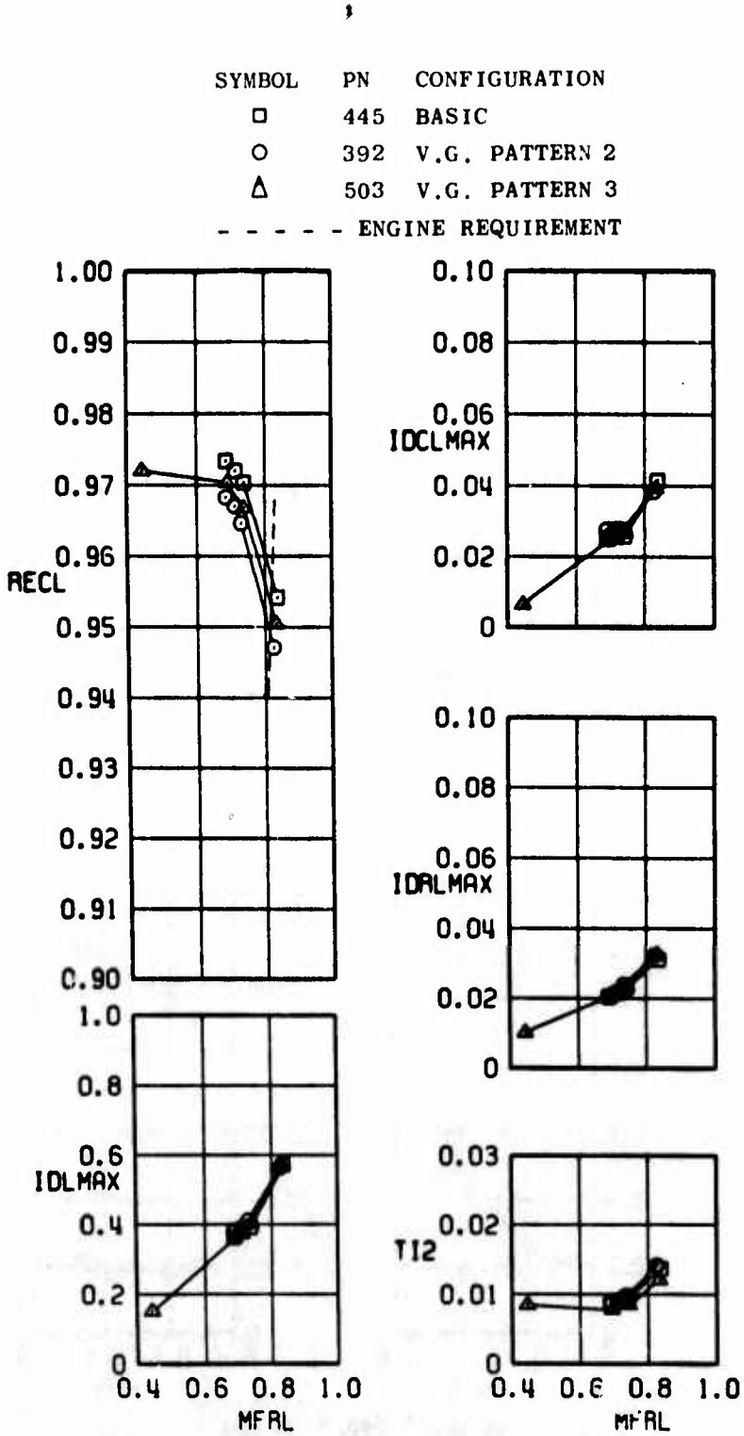

b. α = 10 deg, β = 0 deg

Figure 26. Concluded.

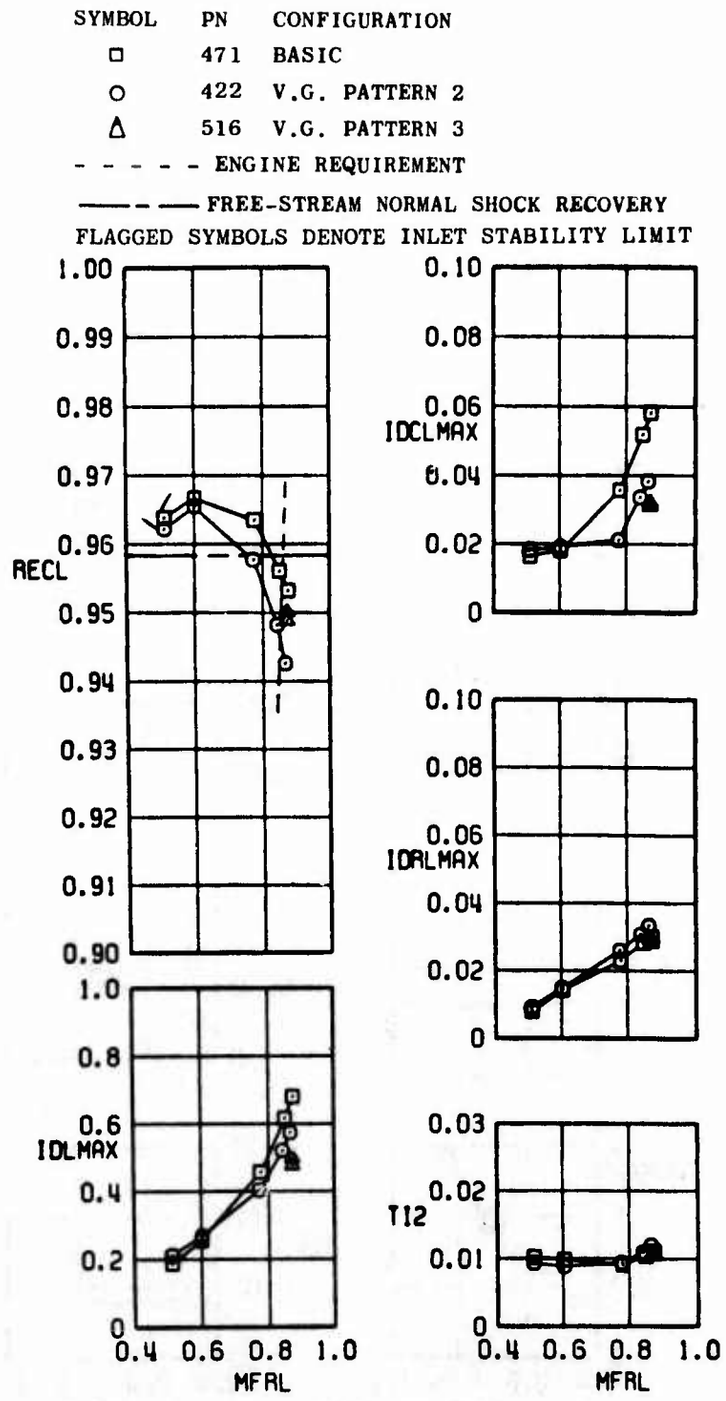

a. α = 5 deg, β = 0 deg

Figure 27. Effect of vortex generator patterns 2 and 3 on inlet performance at M_∞ = 1.40.

SYMBOL	PN	CONFIGURATION
□	475	BASIC
○	426	V.G. PATTERN 2
Δ	521	V.G. PATTERN 3

- - - - -ENGINE REQUIREMENT

——— - ———FREE-STREAM NORMAL SHOCK RECOVERY

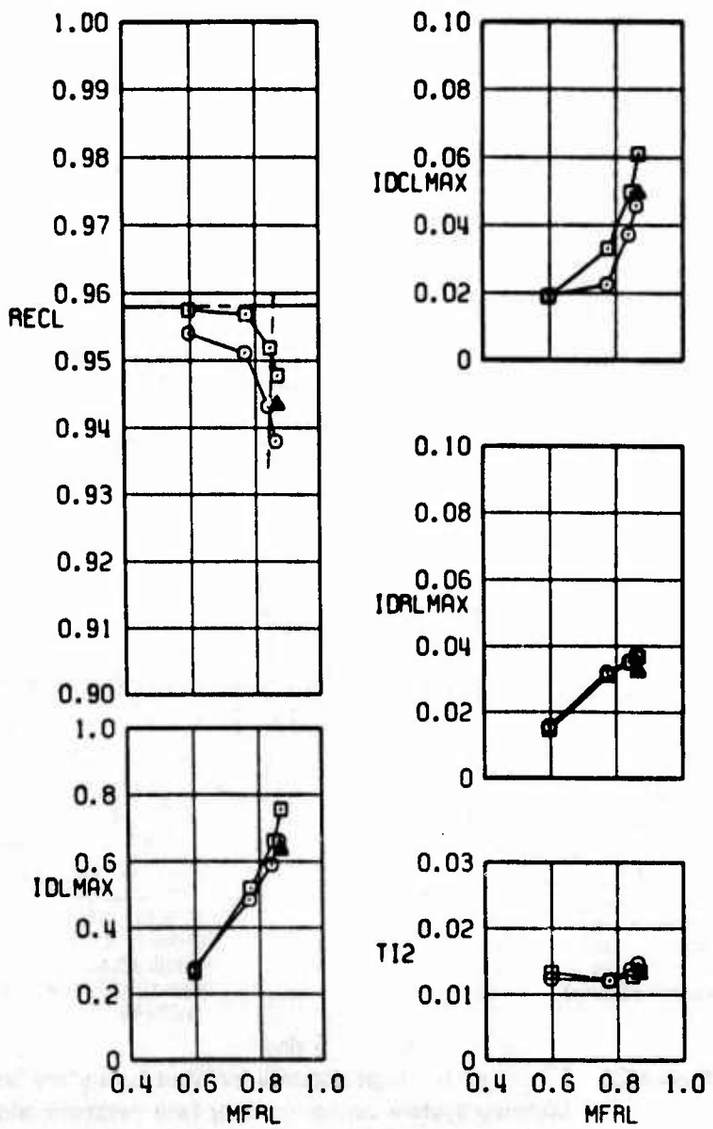

b. α = 10 deg, β = 0 deg

Figure 27. Concluded.

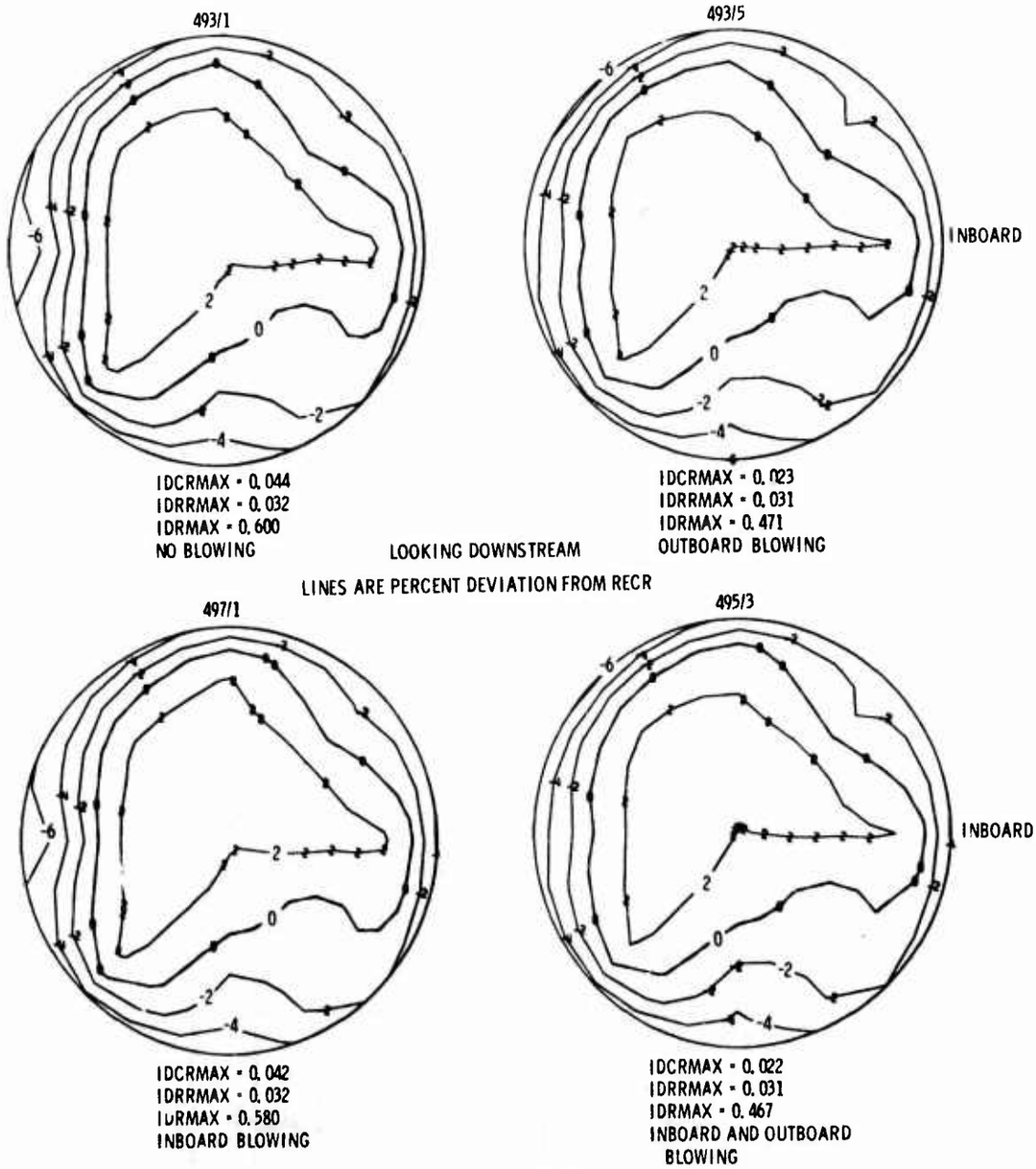

a. α = 5 deg

Figure 28. Effect of the high-pressure air duct boundary-layer blowing system on compressor-face pressure contour at at M_{∞} = 0.85, β = 0 deg.

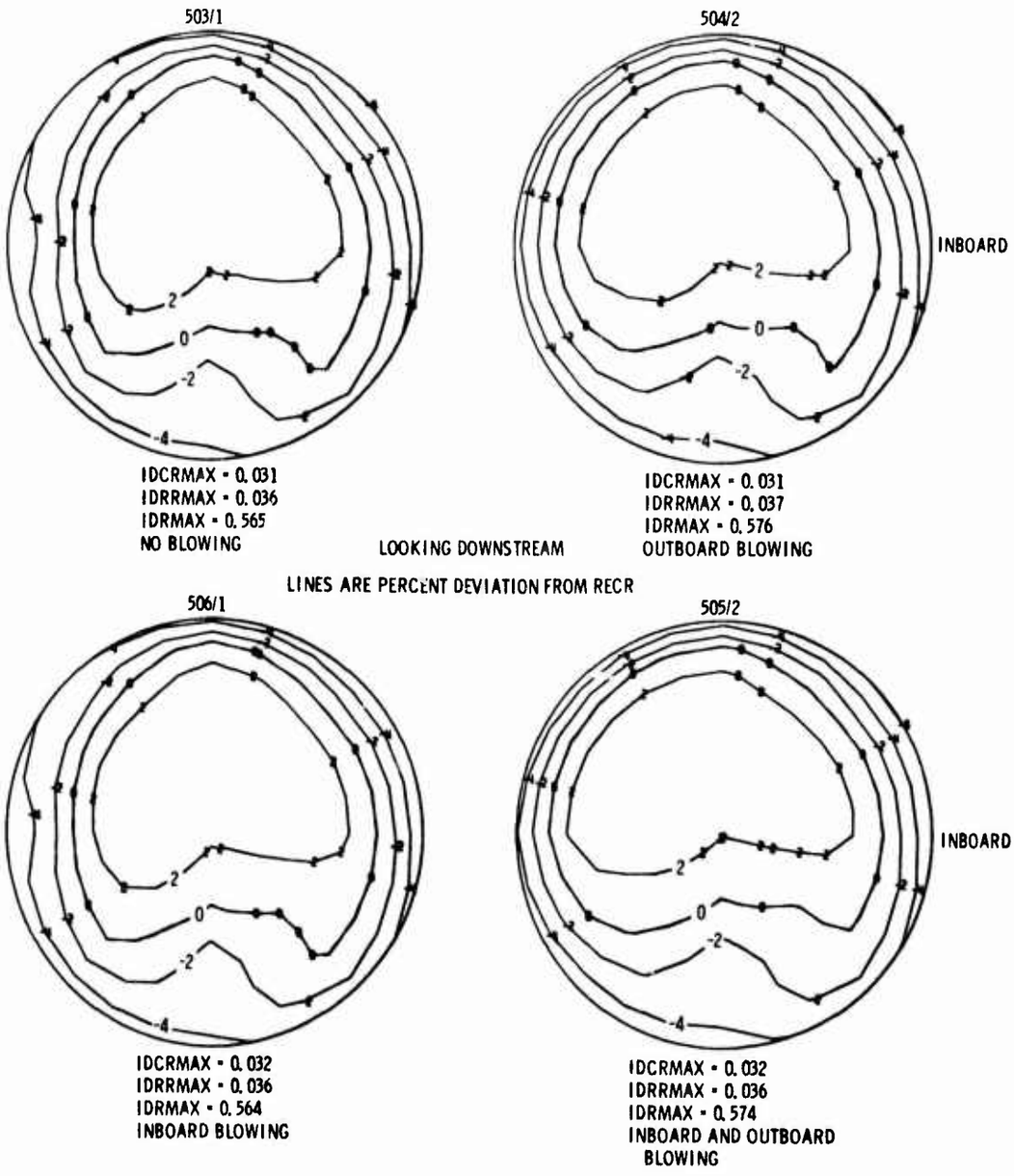

b. α = 10 deg

Figure 28. Concluded.

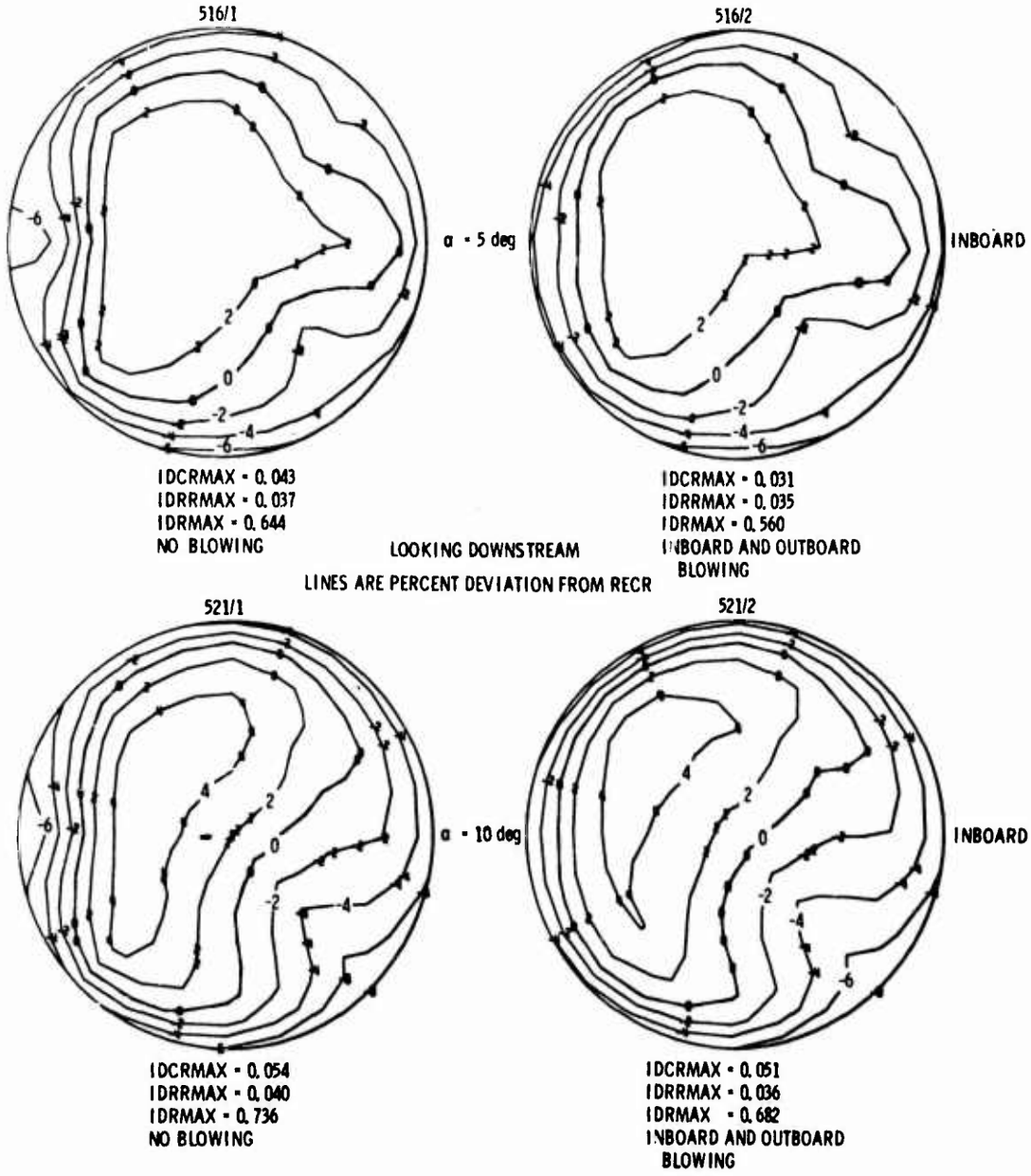

Figure 29. Effect of high-pressure air duct boundary-layer blowing system on compressor-face pressure contour at contour at M_∞ = 1.40, β = 0 deg.

Table 1. Inlet Configuration Summary

a. Left inlet

Part Number Range	Configuration
12-30 114-173	Basic Splitter; Inlet at B.L. 43.82
35-48	Basic Splitter; Inlet at B.L. 47.45
54-77	Short Splitter; Inlet at B.L. 43.82
81-105	Short Splitter; Inlet at B.L. 45.64
207-226	Basic Splitter; Inlet at B.L. 43.82; Vortex Generator Pattern 1
239-272	Alternate Splitter 2; Inlet at B.L. 43.82
275-372	Basic Splitter; Inlet at B.L. 43.82
379-432	Basic Splitter; Inlet at B.L. 45.64; Vortex Generator Pattern 2
434-482 527-558	Basic Splitter; Inlet at B.L. 45.64
487-525	Basic Splitter; Inlet at B.L. 45.64; Vortex Generator Pattern 3

b. Right inlet

12-30	Basic Splitter; Inlet at B.L. 45.64; Flow-Field Rakes; Side Plate Rakes; Throat Rakes
35-48	Basic Splitter; Inlet at B.L. 45.64; Side Plate Rakes; Throat Rakes
54-77	Basic Splitter; Inlet at B.L. 45.64; Throat Rakes
81-105	Basic Splitter; Inlet at B.L. 45.64
114-173	Basic Splitter; Inlet at B.L. 43.82
207-226	Alternate Splitter 1; Inlet at B.L. 43.82; Throat Rakes

Table 1. Concluded
b. Concluded

239-272	Alternate Splitter 2; Inlet at B.L. 43.82; Throat Rakes
275-372	Basic Splitter; Inlet at B.L. 43.82; Throat Rakes
379-432	Basic Splitter; Inlet at B.L. 43.82; Flow Field Rakes; Throat Rakes
434-482	Alternate Splitter 1; Inlet at B. L. 43.82; Flow Field Rakes; Throat Rakes
487-525	Basic Splitter; Inlet at B.L. 43.82; Duct High-Pressure Air Jets
527-558	Basic Splitter; Inlet at B.L. 43.82; No Splitter Plate Tip; Duct High-Pressure Air Jets

Table 2
Test Conditions

Tunnel 16T

M_∞	PT, psfa	TT, °R	Q, psf
0.55	850	560	150
0.65	2,425	560	540
0.75	1,990	560	540
0.85	1,710	560	540
1.20	1,225	560	509
1.40	1,050	560	453
1.50	1,000	560	430

Tunnel 16S

M_∞	PT, psfa	TT, °R	Q, psf
1.60	850	600	357
1.62	850	600	358
1.70	900	600	368
1.80	950	600	374
1.90	1,025	600	386
2.00	1,100	600	393

Table 3
Design Engine Airflow Requirements

M_∞	WPLFS WPRFS
0.55	313
0.65	337
0.75	353
0.85	355
1.20	353
1.40	343
1.50	333
1.60	323
1.70	310
1.80	295
1.90	280
2.00	270

Table 4
Measurement Uncertainties

M_∞	PT	TT, °R	M_∞	PT, psf	TT, °R	α, deg	β, deg	RECL RECR	TI2	WPLFS WPRFS, lb/sec
0.55	850	560	0.005	2.0	5.0	0.10	0.10	0.001	0.002	0.75
0.65	2,425	↓	0.002	3.3	↓	↓	↓	↓	↓	↓
0.75	1,990	↓	0.002	2.9	↓	↓	↓	↓	↓	↓
0.85	1,710	↓	0.002	2.7	↓	↓	↓	↓	↓	↓
1.20	1,225	↓	0.003	2.3	↓	↓	↓	↓	↓	↓
1.40	1,050	↓	0.004	2.2	↓	↓	↓	↓	↓	↓
1.50	1,000	↓	0.004	2.2	↓	↓	↓	↓	↓	↓
1.60	850	600	0.005	2.0	↓	↓	↓	0.003	↓	↓
1.70	900	↓	0.007	5.0	↓	↓	↓	0.003	↓	↓
1.80	950	↓	0.007	5.1	↓	↓	↓	0.003	↓	↓
1.90	1,025	↓	0.008	5.2	↓	↓	↓	0.002	↓	↓
2.00	1,100	↓	0.008	5.2	↓	↓	↓	0.002	↓	↓

APPENDIX A
EQUATIONS FOR CALCULATING INLET/ENGINE DISTORTION INDEX

$$RECL = \frac{1}{40} \sum_{j=1}^{j=8} \sum_{i=1}^{i=5} \frac{P_{ij}}{PT}$$

i = Ring number for i = 1 to 5

j = Rake number for j = 1 to 8

$$RAVGL_i = \frac{1}{8} \sum_{j=1}^{j=8} \frac{P_{ij}}{PT}, \quad i = 1 \rightarrow 5$$

$RMINL_i$ is defined as the minimum total pressure within the largest low-pressure extent of the ring.

Circumferential distortion for each circumferential ring:

$$IDCL_i = \frac{RAVGL_i - RMINL_i}{RECL}, \quad i = 1 \rightarrow 5$$

Hub circumferential distortion:

$$IDCLHUB = \frac{IDCL1 + IDCL2}{2}$$

Tip circumferential distortion:

$$IDCLTIP = \frac{IDCL4 + IDCL5}{2}$$

Maximum circumferential distortion:

IDCLMAX = larger of IDCLHUB or IDCLTIP

Radial distortion for each circumferential ring:

$$IDRL_i = \frac{RECL - RAVGL_i}{RECL}, \quad i = 1 \rightarrow 5$$

Maximum radial distortion:

$$IDRLMAX = \text{larger of } IDRL4 \text{ or } IDRL5$$

Inlet/Engine Distortion Index:

$$IDLMAX = (BL)\,(KC)\,(IDCLMAX) + (KR)\,(IDRLMAX)$$

where

$$BL = \frac{IDRLMAX/IDCLMAX}{A + B\,(IDRLMAX/IDCLMAX)} + C$$

Constants for Equations in Appendix A

M_∞	KC	KR	A	B	C
0.55	8.00	13.33	-0.55	-0.51	1.0
0.65	8.33	14.30	-0.55	-0.51	1.0
0.75	8.33	14.30	-0.55	-0.51	1.0
0.85	9.48	15.80	-0.56	-0.51	1.0
1.20	9.48	15.80	-0.56	-0.51	1.0
1.40	9.48	15.80	-0.56	-0.51	1.0
1.50	9.48	15.80	-0.56	-0.51	1.0
1.60	9.48	15.80	-0.56	-0.51	1.0
1.70	9.48	15.80	-0.56	-0.51	1.0
1.80	8.33	13.33	-0.55	-0.51	1.0
1.90	8.00	13.33	-0.55	-0.51	1.0
2.00	7.69	11.77	-0.56	-0.92	1.0

The relationship between maximum circumferential and maximum radial distortion for an inlet/engine distortion index equal to unity at the above Mach numbers is shown in Fig. A-1.

Note: Distortion parameters for the right-hand compressor face were calculated in the same manner as those for the left-hand compressor face. The nomenclature used for the right compressor-face distortion parameters is as follows: IDCRMAX, IDRRMAX, and IDRMAX.

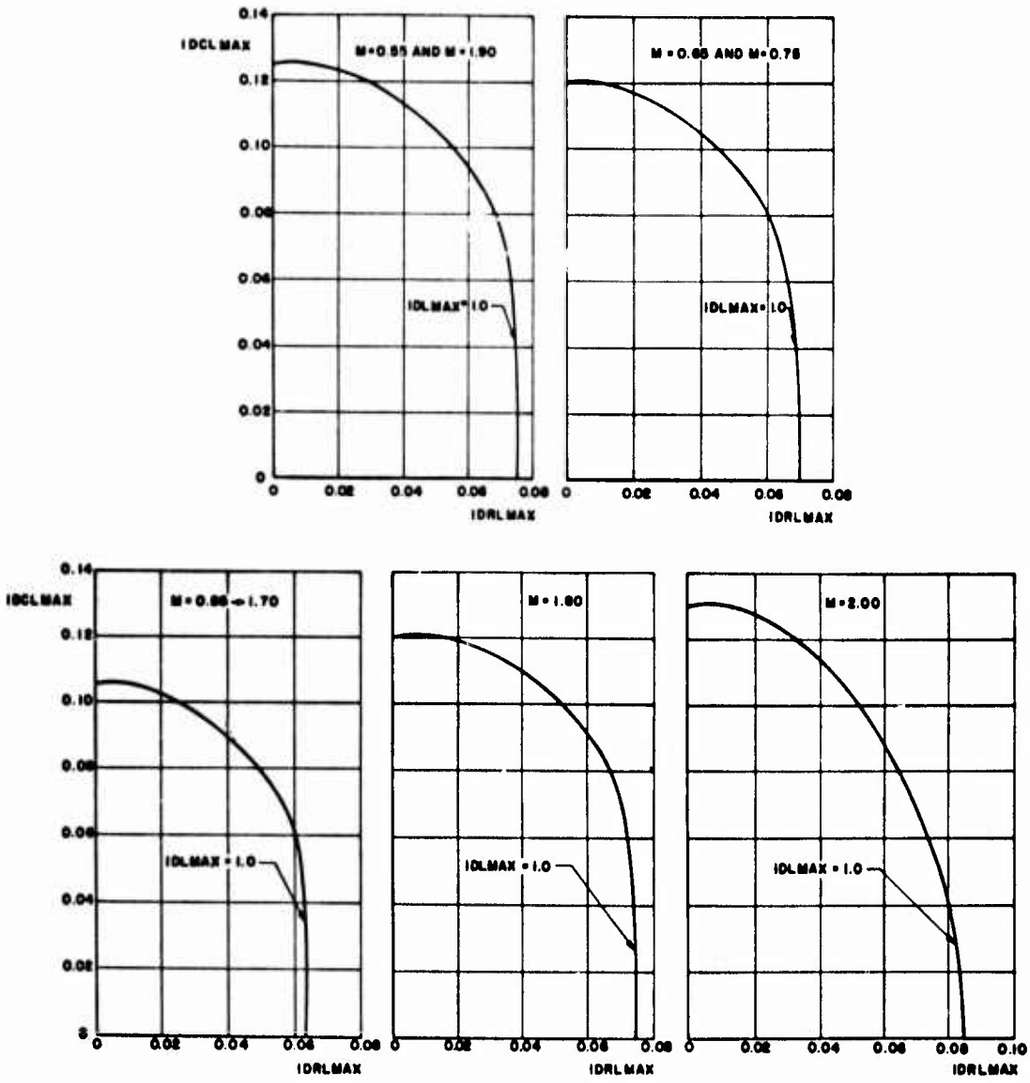

Figure A1. Relationship of IDRLMAX and IDCLMAX at IDLMAX = 1.0 for Mach numbers 0.55 to 2.00.

NOMENCLATURE

B.L.	Buttock line (full scale), in.
C.S.	Cowl station (full scale), in.
F.S.	Fuselage station (full scale), in.
IDCLMAX	Left compressor-face circumferential distortion index, see Appendix A
IDCRMAX	Right compressor-face circumferential distortion index, see Appendix A
IDLMAX	Left compressor-face combined distortion index (or inlet/engine stability index), see Appendix A
IDRLMAX	Left compressor-face radial distortion indes, see Appendix A
IDRMAX	Right compressor-face combined distortion index (or inlet/engine stability index), see Appendix A
IDRRMAX	Right compressor-face radial distortion index, see Appendix A
M_∞	Free-stream Mach number
MFRL	Left engine primary mass-flow ratio: ratio of left compressor-face station mass flow to inlet capture mass flow based on inlet reference area at α = 0 deg
MFRR	Right engine primary mass-flow ratio: ratio of right compressor-face station mass flow to inlet capture mass flow based on inlet reference area at α = 0 deg
P	Total pressure, psfa
PN	Part number
P_{rms}	Root-mean-square (rms) value of total-pressure oscillation (turbulence) at the compressor face ratioed to the average compressor-face total pressure
P_s	Static pressure, psfa
PT	Free-stream total pressure, psfa
PT2L	Left compressor-face average total pressure, psfa
PT2R	Right compressor-face average total pressure, psfa

Q	Free-stream dynamic pressure, psf
RECL	Left compressor-face total pressure recovery
RECR	Right compressor-face total pressure recovery
TI2	Turbulence index: average rms value of total pressure oscillations at the compressor face normalized by the average compressor-face total pressure
TT	Free-stream total temperature, °R
V.G.	Vortex generator
W.L.	Water line (full scale), in.
WPLFS	Left-hand full-scale engine airflow corrected to standard sea-level conditions
WPRFS	Right-hand full-scale engine airflow corrected to standard sea-level conditions
α	Model angle of attack, deg
β	Model angle of sideslip, nose left is positive, deg